5-2013

Interactions between Ions and Lysenin Nanochannels and their Potential Applications as Biosensors

Radwan Awwad Al Faouri
University of Arkansas, Fayetteville

Interactions between Ions and Lysenin Nanochannels and their Potential Applications as Biosensors

Interactions between Ions and Lysenin Nanochannels and their Potential Applications as Biosensors

A dissertation submitted in partial fulfillment
of the requirements for the degree of
Doctor of Philosophy in Physics.

By

Radwan Awwad Al Faouri
Yarmouk University
Bachelor of Science in Physics, 1987
Al-Balqa Applied University
Master of Science in Physics, 2005
University of Arkansas
Master of Science in Physics, 2009

May 2013
University of Arkansas

Abstract

Lysenin is classified as a pore-forming toxin protein that is isolated from the earthworm *Eisenia fetida* and consists of 297 amino acids [1]. Lysenin inserts large conducting pores (3.0-4.7 nm in diameter) into artificial membranes (BLM) which include sphingomyelin. These pores (channels) are open and oriented upon insertion into the bilayer lipid membrane. Lysenin channels gate at positive voltages (voltage-induced gating), but not at negative voltages. Lysenin pores also exhibit activity modulation in response to changes in ionic strength and pH, indicating that electrostatic interaction is responsible for Lysenin conductance activities. In this line of inquiries, and by modulating Lysenin electrostatic interactions, it was hypothesized that the electrical properties of Lysenin pores (channels) could be influenced by multivalent ions.

The macroscopic conductance of Lysenin channels was inhibited by addition of multivalent ions. The inhibition was concentration dependent and reversible by addition of chelating or precipitating agents. The ability of the examined multivalent ions to inhibit pore conductance depended on ionic charge and size. Taken together, these results indicate that the Lysenin channel has a binding site that is placed inside the channel and interacts electrostatically with multivalent ions resulting in a conductance response related to ionic number and size. The high sensitivity of Lysenin pores toward trivalent ions indicates that Lysenin channels could be used to develop novel biosensors for multivalent ion detection in environmental samples.

The dynamic interaction of Lysenin with multivalent ions was modeled based on the conductivity of the bulk solution and the status of Lysenin channels. The purpose of the model was to provide a mechanistic understanding of Lysenin gating. Using the experimental data, an equilibrium rate constant of the interaction between Lysenin and each multivalent ion was estimated. Each rate constant was related to the binding affinity of each ion with the binding site.

This dissertation is approved for recommendation

to the Graduate Council.

Dissertation Director:

_____

Prof. Gregory Salamo

Dissertation Committee:

_____

Prof. William F. Oliver III

_____

Prof. Laurent Bellaiche

_____

Prof. Ralph Henry

_____

Prof. Woodrow Shew

_____

Prof. Daniel Fologea

Dissertation Duplication Release

I hereby authorize the University of Arkansas Libraries to duplicate this dissertation when needed for research and/or scholarship.

Agreed _____
Radwan Awwad Al Faouri

Refused _____
Radwan Awwad Al Faouri

Acknowledgments

I would love to thank all the great people who helped and supported me over the course of my present research. First, I would like to express how much I appreciate my advisor, Professor Gregory Salamo. I would like to thank him for his constant effort in guiding me during my work on this dissertation. Secondly, I would like to thank my committee members, Prof. Ralph Henry, Prof. William Oliver III, Prof. Laurent Bellaiche, and Prof. Woodrow Shew, for their input and the time they spent helping me improve it. I would like to deeply thank Prof. Daniel Fologea for his encouragement and great discussions. I am grateful for the assistance and training he provided me. I would also like to thank my lab mate Eric Krueger for the efforts that he put into helping me, Cooley Pasley for proofreading, and Dr. David Straub for the useful and insightful discussions. Additionally, I would like to thank prof. Ken Vickers for critically reading this dissertation and providing invaluable feedback.

I am very thankful to my lovely and supportive parents for helping me in countless ways throughout my life. I'd like to thank my whole family, sisters and brothers, for all their love and support over the years. A special thank you to my kids Oday, Qusay, Louai, Mahmoud, Own, Shahad, and Jude, I am proud of you all.

Finally, I would like to say a huge thank you to my lovely wife Hedayah for understanding, standing by, and supporting me the whole time she has lived with me.

This work was partially financially supported by HHMI, under the grant number “52005890”

Dedication

This work is dedicated to all researchers past and present who have made efforts for better human health and understanding.

Table of Contents

Chapter 1 Introduction 1
1.1 Introduction to Biomembrane Channels and This Research 1
1.2 The Importance and Motivation 2
1.3 Main Dissertation Problem 3
1.4 Dissertation Structure 4

Chapter 2 Literature Review 5
2.1 The Cell and its Membrane 5
2.2 Diversity of Biomembrane Lipid Structure 7
2.3 Lipid Bilayer Surface Charge 14
2.4 Transport across Biomembranes 14
2.5 Metal Ions 16
2.5.1 Importance and Characteristics of Metal Ions 16
2.5.2 Metal Ions and Biological Interactions 17
2.5.3 Chelation of Metal Ions 19
2.5.4 Influence of Metal Ions on Gating 20
2.6 pH, Buffer and Electrical Conductivity 21
2.6.1 Acidity and Basicity of Solutions 21
2.6.2 Buffer 23
2.6.3 Electrical Conductivity of Electrolyte Solutions 23
2.7 Lysenin: A Pore-Forming Protein 26
2.7.1 Ion Channels versus Lysenin 26
2.7.2 The Structure of Lysenin 29
2.7.3 Interaction of Lysenin with Lipids 30
2.7.4 Voltage Gating, Ligand Gating and Modulation of Channels 32

Chapter 3 Materials and Methods 34
3.1 Materials 34
3.1.1 Chemicals 34
3.1.2 Teflon chamber 35
3.1.3 Measurement devices 35

3.2 Methods 36
3.2.1 Planar BLM Formation 36
3.2.2 Insertion of Lysenin into BLM 38
3.2.3 Addition of Ions and Measuring Conductance 41
3.3 Error Analysis 42

Chapter 4 Results and Discussion 44
4.1 Insertion of Lysenin Channels into BLM, and their Electrical Characterization 44
4.2 Effect of Monovalent Ions Concentrations on Lysenin Channels' Conductance 50
4.3 Influence of Divalent Metal Ions on Lysenin Channel's Macroscopic Conductance 51
4.4 Effect of Trivalent Metal Ions on Lysenin Channel's Macroscopic Conductance 54
4.5 Influence of Monovalent Ions on Lysenin's Gating 56
4.5.1 High Monovalent Concentration Modulates Lysenin's Voltage Gating 56
4.5.2 Monovalent and Multivalent Ions Compete Lysenin's Binding Site 59
4.5.3 Monovalent Ions affect the Transport of Lysenin's Channels 63
4.5.4 Sensitivity of the Lysenin-BLM Biosensor 65
4.6 Charge Impact on Lysenin Channel's Conductance 68
4.7 Hydrated Radius and Charge Density Effects on Lysenin Channel's Conductance 69
4.8 Reversibility 72
4.9 Single Channel Investigation and Mechanism of Conductance Decreasing 75

Chapter 5 Modeling the Dynamic Interaction between Ions and Lysenin 82
5.1 Kinetics of the Dynamic Interaction between Lysenin and Ions 82
5.2 Mathematical Model for Ligand Gating of Lysenin Channels 84
5.2.1 Equilibrium Rate Constant 84
5.2.2 Electric Current Before and After Adding Multivalent Ions 87

Chapter 6 Comparison between Theory and Experiment 91
6.1 Fitting Data of Divalent Metal Ions 91
6.2 Fitting Data of Trivalent Metal Ions 97
6.3 Fitting the Data for High Monovalent Ion Concentration 102

Chapter 7 Conclusions 105

Chapter 8 Future Work 107
8.1 Full Closing versus Partial Closing: a Cu^{2+} Study 107

8.2 The Influence of Lipid Composition on Lysenin Channel Insertion and Activity 110
8.3 Ion-Lipid Interaction Effect on Lysenin Channel Functionality..... 110
8.4 Controlled Molecular Transport 111
8.5 Modulate the Charge on Lysenin Structure 113

References..... 114

Appendix A: Characteristics of Metal Ions..... 119

Appendix B: Chelating Agents and Buffers 121

Appendix C: Conductivity and Electrochemical Reactions..... 123

Appendix D: Conductance Calculations, Uncertainties and Errors..... 127

Appendix E: Capacitance and Electric Field Across BLM..... 132

List of Figures

Figure 2.1: Schematic drawing of a cross section of an animal cell showing the cell membrane and the biomembranes of other cell parts. 6

Figure 2.2: Schematic drawing of bilayer lipid membrane (BLM) shows their two leaflets (layers), which consist of hydrophilic headgroups (polar) and the hydrophobic tails (nonpolar) surrounded by water..... 7

Figure 2.3: The membrane phospholipids and its amphipathic nature. (a) A phospholipid molecule consists of a polar head and two fatty acids (nonpolar tails) attached by a glycerol backbone. PE is an example of the membrane phospholipids, where the polarity of the head results from a positively charged amino group connected to a negatively charged phosphate one. Note that if the 3 hydrogen atoms bonded to the N atom were replaced by 3 methyl groups (CH_3) then we would have Phosphatidylcholine (PC or lecithin). (b) A schematic drawing of this phospholipid molecule (PE or cephalin). Such a molecule is called zwitterion (hybrid ion) because it has both positively and negatively charged groups in its structure 9

Figure 2.4: Chemical structures of the most common functional groups used with phosphatidic acid to form phosphoglycerides, (a) Ethanolamine and (b) Choline are positively charged (c) Serine is zwitterionic even before attached to phosphatidic acid and (d) Inositol headgroup is neutral. 11

Figure 2.5: (a) The chemical structure of sphingomyelin, which is considered as one of the major constituents of animal cell membranes. It can be found in the myelin sheaths of nerve cells . (b) The chemical structure of cholesterol consists of a four-ringed hydrocarbon linked to a hydrocarbon chain..... 12

Figure 2.6: Cholesterol molecules in a lipid bilayer. (a) Cholesterol molecules are present in both lipid monolayers of the membrane of animal cells. (b) Cholesterol forms a hydrogen bond (via its hydroxyl group) with the oxygen atom that is between the glycerol backbone and the fatty acid of the phospholipid molecule. A mixture of lipids and cholesterol was used in this study in preparing the artificial bilayer lipid membrane (BLM) to provide stability and facilitate the pore formation of Lysenin..... 13

Figure 2.7: The periodic table of the elements, showing bulk metals such as Na, trace metals such as Mn, toxic metals such as Pb and beneficial metals like Cr. All elements located to the left of the black bold zigzag line are called metals. 17

Figure 2.8: The ions are hydrated (surrounded by six water molecules). (a) The negatively charged oxygen atoms of the water molecules' dipoles are attracted by the positively charged sodium ion. (b) The positively charged hydrogen atoms in the water molecules' dipoles are attracted by the negatively charged chloride ion. 24

Figure 2.9: The conductivity of potassium chloride without buffer and mixed with 20mM buffer in the range of 0 to 800 mM KCl. The buffer does not change the conductivity of potassium chloride ions in the electrolyte. 25

Figure 2.10: The amino acid is a molecule that has a central carbon atom attached to one hydrogen atom and to three different groups (amino, carboxyl and R group), the R group defines the amino acid. 27

Figure 2.11: (a) Schematic shows three Lysenin channels inserted in artificial bilayer lipid membrane containing sphingomyelin immersed in an aqueous solution (KCl or NaCl), (b) Electron microscopy shows that Lysenin produced a honeycomb structure (pores) in sphingomyelin-containing membranes 28

Figure 2.12: A spiral-and-ribbon model of Lysenin crystal structure showing (a) its two domains: the first one is the N-terminal (red and blue) which is the part of the protein that is inserted inside the membrane, and the second domain is the C-terminal one (cyan) which is the head of the Lysenin protein. (b) The hinge is located at the boundary between the head (C-terminal) and the body of Lysenin (N-terminal), and has a freedom to move about 45^0 30

Figure 2.13: Electrostatic surface representation of Lysenin shows the positively charged regions (blue) at the C-terminus and the negatively charged ones at the N-terminus (red). One of the fatty acid tails of the SM binds with Lysenin along a groove on the surface. 32

Figure 2.14: Two mechanisms of ligand gating: (a) a ligand interacts with the protein's binding site, and then the pathway of the channel is blocked by the ligand (pore-blocking mechanism), (b) a ligand binds to the binding site causing conformational changes leading to pore blocking. 33

Figure 3.1: Three Lysenin channels inserted into a constructed BLM. The electric current through these channels was recorded by using two Ag/AgCl electrodes placed across the BLM in the chamber that contained an aqueous electrolyte..... 36

Figure 3.2: Current versus time graph illustrates a recorded capacitive current in pico amperes (70 pA), evidence of stable BLM formation across the punctured aperture in the Teflon sheet.. 38

Figure 3.3: The insertion process of Lysenin channels into BLM. The current per channel was approximately –48 pA when the biased voltage across the membrane was –80 mV. The value of the current per channel is important because it enables us to estimate the total number of channels..... 39

Figure 3.4: Current versus time graph showing insertion of about 300 Lysenin channels into BLM. Ionic current passing through BLM increases with time and reaches its maximum value and then stabilizes in about 25 minutes. 40

Figure 3.5: The conductance of Lysenin channels was measured by applying a voltage ramp (0 mV: –60 mV: 0 mV) across the inserted channels in the BLM. 42

Figure 3.6: (a) Increasing the concentration of sodium chloride from 50 mM to 800 mM increased the conductivity of the bulk, while (b) addition of 100 μM trivalent ferric ions (Fe^{3+}) to 150 mM KCl bulk solution significantly reduced the channels' conductance. 43

Figure 4.1: The macroscopic current increases with time, showing a rapid growth and leveling of current through the BLM. The behavior of the current indicates a permeability increase of the BLM upon the addition of Lysenin channels by maximizing the number of charge transporters passing through the BLM..... 44

Figure 4.2: The interaction between Lysenin and bilayer lipid membrane affects the latter's permeability, resulting in insertion of pores. A higher resolution graph of open current shows the stepwise nature of this process and its relation with each individual pore (approximately -48 pA/pore at -80 mV bias voltage)..... 45

Figure 4.3: Current versus time graph shows the closing of three embedded channels into the bilayer due to voltage-induced gating. At +15 mV the pores started to gate, and holding the potential at +30 mV closed all three pores (150 mM KCl, 20 mM HEPES/KOH, pH 7). 47

Figure 4.4: Current versus time graph shows the negative applied voltages up to -30 mV did not produce closure in any of the bilayer's three pores (150 mM KCl, 20 mM HEPES/KOH, pH 7). 48

Figure 4.5: Current voltage graph shows the behavior of a population of Lysenin channels in the BLM surrounded by a supporting electrolyte solution of 150 mM KCl, 20 mM HEPES/KOH pH 7. The linearity in the negative voltage shows no rectification, while it can clearly be seen in the positive voltage region due to the voltage-induced gating of Lysenin. 49

Figure 4.6: (a) The conductance of Lysenin channels linearly increased with monovalent ion concentration in the range 50mM to 900 mM, which is consistent with the conductivity curve in (b), indicating no changes in the geometry of the channels in that range. (b) K^+ and Na^+ increased the conductivity at a constant rate in the range of 50-900 mM, with the difference between the two ions due to sodium's lower mobility..... 50

Figure 4.7: (a) $Mg^{2+}$and Ca^{2+}decreased the conductance of Lysenin channels by about 30% (b) Mn^{2+} also reduced the conductance of channels but was less efficient than Ni^{2+} and Co^{2+}. The most efficient divalent ion was Fe^{2+} and the linear increase after the minimum conductance was due to the subsequent increase in the bulk conductivity. 52

Figure 4.8: Zn^{2+} was more efficient and caused a greater reduction in Lysenin's channels conductance than Cd^{2+} and at a lower concentration range. 53

Figure 4.9: Lanthanides ions were very effective inhibitors of ionic transport through Lysenin channels, and lowering the conductance to approximately zero in ranges of 130 μM-650 μM... 54

Figure 4.10: Among the tested ions, Al^{3+} was the most effective inhibitor, bringing the conductance of Lysenin channels to zero in the range of zero to 1.5 μM. 55

Figure 4.11: A Lysenin channel in its open state. The structure shows just two of the six Lysenin proteins with their dipole moments interacting with the external electric field across the BLM and the channel. The blue and red colors represent the positive and negative charged regions (inside the lumen) respectively. The interaction between ($Eext$) and (p) that is ($p.E$) forces the channel to stay open. 57

Figure 4.12: The positive voltage is applied across the BLM and the channel. The Lysenin channel starts to gate when this voltage exceeds the critical voltage, proposing that the main cause for voltage gating is the dipole-electric field interaction ($p.E$). 57

Figure 4.13: Current versus voltage graph shows the shift in the critical voltage of Lysenin as a result of the electrostatic interaction of monovalent ions and the voltage sensor of Lysenin channels. In the negative region, the slopes of the straight lines increased because of the increase in the conductivity of the solution. 59

Figure 4.14: The behavior of the conductance of Lysenin channels versus concentration of monovalent concentrations shows the sensitivity of Lysenin towards trivalent cations (Ce^{3+}) at low monovalent ion concentrations. This sensitivity became weaker as the monovalent ion concentration increased. 61

Figure 4.15: Divalent ions modify the voltage gating of Lysenin. A notable shift in the critical voltage before and after adding Mg^{2+} was recorded. The critical voltage was shifted from 20 mV to 40 mV before and after adding Mg^{2+} respectively. 62

Figure 4.16: The measurement of the conductance of single Lysenin channel shows its nonlinear and linear behavior in the ranges of 1 mM to 50 mM and 50 mM to 900 mM KCl respectively. 64

Figure 4.17: The measurement of the conductance of single Lysenin channel shows its nonlinear behavior with the conductivity of KCl bulk upon increasing its concentration from 1 mM to 50 mM. The differences in slopes of the segments indicate a change in the geometry of the channel. 65

Figure 4.18: The linearity of the conductance versus bulk concentrations of one single channel indicates that the geometry of the channel is not affected at very low monovalent ion concentrations. 66

Figure 4.19: Lysenin channels show more sensitivity to Co^{2+} at the lowest monovalent ion bulk concentrations. 67

Figure 4.20: Trivalent ferric ions (Fe^{3+}) reduced the conductance of Lysenin much more effectively than divalent ferrous ions (Fe^{2+}), indicating the irrelevance of chemical identity to changes in Lysenin's conductance. 69

Figure 4.21: The chemical structure of (a) $Spermidine^{3+}$ and (b) $Spermine^{4+}$ 70

Figure 4.22: The effects of (a) trivalent Spermidine and (b) quatrovalent Spermine on conductance of Lysenin channels were similar to those of divalent ions. 71

Figure 4.23: Chelators' or precipitators' effect on recovering the current through closed Lysenin channels. The fast recovery of the current indicated that these channels were functioning in the BLM. (a) Addition of EDTA chelated La^{3+}; as a result the channels reopened again. (b) Phosphate ions precipitated Al^{3+}; the channels reopened quickly. 73

Figure 4.24: (a) The kinetic process of inserting three Lysenin channels in the BLM increased current in three discrete steps. (b) The inhibition of the current through these channels in a similar manner as they closed upon addition of La^{3+}. The noise was higher in (a), so the recorded line is thicker than (b). 78

Figure 4.25: (a) The kinetic process of inserting three Lysenin channels in the BLM increased current in three discrete steps. (b) The addition of Ca^{2+} decreased open current in a similar manner to La^{3+} with approximately half amplitude steps indicating a sub-conducting state. The noise was higher in (b), so the recorded line is thicker than (a). 80

Figure 5.1: La^{3+} ions interacted with Lysenin channel and caused a fluctuation in current revealing the dynamic interaction between them. The status of the channel was switched between partially closing and reopening according to the dynamic interaction with ions. 83

Figure 5.2: Addition of Ca^{2+} to a bulk of 150 mM KCl linearly increases the conductivity of the bulk. The linear fit gives the value of the parameter "b" which is the slope of line. 89

Figure 6.1: The model successfully predicted a stable sub-conducting state of Mg^{2+}. As indicated by the graph, the macroscopic current decreased at low divalent ion concentrations was followed by a linear increase due to the subsequent increase in conductivity of the bulk. 92

Figure 6.2: Fitting the experimental data of Ca^{2+}. 92

Figure 6.3: Fitting the experimental data of Mn^{2+}. 93

Figure 6.4: Fitting the experimental data of Ni^{2+} 93

Figure 6.5: Fitting the experimental data of Co^{2+}. 94

Figure 6.6: Fitting the experimental data of Fe^{2+} 94

Figure 6.7: Fitting the experimental data of Cd^{2+}. 95

Figure 6.8: Fitting the experimental data of Zn^{2+}. 95

Figure 6.9: The model successfully predicted a non-conducting state. As indicated by the graph, the macroscopic current decreased at very low aluminum trivalent ion concentrations. 97

Figure 6.10: Fitting the experimental data of Ce^{3+}. 98

Figure 6.11: Fitting the experimental data of La^{3+}. 99

Figure 6.12: Fitting the experimental data of Eu^{3+}. 99

Figure 6.13: Fitting the experimental data of Tb^{3+}. 100

Figure 6.14: Fitting the experimental data of Fe^{3+}..... 100

Figure 6.15: Fitting the experimental data of Ce^{3+} at 75 mM KCl. 102

Figure 6.16: Fitting the experimental data of Ce^{3+} at 150 mM KCl. 103

Figure 6.17: Fitting the experimental data of Ce^{3+} at 300 mM KCl. 103

Figure 6.18: Fitting the experimental data of Ce^{3+} at 600 mM KCl. 104

Figure 6.19: Fitting the experimental data of Ce^{3+} at 900 mM KCl. 104

Figure 8.1: Among all tested divalent ions, Cu^{2+} demonstrated the greatest conductance reduction effect on Lysenin channels, requiring only 200 μM to almost completely shut them.107

Figure 8.2: (a) Two Lysenin channels opening. (b) Full closure of Lysenin channels in two steps as induced by Cu^{2+} with brief transitional periods between them. (c) The channels reopen with similar transitional states upon Cu^{2+} chelation. 108

Figure 8.3: The model provided the value of the equilibrium rate constant of the interaction between copper divalent ions and the binding site of Lysenin. 109

Figure 8.4: Fluorescent giant unilamellar vesicle (GUV)..... 112

List of Tables

Table 1: The deficiency of some ions in humans and their corresponding diseases..... 18

Table 2: pH values of some common substances..... 22

Table 3: The hydration numbers of some ions..... 24

Table 4: predicted values of equilibrium rate constants and the fraction numbers "*f*" for divalent ions..... 96

Table 5: predicted values of equilibrium rate constants for trivalent ions..... 101

Table 6: Biological classification, ionic and hydrated radii 119

Table 7: Electronic configurations of elements and ions..... 120

Table 8: The estimated values of the electrical conductance of Lysenin channels before adding ions..... 130

Table 9: The estimated values of the electrical conductance of Lysenin channels after adding ions..... 130

Chapter 1 Introduction

1.1 Introduction to Biomembrane Channels and This Research

In any biological membrane there are pathways called ion channels for ions or biomolecules to pass through. They are responsible for controlling the movement of biomolecules or ions in and out of these membranes [2], and can be considered as controlled pores in the membrane. They control the traffic across the biological membrane by gating, so they open and close according to the need of the cell or the organelle inside it. There are different types of gating; voltage and ligand gating are two common examples. In voltage gating, for instance, the channel responds to a voltage to switch its state from open to close state or vice versa [3].

The investigation of ion channels in the cell or organelle membranes has many limitations and difficulties. To overcome these difficulties in this research, a self- inserted protein (called Lysenin) in a membrane containing sphingomyelin is used.

This work is a valuable addition to previous studies in the field of ligand gating and its uses in biosensing applications. In this study, Lysenin, which is categorized as a pore-forming toxin, is used to insert channels in an artificial planar bilayer lipid membrane (BLM). The mechanism of Lysenin's gating was inspected under the influence of multivalent ions in order to reveal the functionality of such a protein in the BLM. This work proposes that Lysenin channels have a binding site that interacts electrostatically with multivalent ions and senses them differently according to their ionic numbers and sizes. This gives Lysenin the capability to be used as a sensor for biological applications like detecting the amount of different ions such as lead, potassium, copper and sodium in our drinking water. In addition, the interaction of Lysenin

and multivalent ions was modeled based on the conductivity of the bulk solutions and the status of Lysenin channels. The purpose of that modeling is to provide more evidence that enhance us to comprehend the mechanism of Lysenin gating. Accordingly, by fitting the experimental data, the equilibrium rate constants of the interaction between Lysenin and metal ions were estimated.

1.2 The Importance and Motivation

The incentive of this study was first to understand the gating process of ion channels by investigating the dynamic interaction between metal ions and Lysenin channels, and then to establish a biological sensor setup to detect various metal ions in environmental samples.

Ion channels are central in performing many biological processes; they can be found either in external membranes (plasma), or the in the membranes of organelles inside the cell such as lysosomes and mitochondria [2].

The importance of this investigation arises from the fact that all living cells have biological membranes (biomembranes), which define either their boundaries or the boundaries of their constituent organelles. A Biological membrane consists of lipids (mainly phospholipids) and proteins either attached (associated protein) or embedded (integral protein), in addition to some other complexes [4].

Providing a compartment for the cell's constituents is not the only function of the membrane. The plasma cell membrane (exterior) for example, has a potential difference between its interior and exterior sides due to the differing concentrations of various types of ions. This potential difference provides what is called the resting membrane potential which lies in the range (-60mV — -80mV) [5]. In order to maintain this resting potential the biomembrane should

contain controlled pathways within its structure; called ion channels [6]. These ion channels are regulated (controlled) by the cell where the biomembrane is said to be selective [4].

Understanding the mechanism of Lysenin's gating would enrich our knowledge of the functionality of ion channels in living systems and cells. The role of ion channels is not only in controlling their pathways across their biomembranes, although these channels have several other functions. For example, they are responsible for regulating the pH and the size of the cell itself or the organelles inside it; in addition, they are significant for the transport of salt and water. Any failure in their functionality may lead to severe medical consequences. Epilepsy is an ion channel disease which affects the neuromuscular system [2].

1.3 Main Dissertation Problem

My main passion is to understand how cellular transport takes place. In this direction of investigation, the efforts of this research focus on the field of microcarrier drug delivery, with particular emphasis on transport of medications and/or therapeutic material across biomembranes.

This dissertation endeavors to investigate the mechanism of ligand-induced gating of Lysenin as a pore-forming toxin under the influence of multivalent ions, to further explore the potential of this setup for use in biosensing applications, and finally to investigate theoretically the kinetics of these ions and Lysenin channels by modeling the experimental data.

1.4 Dissertation Structure

This dissertation consists of eight chapters. In chapter one, the introduction; it consists of a brief overview of ligand-gating and the significance of this study within this field.

Chapter two is the literature review, where it begins by explaining the importance of the tiny sizes of cells and the transport through biomembranes. The definition of biomembrane and the significance of diversity of its lipid structure, its charge surface and their influence on functionality. Then full description of Lysenin, the protein that has been used in this research, metal ions and the definitions of pH, electrical conductivity.

Chapter three, materials and methods, a full explanation of the required chemicals, lipids and the instrumentation that has been used will be presented and fully explained. In chapter four, results and discussion, the sensing of multivalent ions by Lysenin and the mechanism of Lysenin's gating will be discussed in detail.

Chapter five is the modeling of the dynamic interaction between ions and the binding site of Lysenin. In chapter six the experimental data are fitted by using the suggested mathematical model to estimate the equilibrium rate constant. Chapter seven is the summary of the experimental results and conclusion and finally, Chapter eight, the future work; some projects are proposed that can be conducted by any interested future student or researcher in this field.

Chapter 2 Literature Review

2.1 The Cell and its Membrane

Cells are divided into two types, prokaryotic and eukaryotic. The prokaryotes, such as bacteria, do not have a nucleus, while the eukaryotes such as plants, animals and fungi do [7].

Cells have different shapes and sizes. Bacteria, for example, range in diameter from about 1-5 μm in diameter; while animal cells are about 10-100 μm. Some cellular duties, such as the transport of biomaterials across the cell membrane, are related to the proportion of its surface area to its volume [4]. The surface area effectively represents the amount of cell membrane available for the uptake of nutrients and the excretion of waste [7]. The volume of a spherical shape increases more than its surface area ($V \alpha r^3$, whereas $A \alpha r^2$) and the cell has very small dimensions. The ratio of its surface area to volume is quite large which explains the tiny size of the cell, which enhances the membrane of the cell in performing the cell's duties and puts a constraint on the size of the cell. Its size can increase only as long as the membrane's surface area is adequate to transport biomaterials across it.

One organelle which all cells have in common is the cell membrane (plasma membrane), which defines the cell's boundary and provides it with its distinct compartment. The plasma membrane controls the traffic of biomolecules and ions across it. The membrane of the cell has pathways (channels) which control the quantity and the quality of biomolecules and ions that pass across the membrane. The mechanism of controlling the membrane channels is called gating and selectivity [4]. A schematic of a cross sectional area of an animal cell with some of its constituents is illustrated in Figure 2.1 [7], demonstrating the importance of the biomembrane for the cell as a whole and for its constituents such as the nucleus and mitochondrion.

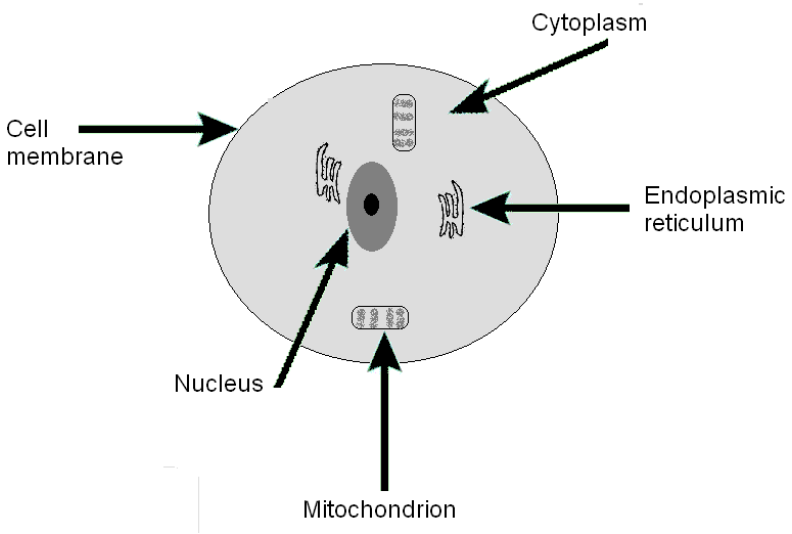

Figure 2.1: Schematic drawing of a cross section of an animal cell showing the cell membrane and the biomembranes of other cell parts.

The plasma membrane and other cellular membranes are composed primarily of two layers of phospholipid molecules (4-5 nm thick) [7]. The two phospholipid layers arrange themselves such that all the hydrophilic ends directed toward the inner and outer membrane surfaces, while the hydrophobic ends are hidden within the interior (see Figure 2.2). In addition to the phospholipid, the cellular membrane has smaller amounts of other lipids, such as cholesterol, and many kinds of proteins, which are inserted into the phospholipid structure [8].

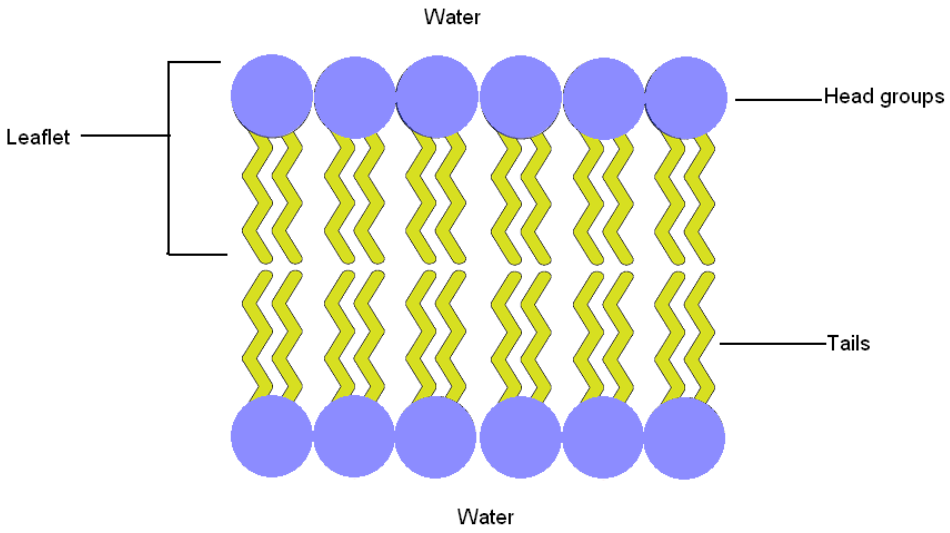

Figure 2.2: Schematic drawing of bilayer lipid membrane (BLM) shows their two leaflets (layers), which consist of hydrophilic headgroups (polar) and the hydrophobic tails (nonpolar) surrounded by water.

2.2 Diversity of Biomembrane Lipid Structure

Biomembranes usually contain different kinds of lipids; more than what is required to form their bilayer. Each lipid species has its own diverse role. Sphingomyelin (SM), a major sphingolipid, is one of the constituents of the plasma membrane of animal cells (in the outer leaflet). Sphingomyelin interacts with cholesterol that found in the membrane and forms what is called lipid rafts [9].

The biological membrane consists of proteins embedded in (integral proteins) or attached to (peripheral proteins) bilayers, which are mainly constructed of lipids. Most membrane lipids and proteins are not simply hydrophilic (water loving) or hydrophobic (afraid of water), but in fact have both hydrophobic and hydrophilic sections. In the presence of water, the hydrophilic polar heads orient themselves to self-assemble at the outer surface of the bilayer lipid membrane and their hydrophobic hydrocarbon tails become hidden inside [10] as illustrated in Figure 2.2.

Because of their amphipathic nature, (hydrophilic and hydrophobic regions within the same structure) lipids are insoluble in water, but are highly soluble in organic solvents such as n-Decane or chloroform [11]. An example of the structure of amphipathic molecule, phosphatidyl ethanolamine (PE or cephalin), is illustrated in Figure 2.3.

The length of the hydrocarbon chains plays an important role in the stability and fluidity of the membrane. The shorter the hydrocarbon tails (chains), the weaker the interaction between them, accordingly, the lipid is less rigid and become fluid, especially at low temperatures. In addition, the kinks in the hydrocarbon tails (double bond between two CH molecules in the chain as shown in Figure 2.3) also increase the fluidity of the membrane because these kinks impede the packing of fatty acids [6].

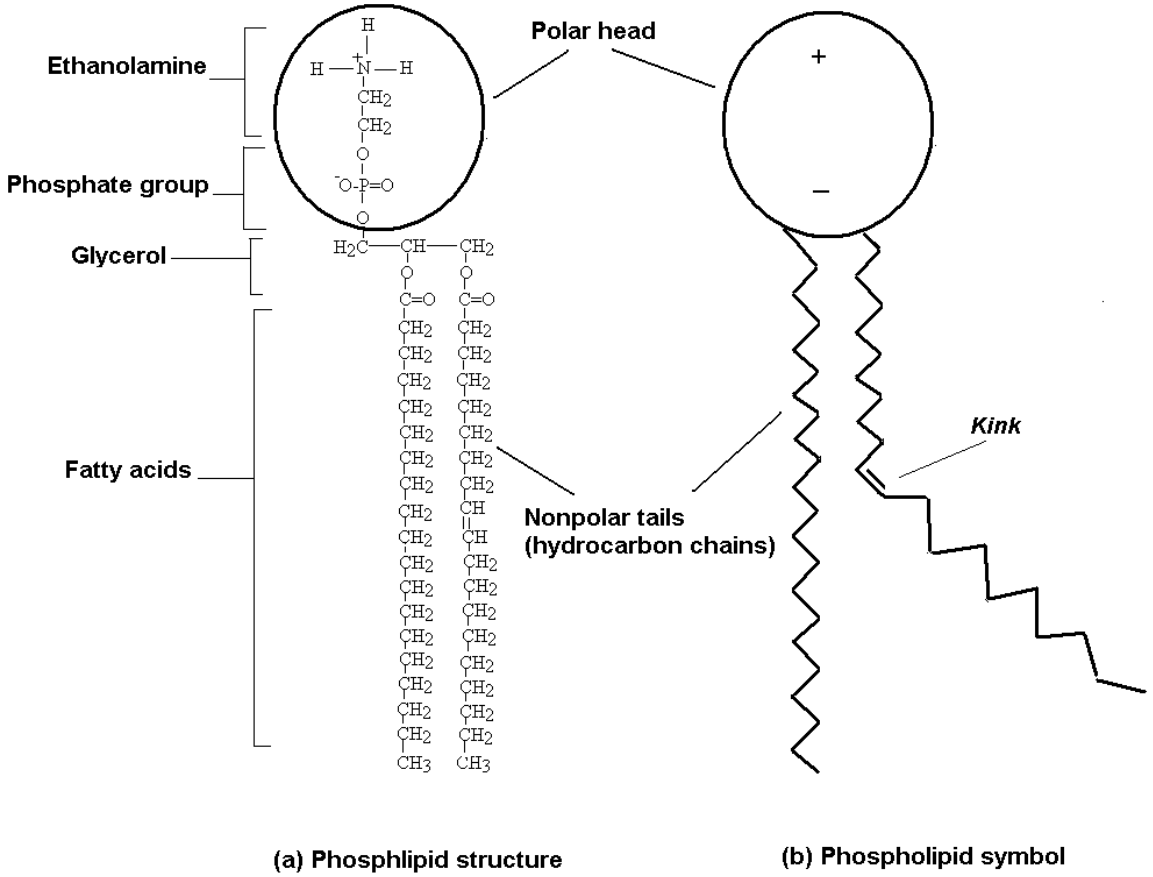

Figure 2.3: The membrane phospholipids and its amphipathic nature. (a) A phospholipid molecule consists of a polar head and two fatty acids (nonpolar tails) attached by a glycerol backbone. PE is an example of the membrane phospholipids, where the polarity of the head results from a positively charged amino group connected to a negatively charged phosphate one. Note that if the 3 hydrogen atoms bonded to the N atom were replaced by 3 methyl groups (CH_3) then we would have Phosphatidylcholine (PC or lecithin). (b) A schematic drawing of this phospholipid molecule (PE or cephalin). Such a molecule is called zwitterion (hybrid ion) because it has both positively and negatively charged groups in its structure [12].

In terms of chemical structure, the six main classes of lipids are fatty acids, composed of a long, unbranched hydrocarbon chain with a carboxyl group at one end, phospholipids such as PE, triacylglycerols (also called triglycerides) which contain a glycerol group attached to three fatty acids, glycolipids, steroids such as cholesterol, and terpens [4, 7].

A cellular membrane is essentially a hydrophobic permeability barrier that consists of phospholipids, glycolipids, cholesterol, and membrane proteins. With the exception of bacteria, the membranes of most cells contain sterols (such as cholesterol). Phospholipids are considered crucial since they are the main lipid constituents of most biological membranes and they have amphipathic nature too. Phospholipids have asymmetrical distribution between the inner and outer leaflet of biomembrane. Sphingomyelin (SM) for example is found in the outer leaflet, while Phosphatidylethanolamine (PE) resides in the inner one [7].

In terms of structure, phosphatidic acid (PA) (two fatty acids and a phosphate group attached to a glycerol), is essential in the synthesis of other phospholipids. The phosphatidylethanolamine (PE), illustrated in Figure 2.3, is just one of the phospholipids that can be synthesized from PA, and if we replaced the ethanolamine in its head with serine, inositol, or choline we would get phosphatidylserine (PS), phosphatidylinositol (PI), and phosphatidylcholine (PC or lecithin) respectively. The latter in particular (PC) is one of the predominant phospholipids in biomembranes, with a large fraction of their surfaces being occupied by phosphocholine groups [13]. Along with these phospholipids (PE, PC, PI, PS), (Phosphatidylglycerol) and diphosphatidylglycerol (Cardiolipin) also count among the most common phospholipids [6].

PE, PC and PS are examples on the zwitterionic lipids, which have both positive and negative charges (polar) on their head groups [12]. The positively charged groups of ethanolamine and choline attached to phosphatidic acid, via phosphate group (negatively charged), and form a polar head groups. Serine group caries both positively and negatively charged and when attached to the phosphate it forms also a polar head group. On the other hand the inositol is neutral and when attached to the negatively charged phosphate group, they form a

negatively charged (PI) lipid. The chemical structures of ethanolamine, choline, serine and inositol are illustrated in Figure 2.4 [7].

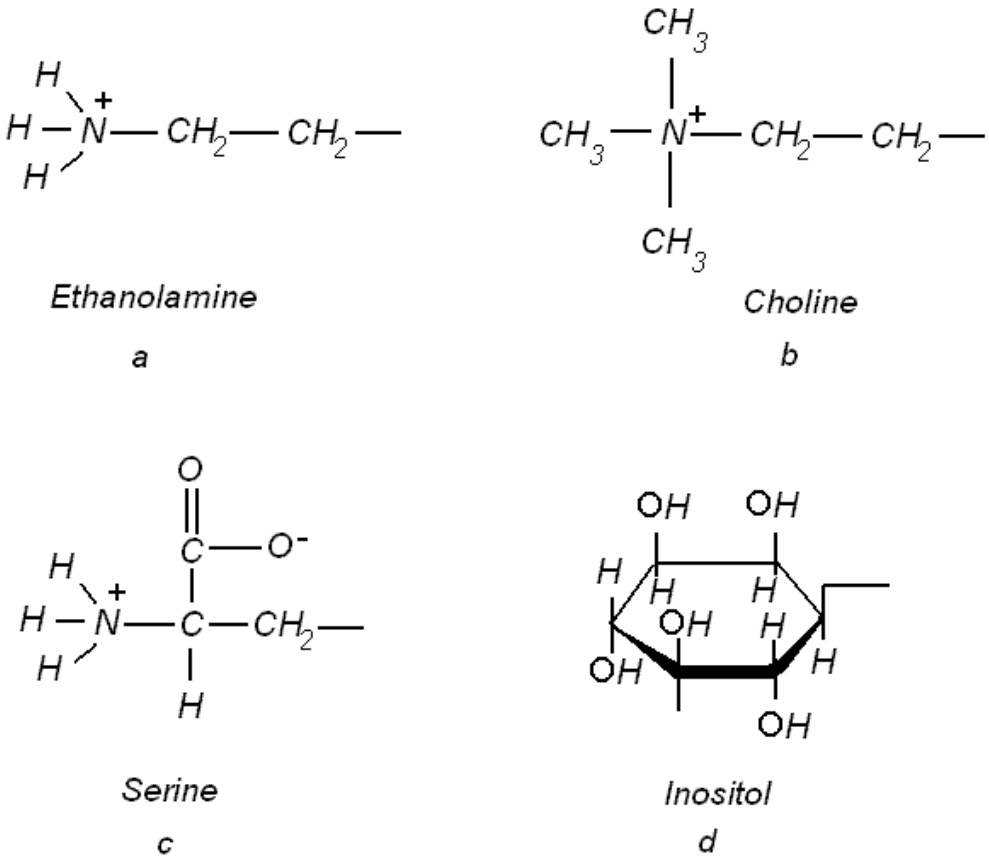

Figure 2.4: Chemical structures of the most common functional groups used with phosphatidic acid to form phosphoglycerides, (a) Ethanolamine and (b) Choline are positively charged (c) Serine is zwitterionic even before attached to phosphatidic acid and (d) Inositol headgroup is neutral.

Based on their chemistry, phospholipids are classified as either phosphoglycerides (as those mentioned above) or sphingolipids. Sphingolipids are also important for their wide use in biomembranes. Sphingomyelin (SM), as mentioned before, is found concentrated in the outer leaflet of the membrane of animal cells [9] with a significant role in both natural and artificial membranes. In fact, without sphingomyelin, it would not be possible for Lysenin to create the

membrane channels that it does. Lysenin was used to detect the presence of the sphingomyelin in the membranes [14].

As a result of interaction between SM and the membranes' cholesterol, lipid rafts are formed. They have a significant role in many cellular functions, such as membrane trafficking and cell signaling. Accordingly the insertion of lysenin channels in any membrane depends significantly on the presence of these lipid rafts [9]. Cholesterol, a steroid, proved critical in this research, both for stable BLM construction and its interaction with sphingomyelin to facilitate Lysenin's channel-forming abilities. The chemical structures of sphingomyelin and cholesterol are illustrated in Figure 2.5 (a) and (b).

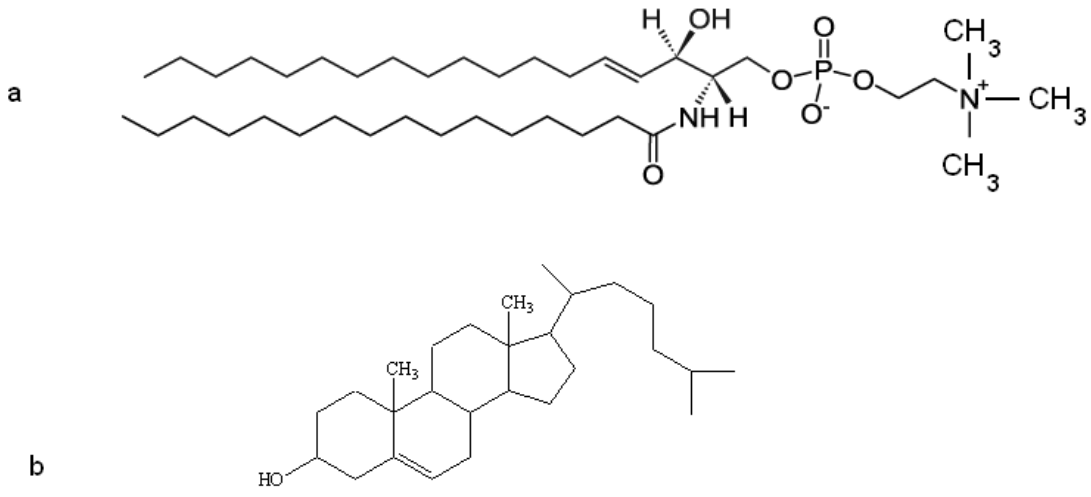

Figure 2.5: (a) The chemical structure of sphingomyelin, which is considered as one of the major constituents of animal cell membranes. It can be found in the myelin sheaths of nerve cells [14]. (b) The chemical structure of cholesterol consists of a four-ringed hydrocarbon linked to a hydrocarbon chain.

Membrane fluidity is affected by the presence of cholesterol in an animal cell, which is about 50% of the total membrane lipid. Cholesterol is usually found in both layers (leaflets) of

the plasma membrane. The cholesterol molecule binds to a neighboring phospholipid molecule, where it can form a hydrogen bond with the oxygen atom that is between the glycerol backbone and the fatty acid of the phospholipid molecule [7]. In this research, the presence of cholesterol molecules in both leaflets of the BLM enhances its stability and facilitates Lysenin's channel-forming abilities. The chemical bond between cholesterol and phospholipid is illustrated in Figure 2.6.

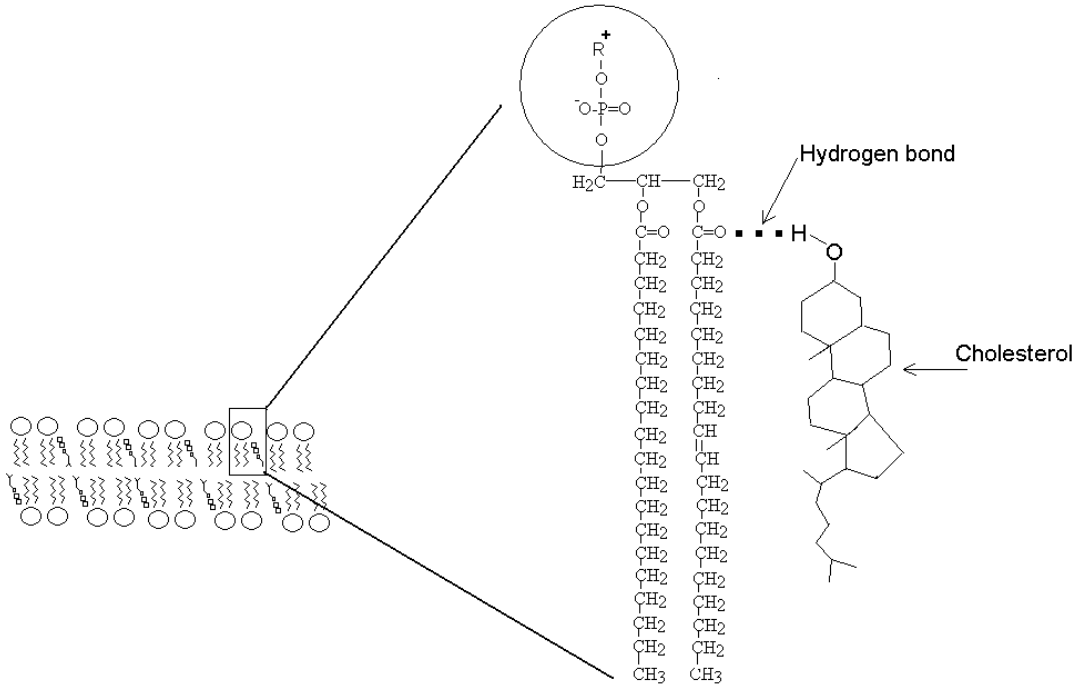

Figure 2.6: Cholesterol molecules in a lipid bilayer. (a) Cholesterol molecules are present in both lipid monolayers of the membrane of animal cells. (b) Cholesterol forms a hydrogen bond (via its hydroxyl group) with the oxygen atom that is between the glycerol backbone and the fatty acid of the phospholipid molecule. A mixture of lipids and cholesterol was used in this study in preparing the artificial bilayer lipid membrane (BLM) to provide stability and facilitate the pore formation of Lysenin.

2.3 Lipid Bilayer Surface Charge

For a better understanding of the influence of ions on Lysenin function, charged lipids were investigated in this research. Charged lipids were provided by using Asolectin (see chapter 3). The charge of Asolectin is due to the lipid's composition since it is composed of roughly equal portions of phosphatidylcholine (PC), phosphatidylethanolamine (PE) and phosphatidylinositol (PI) [15]. There is no net charge carried by the head groups of the zwitterionic lipids either (PE) or (PC), and the (PI) component is negatively charged as illustrated in Figure 2.4. The charge of the head group of the zwitterion can be affected by the pH of the solution surrounding it [16], therefore the charge of Asolectin, that is on (PI) was kept constant (during the conducted experiments in this study) by using HEPES/KOH buffer (i.e. maintain a neutral pH).

2.4 Transport across Biomembranes

Cell membranes (as defined previously) are composed of two layers of lipid molecules and are therefore relatively impermeable to ions. The cell membrane is crucial because it separates the interior and the exterior of the cell, such that it keeps them at different concentrations and compositions [17]. The movement of a neutral molecule is regulated by the concentration gradient of that molecule across the membrane (diffusion); on the other hand, the movement of an ion is controlled by its electrochemical potential (gradient) which is the concentration gradient in addition to the charge gradient of the ion across the membrane.

Most cells have a negative membrane potential, which means the outside is at higher potential than the inside of the membrane [7]. Although, potassium ions are more concentrated inside the cell (~150mM inside to ~4mM outside), there is an excess of negative charges inside it because of the other negatively charged species such as proteins and RNA [18]. On the other hand, the exterior side of the membrane is at a higher potential because of the higher concentration of sodium ions (~140mM outside to ~5mM inside). Additionally, other cations (such as Ca^{2+}) are found outside the cell membrane, which participate in causing the outer surface of the membrane to be at a higher potential.

The transport of materials and ions across the cell membrane, or between different intracellular compartments, is mediated by membrane proteins called ion channels. They are mainly responsible for the transport of specific ions such as potassium (K^+), sodium (Na^+), calcium (Ca^+) hydrogen (H^+) and chlorine (Cl^-) [17]. Ion channels regulate the amount and concentrations of hormones and they control the body electrolyte and volume homeostasis [19]. The significance of these membrane proteins arises from its relation with several diseases. Malfunctioning of ion channels may lead to many various human diseases such as cystic fibrosis or epilepsy [17]. The ability to control the gating of these cellular transporters may open a new window for drug delivery applications.

Among different types of ion channels, Na^+, K^+, Ca^+, and Cl^- are considered the most common examples. The gating mechanism is one significant characteristic of an ion channel. The gating process changes the status of the channel from an open (activation) to a close (inactivation) state or vice versa. Ion channels also exhibit selectivity, which enables them to control the quality of biomolecules that passes through the membrane [20]. The most important characteristic of ion channels is the selectivity, where they have the ability to distinguish

between ions and other species [21]. It gives ion channels that impressive property of not only controlling the traffic of ions but also determining the kind of required ions (selectivity filter) that are allowed to enter or leave the cell through the membrane.

2.5 Metal Ions

2.5.1 Importance and Characteristics of Metal Ions

Metal ions could be used as a tool to investigate biological mechanisms or structures. Their availability, simplicity and well-defined structures make them a powerful tool in many scientific investigations, especially in biological applications [22]. One of the reasons to use metal ions in this research is their potential toxicological effect at higher concentrations in biological media and their strong relevant and association with different biological functions. Their ability to be used as tools to analyze the structure and function of ion channels is another significant reason to use them in order to address the problem of mechanism of gating of Lysenin as a pore-forming toxin.

Metals cover more than 77% of the elements in the periodic table. The alkali and the alkaline earth metals, which are groups 1 and 2 respectively, (Figure 2.7) are considered very reactive elements [23]. Elements 21 (Scandium) through 30 (Zinc) and 39 (Yittrium) through 48 (Cadmium) are the first two rows of the block known collectively as the transition metals. Elements 58 (Cerium) through 71 (Lutetium) are called the lanthanides. Correspondingly, another 14-elements series starting from element 90 (Thorium) to element 103 (Lawrencium) is called actinides [12].

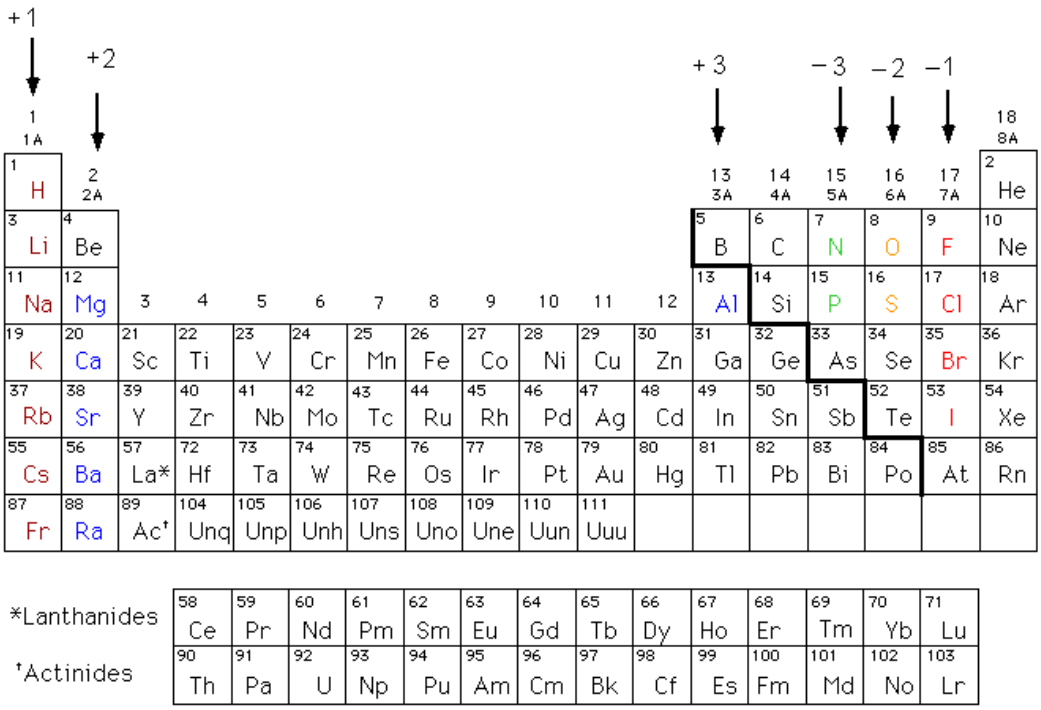

Figure 2.7: The periodic table of the elements, showing bulk metals such as Na, trace metals such as Mn, toxic metals such as Pb and beneficial metals like Cr. All elements located to the left of the black bold zigzag line are called metals [24].

Metal ions have various ionic sizes (relative to their parents) and the size of each ion depends on its charge number. Cations, for example are smaller than their parents, while anions, on the other hand, are larger [12]. The biological classification and the ionic and hydrated radii of the metal ions in this research are shown along with their electron shell configuration in Appendix A.

2.5.2 Metal Ions and Biological Interactions

Although metal ions might be used for treating some diseases, such as using Mg^{2+} for the treatment of intestinal disorders and Fe^{2+} for anemia [25], they may threaten human health when

they enter our food chain or water supplies. Some soluble metal ions such as Fe^{2+} and Mn^{2+} are toxic to plants at high levels [26].

Since metal ions are positively charged, then they look to share electron pairs with other atoms to achieve a bond or charge-charge interaction. Metal ions have large ionic sizes and their charges are greater than one. Accordingly, they have the ability to bind to many ligands around them [27] and could serve to maintain the enzyme molecule in the structure needed for biological activity.

The treatment of complicated neurological diseases such as Alzheimer's or Parkinson's could be improved by understanding the mechanism of metal ion interactions with the central nervous system. Many other diseases such as tuberculosis could be treated by using Lanthanides [22]. Some essential metals and medical consequences resulting from their deficiency in our bodies are shown in Table 1 below [29].

Table 1: The deficiency of some ions in humans and their corresponding diseases

Metal ion	Related disease
Iron deficiency	pernicious anemia
Insufficient dietary zinc	growth retardation, skin changes
Copper deficiency	brain disease, anemia, heart disease
Excess of mercury and lead	toxicity in humans
Calcium deficiency	bone deterioration
Cobalt deficiency	anemia
Excess of manganese	symptoms similar to Parkinson's disease
Chronic exposure to cadmium & lead	neurological, and kidney toxicity

The following ions were used in this research: Na^{+}, K^{+}, Ca^{2+}, Mg^{2+}, Co^{2+}, Mn^{2+}, Zn^{2+}, Ni^{2+}, $Fe^{2,\ 3+}$, Cd^{2+}, Al^{3+}, La^{3+}, Ce^{3+}, Eu^{3+}, and Tb^{3+}. In addition, some non-metal ions such as SPD^{3+} and SPM^{4+} were used as well.

2.5.3 Chelation of Metal Ions

The chelation is an interaction process between metal ions and other compounds called chelating agents (ligands), resulting in binding these metal ion to a central atom in the ligand. Some ligands bind to one metal ion, and accordingly they are called monodentate. On the other hand, polydentate (multidentate) is a ligand that has the ability to bind with a metal ion through several atoms, holding it like a claw. When a chelating agent binds to a metal ion, it holds it tightly, such that it is prevented from reacting with other species in the solution [12]. The Ethylenediaminetetraacetate ion (EDTA) is a common example of the polydentate ligands [28].

Chelating agents may have different functional groups in which they provide the required electrons that are essential in binding with metal ions. Additionally, a precipitator could be used as an alternative to chelation to inhibit metal ion interaction in solution. Potassium phosphate was used in this research to precipitate aluminum and copper ions. Carboxylate, Phenoxide and Phosphate are some of the common functional groups [26]. The chemical structures of these groups along with EDTA and EGTA are explained in Appendix B.

Most proteins are able to bind to metal ions, so metal proteins are significant in biological studies and applications [29]. It was crucial for this research to examine the stability of Lysenin channels in the BLM during their dynamic interaction with multivalent ions. Checking the stability of Lysenin channels would be essential in this study because it determines whether these channels were functioning reversibly (closed to open state) or were simply removed from the BLM. Chelating agents played a crucial role in the investigations in this direction.

Along with EDTA and EGTA as chelating agents for most metal ions, potassium phosphate (KH_2PO_4) was used as a precipitator in some experiments in this research to precipitate aluminum and copper ions from the bulk solution.

2.5.4 Influence of Metal Ions on Gating

Metal ions modify the gating of ion channels or block the pathway of these ion channels. For voltage-gated channels (such as sodium channel), metal ions interact with the voltage domain sensor causing that modification [30]. On the other hand, channels that gate in response to external stimuli such as K^+ metal ions are considered ligand-gated channels (such as potassium channel) [31].

The mechanism of gating is governed by the interaction between metal ions and protein channels. Some mechanisms assume that metal ions screen the voltage domain sensor of the voltage-gated channel, while other mechanisms propose a dynamic charge-charge interaction between metal ions and the protein's voltage domain sensor [22].

The investigation of this study considered the effect of metal ions on the conductance of a Lysenin channel, which is different from ion channel (see sec.2.7.1) in that Lysenin channels lack selectivity. According to the experimental results (chapter 4), a pore-blocking mechanism is consistent with all observations and findings. As a result, the experimental data was compared with a proposed model that assumes a dynamic equilibrium between a charged site on the protein and ions passing through the pore. The model also assumes competition between different ions for occupation of the site. However, it is also possible that neutralization of the charge at the protein site may cause a conformational change that also plays a role in reducing ion transport.

2.6 pH, Buffer and Electrical Conductivity

2.6.1 Acidity and Basicity of Solutions

Acid and base quantities must be in equilibrium in the human body so that it maintains a neutral pH. In solutions such as those found inside or outside body cells, acids dissociate into hydrogen ions (H^+) and anions. Bases, on the other hand, dissociate into hydroxide ions (OH^-) and cations. Any big changes of the normal H^+ and OH^- concentrations may greatly modify cell functions and disrupt homeostasis [32]. In our bodies, hydrolysis of CO_2 produces a weak acid that plays a major role in maintaining the acid-base balance necessary to assure normal functioning [12]. Because of that it is very important to keep the balance of acids and bases in our bodies.

The pH of a solution describes the hydrogen ion concentration $[H^+]$ in it. The Danish biochemist Soren Sorenson (1868-1939) proposed a scale for expressing acidity and basicity based on the concentration of Hydrogen ions [12]. This pH scale (0 to 14) was built based on the mathematical formula which defines the pH as the negative logarithm to the base 10 of $[H^+]$, that is $pH= -\log[H^+]$. For instance, a pH=0 represents 1M concentration of Hydrochloric acid (HCl), and pH=14 represents 10^{-14} M concentration of sodium hydroxide (NaOH). The pH values of some common substances are given in Table 2 [10, 12].

Table 2: pH values of some common substances

Substance	pH	Acidity and basicity
Hydrochloric acid (HCl)	0	More acidic (lower pH)
Stomach acid	1.5-2.0	
Lemon	2.3	
Beer, vinegar	2-3	
Oranges	3.5	
Tomatoes	4.5	
Black coffee	5	
Urine	6	
Saliva	6.5	
Distilled water	7	Neutral
Human Blood	7.4	
Sea water	8.2	
Baking soda	8.3	
Household ammonia	11.7	
Bicarbonate of soda	12	
Oven cleaner	13	
Sodium hydroxide (NaOH)	14	More basic (higher pH)

It was found that highly charged metal cations (such as Al^{3+}) are acidic. Therefore, when salts containing these ions dissolve in water, the pH of the solution is affected. In fact, when they dissolve in water, metal ions behave like Lewis acids. According to the Lewis acid-base definition, a base is a substance that provides an electron pair, and an acid is a substance that receives an electron pair [23].

2.6.2 Buffer

Buffers may be defined as salts of weak acids or bases which maintain a constant hydrogen ion concentration in the solution. Buffers are significant because most functions of biological organisms critically depend on the pH [33]. On the other hand, not all types of buffers fit with every experimental requirement. In this research, it was very critical to choose a buffer with relatively weak binding of metal ions, so HEPES/KOH buffer was chosen. It keeps a neutral pH of either KCl, or NaCl electrolyte solutions. Further information about HEPES/KOH buffer can be found in Appendix B.

2.6.3 Electrical Conductivity of Electrolyte Solutions

The electrolyte solutions of either sodium chloride (NaCl) or potassium chloride (KCl) dissociate in water and increase its electrical conductivity according to their concentrations. An electrolyte is classified as weak or strong, based on whether its solution is a poor or good conductor of electricity. With water as the solvent, some examples of weak electrolytes are NH_3 and CO_2, while NaCl and KCl are considered strong electrolytes [34]. A crystal of NaCl, for instance, consists of positive and negative ions, and when it dissolves in water, the ions break off from the crystal and go into solution as hydrated ions. Upon its motion, the ion becomes hydrated, that is, surrounded by a number of water molecules (hydration number) that form a sphere of hydration [12]. The hydration number is different from the coordination number [34], which can be defined as the average number of water molecules that are the closest neighbors of

the ion [28]. The values of the hydration numbers (n_h) of some ions, which have been used in this study are listed in Table 3 below [12, 34].

Table 3: The hydration numbers of some ions

Ion	Na^+	K^+	Cl^-	Mg^{2+}
$\mathbf{n_h}$	6	3	6	12

Within a sphere of hydration; the water molecules closest to an ion are oriented so that their oxygen atoms are directed toward a cation such as sodium cation in Figure 2.8-a.

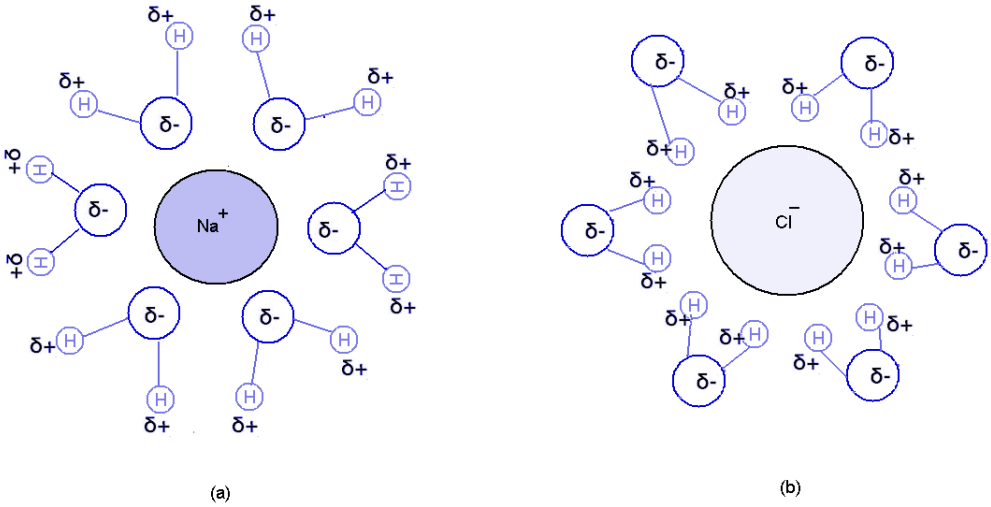

Figure 2.8: The ions are hydrated (surrounded by six water molecules). (a) The negatively charged oxygen atoms of the water molecules' dipoles are attracted by the positively charged sodium ion. (b) The positively charged hydrogen atoms in the water molecules' dipoles are attracted by the negatively charged chloride ion.

The electrolyte solution used in the experiments of this investigation was mixed with the buffer, which does not affect the conductivity of the electrolyte itself. The conductivity of potassium chloride, with and without HEPES/KOH (buffer), is measured and shown in Figure 2.9.

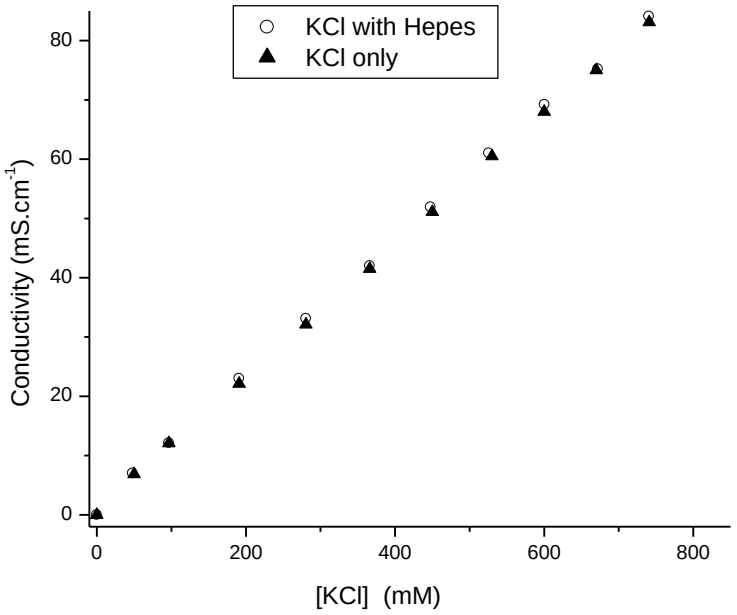

Figure 2.9: The conductivity of potassium chloride without buffer and mixed with 20mM buffer in the range of 0 to 800 mM KCl. The buffer does not change the conductivity of potassium chloride ions in the electrolyte.

Although the conductance "G" is just a constant multiplied by the conductivity "k" (see Appendix C) in the study of ionic channels, the electrical conductivity is related to the solution, while conductance is associated with the ionic channel or the pathway of ions through the membrane [19, 35]. For example, Lysenin as mentioned before creates pores or channels through the membrane. Accordingly these Lysenin channels would have conductance as a physical property, while the conductivity is the physical property of electrolyte solution surrounding these channels. Conductance, conductivity and electrochemical reactions in electrolytes and between electrodes and electrolytes are clarified in Appendix C.

2.7 Lysenin: A Pore-Forming Protein

2.7.1 Ion Channels versus Lysenin

There are many limitations in using transmembrane proteins, like ion channels, in experimental investigations. They may lose their functionality as they leave their original environment in the cell membrane. In addition, it is not an easy process to reconstitute these ion channels again in an artificial membrane and it is difficult to distinguish between different types of ion channels when using the patch clamp approach. An important and unique characteristic of ion channel is the selectivity, which enables the ion channel to allow one subset of ions (anions or cations) to pass through its pathway [36].

An interesting model for studying ion transport proteins is provided by pore-forming proteins (Lysenin channels), which are unusual in that they function in lipid bilayers and also exist stably in the aqueous phase. Lysenin, a self-inserted protein, makes a large pore in a membrane that contains sphingomyelin causing a malfunction of the cell's electrochemical gradient leading to cell death [37]. The major difference between Lysenin channels and ion channels is the selectivity. Unlike ion channels, Lysenin channels allow both subsets of ions (anions or cations) to flow through their pathways [38]. Their functionality feature makes it possible to produce pore-forming proteins as recombinant proteins, which can subsequently be used to reconstitute functional pores in artificial membranes.

Lysenin, a pore-forming protein that consists of 297 amino acids, (33kDa as a monomer [39]), extracted from the earth worm *E. fetida,* is water-soluble and interacts with cell membranes containing sphingomyelin to form large conductance pathways (the entrance of the

pore 3 nm to 5.7 nm in diameter [40, 41]). In fact, Lysenin was used to detect the presence of sphingomyelin in membranes [40].

It is known that if most of the amino acids in a protein were hydrophobic, the protein would be virtually insoluble in water and would be found instead in a nonpolar environment [7]. This means that most of the amino acids of Lysenin are hydrophilic. Since any hydrophilic amino acid is polar, due to the charge on its R group [12] (see Figure 2.10), then Lysenin has the capability to electrostatically interact with other charged molecules or ions.

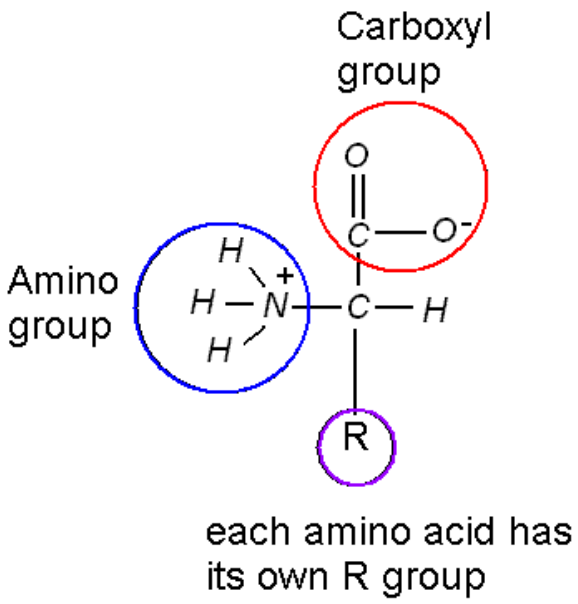

Figure 2.10: The amino acid is a molecule that has a central carbon atom attached to one hydrogen atom and to three different groups (amino, carboxyl and R group), the R group defines the amino acid.

As it provides an excellent method to investigate the structure-function of biomembranes, a planar lipid bilayer (BLM) has been used along with Lysenin in order to investigate the

formation of Lysenin's pores and its gating. The insertion of Lysenin's stable channels in an artificial bilayer lipid membrane containing sphingomyelin is illustrated in Figure 2.11-a.

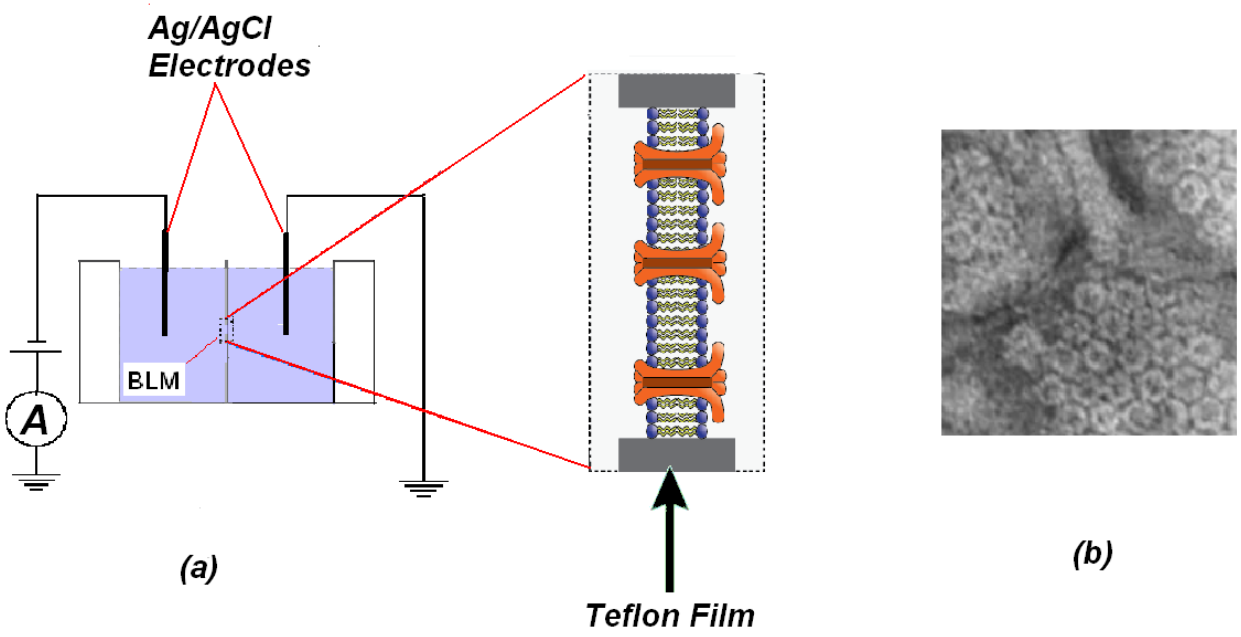

Figure 2.11: (a) Schematic shows three Lysenin channels inserted in artificial bilayer lipid membrane containing sphingomyelin immersed in an aqueous solution (KCl or NaCl), (b) Electron microscopy shows that Lysenin produced a honeycomb structure (pores) in sphingomyelin-containing membranes [9]

2.7.2 The Structure of Lysenin

Revealing the structure of a protein is crucial in understanding and explaining its functionality and its interaction with the lipid membrane or other kinds of proteins. Lysenin, as explained in the previous sections, requires sphingomyelin to interact and make pores in the membrane. Investigating the structure of Lysenin bound to SM is crucial to this research because it enhances our understanding to better propose mechanisms either for insertion in the BLM or for gating.

The mechanism of Lysenin's pore-forming in the BLM is yet to be known. One of the suggested mechanisms is that the Lysenin protein units assemble themselves on the surface of the BLM then they insert and make the pore [41].

Defining the structure of Lysenin is still under investigation. Since it expands our understanding of the influence of the protein's charge on its activity in the membrane (functionality), determining the charged amino acids among its structure is of great interest to this research. The investigation of Lysenin's structure will lead to better understanding of both protein-lipid interaction and protein-protein interaction. A newly published structure of Lysenin [41] shows that Lysenin has N-terminal domain that is divided into two subdomains and the C-terminal domain. This structural investigation uncovered the interaction between one of the hydrophobic tails of sphingomyelin and two tyrosine molecules on one side of Lysenin. It was surmised that the opposite side of the protein should therefore be along the inner lumen of an assembled channel. The electrostatic surface representation revealed an area of negative charge located in the suspected inner channel wall region (two adjacent glutamate amino acids), which

was hypothesized to be responsible for the interaction with positive ions [42]. The structure of Lysenin is illustrated in Figure 2.12.

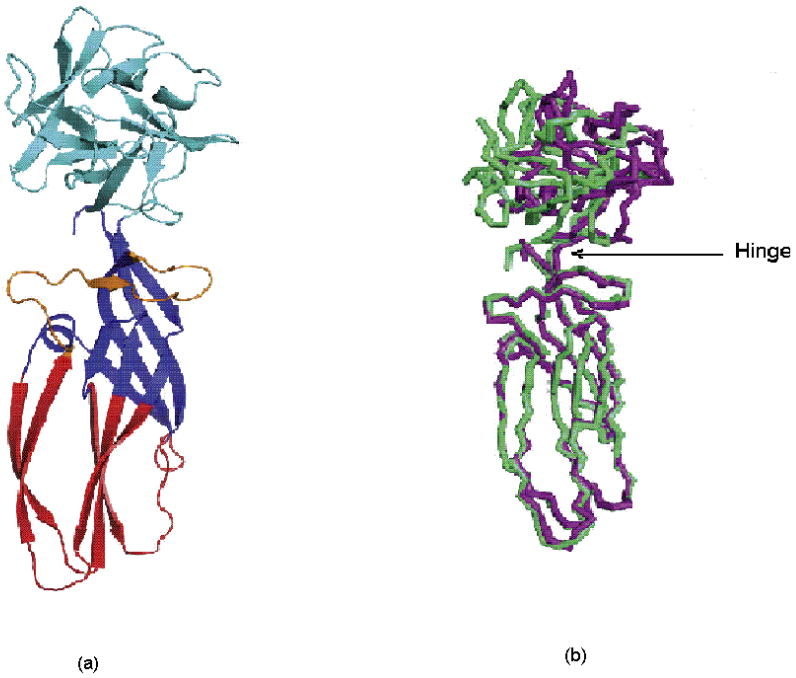

Figure 2.12: A spiral-and-ribbon model of Lysenin crystal structure showing (a) its two domains: the first one is the N-terminal (red and blue) which is the part of the protein that is inserted inside the membrane, and the second domain is the C-terminal one (cyan) which is the head of the Lysenin protein. (b) The hinge is located at the boundary between the head (C-terminal) and the body of Lysenin (N-terminal), and has a freedom to move about 45^0 [41].

2.7.3 Interaction of Lysenin with Lipids

Lysenin contains charged amino acids [43] and analysis of its surface charge shows the accumulation of positive charges at its head side (C-terminal) [41] as shown in Figure 2.13 (dark blue color). This indicates that the head group of Lysenin (C terminus) electrostatically interacts and binds with the phosphocholine group of sphingomyelin, or from phosphocholine lipids.

Accordingly, the initiation of the insertion of Lysenin in a membrane containing SM is governed by charge-charge interaction [44].

Lysenin's hinged region plays a role enabling the remainder of its structure (N-terminal domain) to bind with sphingomyelin and insert into the membrane (see Figure 2.13). This insertion into the BLM creates a pore with either a hexamer assembly (six proteins are required to form a single pore), or a trimeric assembly (three proteins per pore), which leads to different measurements of the diameter of the mouth of the pore (3 nm-5.7 nm) [9, 40, 41]. These measurements of the pore size do not mean that the channel has a cylindrical shape with the same diameter along its inner lumen of the assembled channel. For example, most ion channels, such as the potassium channel, have a larger diameter at the entrance of the channel (mouth) than along the interior [19, 30, 31].

As explained in sec.2.7.2, the location within the structure of Lysenin that is responsible for the interaction with positive ions was proposed to be inside the channel lumen. Accordingly, it was hypothesized that the two glutamate amino acids are facing the interior of the pore, and hence are responsible for the electrostatic interaction between ions and Lysenin (see Figure 2.13). This hypothesis proposes a preferred mechanism of ligand-induced gating of Lysenin.

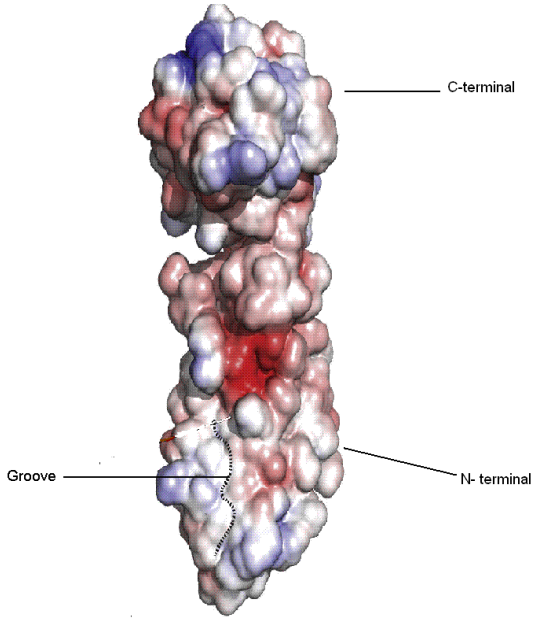

Figure 2.13: Electrostatic surface representation of Lysenin shows the positively charged regions (blue) at the C-terminus and the negatively charged ones at the N-terminus (red). One of the fatty acid tails of the SM binds with Lysenin along a groove on the surface [41].

2.7.4 Voltage Gating, Ligand Gating and Modulation of Channels

Lysenin channels lack the selectivity as a distinct character of ion channels, while they show voltage-induced gating and activity modulation by ionic strength and pH, indicating that electrostatic interactions play a major role in establishing their electrical activity. Previous studies of Lysenin's voltage gating [1] observed that Lysenin channels (which was formed in a BLM that was made of asolectin) closed their pathways when a positive voltage across the membrane was held, but did not notice any voltage dependence. Instead, our investigations (see chapter 4) proved that Lysenin channels are voltage dependent and respond to changes in the positive voltages across the asolectin bilayer lipid membrane in which they are imbedded [45].

Voltage gating as a distinct characteristic of Lysenin was one of the main reasons to investigate the ligand gating for such a protein under the influence of metal and nonmetal ions.

The mechanism of the gating of ion channels could be modulated by monovalent or divalent cations such as H^+ and Ca^{2+} [19]. The ligand binds to the protein's binding site and as a result, it might gate its pore by directly limiting transport without significant protein conformational change or by driving the protein to undergo conformational changes (rearrangement of the tertiary structure) [21] as illustrated in Figure 2.14 (a) and (b) respectively.

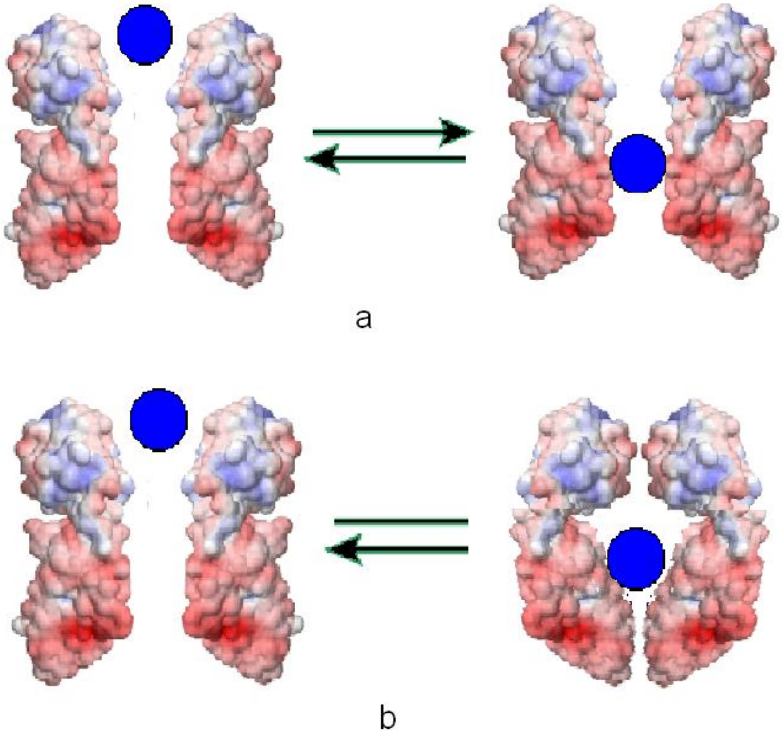

Figure 2.14: Two mechanisms of ligand gating: (a) a ligand interacts with the protein's binding site, and then the pathway of the channel is blocked by the ligand (pore-blocking mechanism), (b) a ligand binds to the binding site causing conformational changes leading to pore blocking.

Chapter 3 Materials and Methods

3.1 Materials

For all experiments, the following materials were used: chemicals, Teflon chamber, and a measurement device. Chemicals were essential to prepare the lipids used in constructing the bilayer lipid membranes (BLM) within the two-compartment Teflon chamber, and the Molecular measurement device (Axopatch 200B amplifier and the DigiData 1440A digitizer) was used to record the electrical signals across the BLM.

3.1.1 Chemicals

Asolectin (Aso) from soybean, Lysenin, Sphingomyelin (SM) and Cholesterol (Chol) were purchased from Sigma-Aldrich. Other chemicals were purchased commercially and used without further purification.

The lipids were dissolved using n-decane, and deionized water was used for dissolving all salts and multivalent ions that came in powder form. HEPES/KOH buffer was added to sodium chloride and potassium chloride solutions due to its solubility, stability, minimum complexation with metal ions [46], and to keep the pH of the solution around physiological conditions (pH 7). A stock solution of approximately 30 µM of Lysenin was prepared by dissolving 50 µg of Lysenin in 50 µl of solution (50% of 60 mM KCl and 50% Glycerol) buffered with 20 mM HEPES/KOH to maintain a neutral pH.

The bulk solution (NaCl, or KCl) was used as a supporting electrolyte to observe the bilayer formation and Lysenin insertion, and to measure the conductance before and after adding the multivalent ions. All tested multivalent metal ions were in chloride form.

3.1.2 Teflon chamber

The chamber consisted of two compartments with a volume of 1.6 ml each and a thin Teflon film placed vertically between the two compartments. A single aperture of diameter of 70 μm to 100 μm was made in the middle of the Teflon film. The voltage was applied across the film (and across the BLM) via two Ag/AgCl electrodes which were used to apply the required voltage and to record the subsequent electrical current.

3.1.3 Measurement devices

The silver-silver chloride electrodes were placed across an artificial planar bilayer lipid membrane (BLM). One electrode was placed in one compartment and grounded, and the other was connected to a head stage and placed in the other compartment as Figure 3.1 depicts. Since the recorded current was on the order of picoamperes, the entire set-up was electrostatically isolated inside a Faraday cage to minimize external electrical noise.

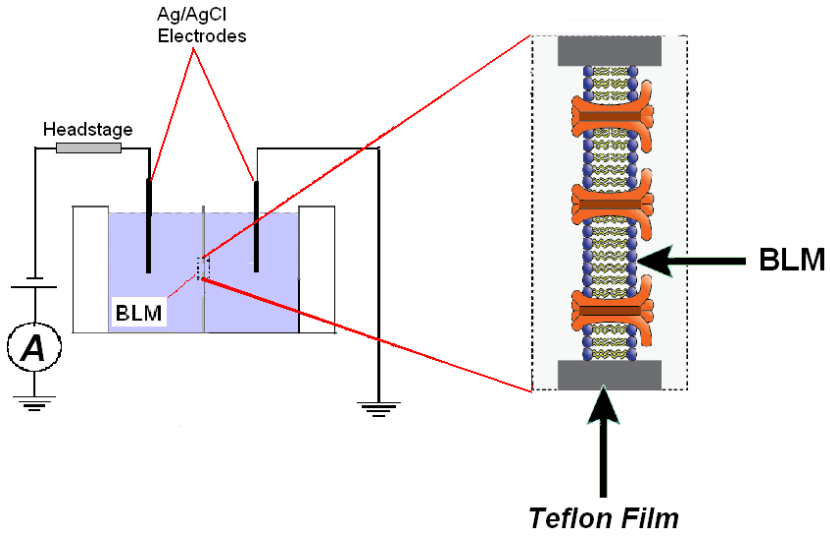

Figure 3.1: Three Lysenin channels inserted into a constructed BLM. The electric current through these channels was recorded by using two Ag/AgCl electrodes placed across the BLM in the chamber that contained an aqueous electrolyte.

3.2 Methods

A full explanation of the artificial bilayer lipid membrane (BLM) formation, insertion of Lysenin protein into the BLM, and the method of conductance measurements before and after adding multivalent metal ions will be provided in this section.

3.2.1 Planar BLM Formation

The painting technique [47] was used to construct a planar bilayer lipid membrane. To form a BLM using the painting method, lipids were dissolved in an organic solvent (n-decane) and then spread over an aperture punctured in the Teflon sheet [48, 49]. The Teflon sheet was mounted vertically between two compartments which were filled with electrolyte solution.

The negatively charged mixture of lipids used in all experiments consisted of 10 mg Asolectin, 5 mg Cholesterol and 5 mg Sphingomyelin dissolved in 400 μl of n-decane.

The diameter of the aperture was about 70-100 μm punctured in the middle of a Teflon sheet (3 cm x 1.7 cm), which separated two reservoirs or compartments, each filled with 1.0 ml of buffered electrolyte (150 mM KCl, 20 mM HEPES/KOH buffer, pH 7).

The solutions in each compartment were continuously stirred with two small bar magnetic stirrers, which were part of the stirrer system spin-2 controller (Warner Instruments). The ionic current was recorded by immersing the two Ag/AgCl electrodes in these compartments. The two electrodes were connected to an amplifier device (Molecular Device called Axopatch 200B), which was then connected to a digitizer (Molecular Device called DigiData 1440A). For data analysis P.Clamp 10.2(Molecular Device) and Origin (OriginLab) were used.

Forming a stable BLM required a capacitive current of about 60-90 pA. These values were estimated because the measured value of the BLM capacitance is approximately $1\mu F/cm^2$, and the formation BLM area, in the conducted experiments in this research, lies between $(0.6\text{-}0.9)x10^{-4}$ cm^2 then the expected capacitive current would be between 60 pA to 90 pA. More details and explanations of BLM capacitance can be found in Appendix E. A recorded capacitive current of a stable BLM is displayed in Figure 3.2 where the capacitive current is about 70 pA.

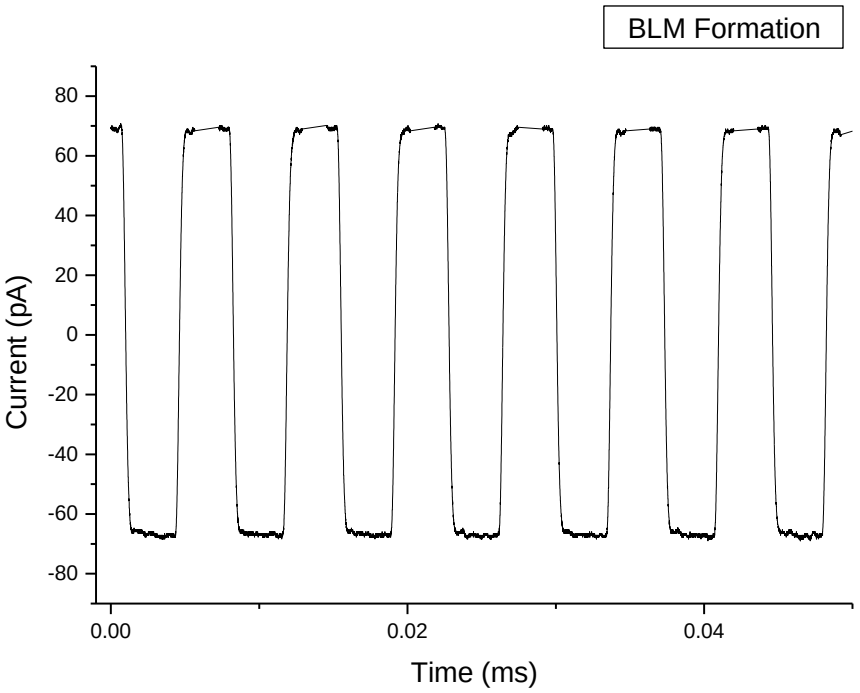

Figure 3.2: Current versus time graph illustrates a recorded capacitive current in picoamperes (70 pA), evidence of stable BLM formation across the punctured aperture in the Teflon sheet.

3.2.2 Insertion of Lysenin into BLM

An external transmembrane voltage of –80 mV was applied across the formed bilayer lipid membrane. The head stage compartment was at negative voltage while the other compartment was grounded. Lysenin was added to the grounded compartment in minor amounts (0.6-1.5 μl of 0.3 μM), and the solution was stirred by the magnetic stirrer to enhance the Lysenin-lipid interaction. Lysenin started to insert channels in the BLM after approximately 4 minutes. Although the insertion of Lysenin channels seemed to be fast process, the entire process of reaching the maximum number of inserted channels was slow. The insertion of Lysenin

depended on the concentration of protein in the solution; therefore, it might take minutes or even hours. According to the increase in the recorded ionic current, which was in discrete steps, the step-current represented the ionic current passing through that channel. The current per channel was approximately -48 pA (at -80 mV) as Figure 3.3 depicts, while the current through the aperture (without the membrane) exceeded 10^6 pA at about 4 mV applied voltage.

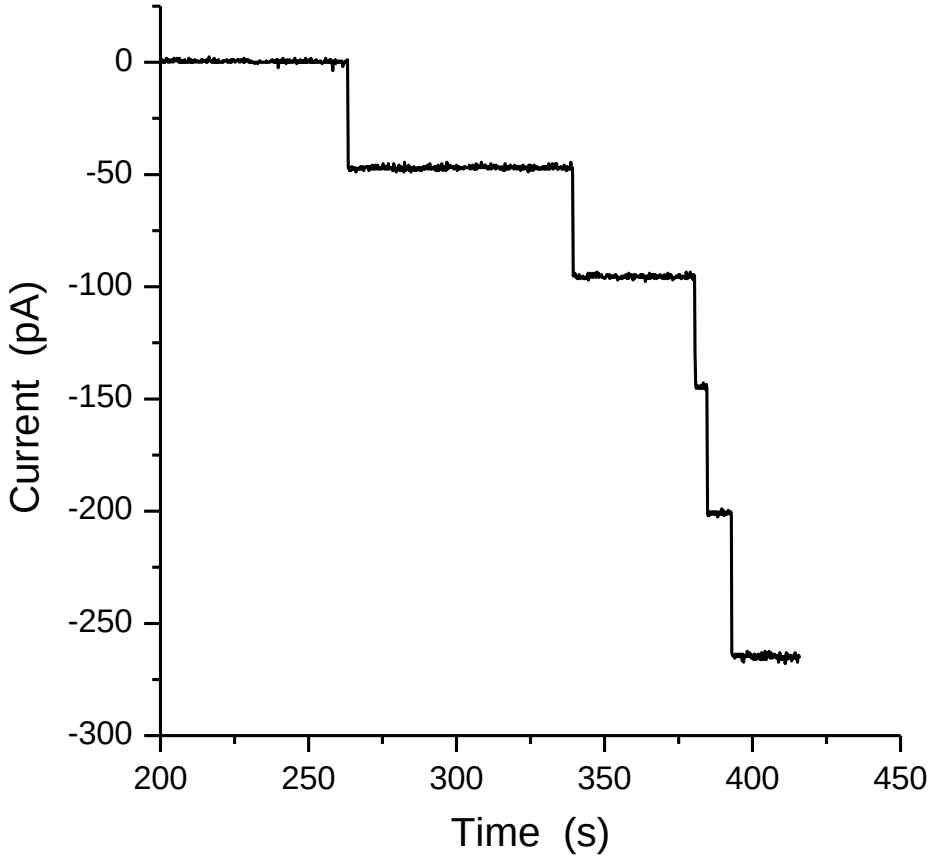

Figure 3.3: The insertion process of Lysenin channels into BLM. The current per channel was approximately –48 pA when the biased voltage across the membrane was –80 mV. The value of the current per channel is important because it enables us to estimate the total number of channels.

The kinetic process of Lysenin insertion into the BLM required waiting about an hour to reach a state of equilibrium, which was observed by optimization of the macroscopic ionic

current through the BLM (open current). The kinetic process and the equilibrium state of Lysenin insertion into the BLM are illustrated in Figure 3.4. It took more than 25 minutes to reach a steady state of open current (the current through all pores).

The approximate number of all inserted channels in the BLM was estimated by dividing the value of the open current by its value per channel. According to Figure 3.4 the estimated number of channels in the BLM is about 300 channels (that is the total current through all pores divided by the current per pore).

The data recording protocols were adopted for each measurement. That is, for the insertion of channels and the opening or closing of these channels, the gap-free protocol was used. The conductance measurements were made with the episodic stimulation protocol [50].

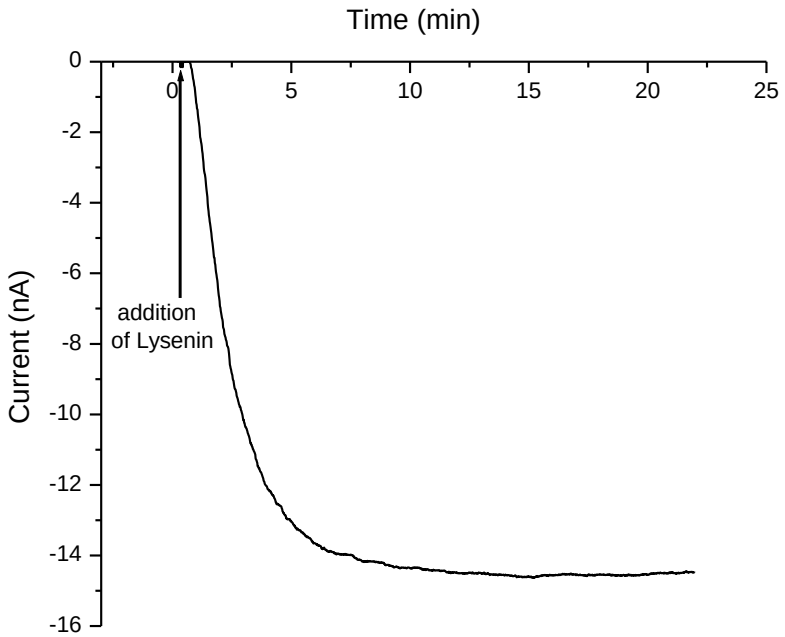

Figure 3.4: Current versus time graph showing insertion of about 300 Lysenin channels into BLM. Ionic current passing through BLM increases with time and reaches its maximum value and then stabilizes in about 25 minutes.

3.2.3 Addition of Ions and Measuring Conductance

After reaching a steady state of open current i.e. current through all-open pores, and before adding the multivalent metal ions, the grounded compartment (trans) was flushed and refilled with a fresh electrolyte solution so that no more Lysenin channels would be inserted. Then multivalent ions were added to the buffered electrolyte solution. The addition of the multivalent ion concentration was gradual and to both sides of the channels (both sides of the chamber). Accordingly, the conductance of the channels has been reduced as a result of the dynamic interaction between multivalent ions and the Lysenin.

In order to measure the conductance of these channels (before and after adding ions) a linear voltage ramp was applied across Lysenin channels, which was defined by using the episodic Stimulation protocol (0 mV: -60 mV: 0 mV, 0.5 mV/ 5 scan rate), each run consisted of three identical voltage sweeps, that is a total of six I-V curves in the range of (0 mV: -60 mV: 0 mV). This voltage ramp is illustrated in Figure 3.5. The average slope of the linear ramps was calculated to obtain the channels' conductance before the addition of ions (G_0), and after (G).

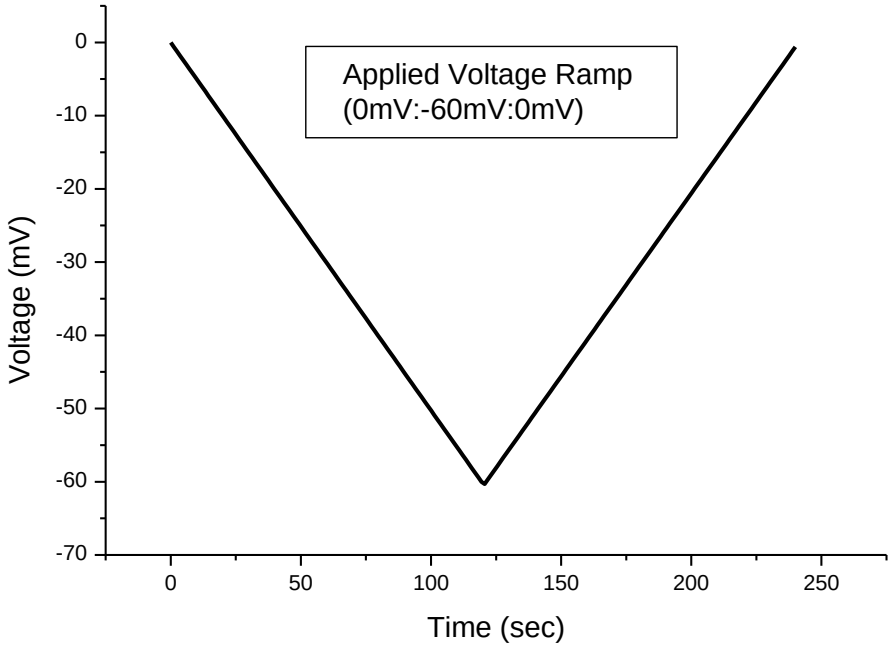

Figure 3.5: The conductance of Lysenin channels was measured by applying a voltage ramp (0 mV: –60 mV: 0 mV) across the inserted channels in the BLM.

3.3 Error Analysis

The differences in the slopes (Figure 3.6-a) showed how the addition of monovalent ions (in mM) increased the solution conductivity. However, the addition of significantly fewer amounts of trivalent ions (in μM) dramatically decreased the channels' conductance but not the conductivity of the bulk solution (Figure 3.6-b).

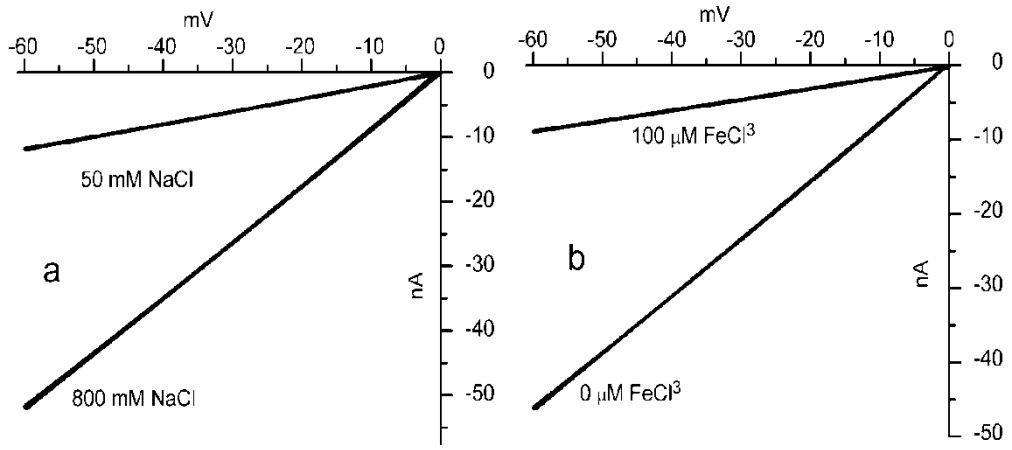

Figure 3.6: (a) Increasing the concentration of sodium chloride from 50 mM to 800 mM increased the conductivity of the bulk, while (b) addition of 100 μM trivalent ferric ions (Fe^{3+}) to 150 mM KCl bulk solution significantly reduced the channels' conductance.

For each experiment, the overlap of the six curves recorded (Figure 3.5) at a specific concentration demonstrated the steady state stability and yielded very small errors in measuring the conductance. However, the conductances measured at the same concentration for multiple experiments yielded a range of values. The reported conductance is the average of these conductances with their standard deviation. The uncertainties appear on the graphs in the form of error bars. Further explanation of error analysis can be found in Appendix D.

Chapter 4 Results and Discussion

4.1 Insertion of Lysenin Channels into BLM, and their Electrical Characterization

After achieving a stable and proper BLM (see the Materials and Methods chapter), minute amount of Lysenin at a final concentration of approximately 200 pM was added to the grounded side of the bilayer setup under continuous stirring. Under voltage clamp conditions of -80 mV, Lysenin addition yielded increasing open current that stabilized to approximately 12 nA in approximately 30 minutes as illustrated in Figure 4.1. This open current indicated that Lysenin disturbed the intrinsic barrier function of the BLM and allowed the charged transporters to move through the membrane.

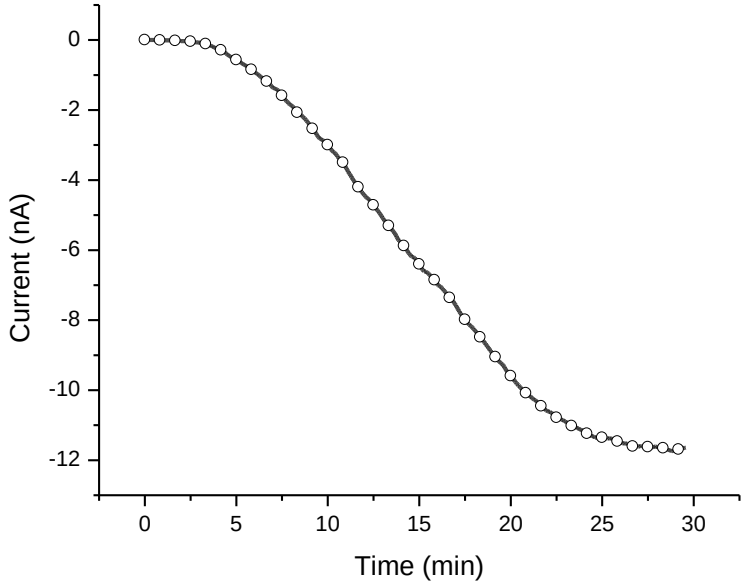

Figure 4.1: The macroscopic current increases with time, showing a rapid growth and leveling of current through the BLM. The behavior of the current indicates a permeability increase of the BLM upon the addition of Lysenin channels by maximizing the number of charge transporters passing through the BLM.

A closer inspection of the current traces performed at higher resolution indicated that the open current increased in steps, where each step represents one channel, as Figure 4.2 depicts, as opposed to a monotonic decrease. Each individual step changed the open current by approximately 48 pA as illustrated in Figure 4.2, demonstrating that Lysenin inserted uniformly large conductance channels in artificial planar membranes BLMs [1, 51].

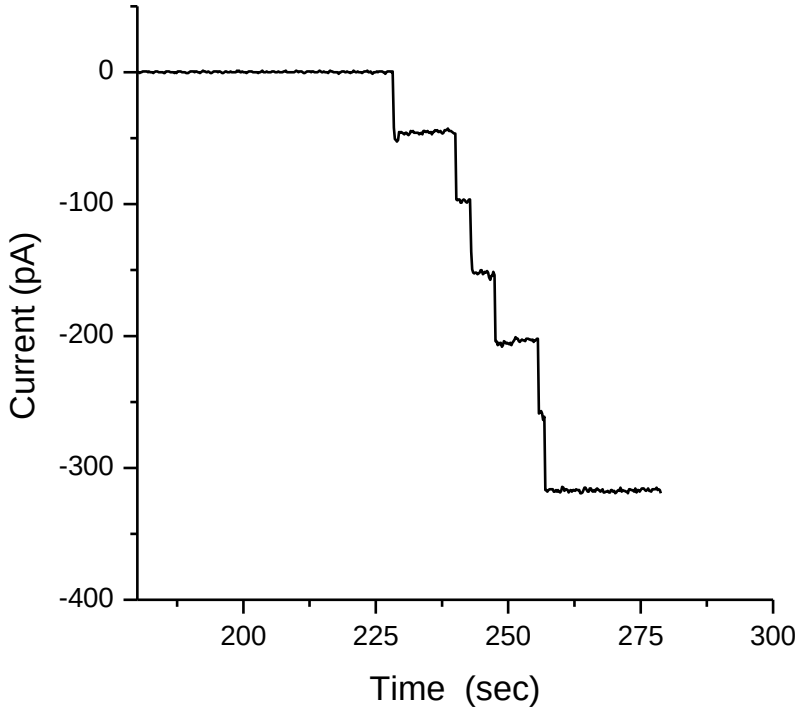

Figure 4.2: The interaction between Lysenin and bilayer lipid membrane affects the latter's permeability, resulting in insertion of pores. A higher resolution graph of open current shows the stepwise nature of this process and its relation with each individual pore (approximately -48 pA/pore at -80 mV bias voltage)

When the BLM was biased by positive voltages, the ionic current through Lysenin channels dramatically decreased [1, 43, 45, 52]. Although no direct evidence was provided previously, Lysenin's structure underwent conformational changes causing its channel to switch from open to closed state [1, 45]. This voltage-induced gating may interfere with other changes in conductance induced by other external factors, thus this research directly addressed this problem by analyzing the response of single Lysenin channels to external voltages. For this purpose, a very small amount of Lysenin, approximately 20 pM at final concentration, was added to the grounded reservoir side, where it yielded only three inserted channels in approximately 30 minutes. The insertion of further channels was prevented by flushing the grounded reservoir with 20 ml fresh buffered electrolyte and removing the free protein from the bulk.

The ionic currents measured through the three channels in response to positive step voltages, as illustrated in Figure 4.3, indicated extended stability at +5 mV. At +10 mV, transient changes in the open current indicated voltage-induced gating. The flickering in current became more persistent at +15 mV, while at +30 mV all three channels closed in a few seconds.

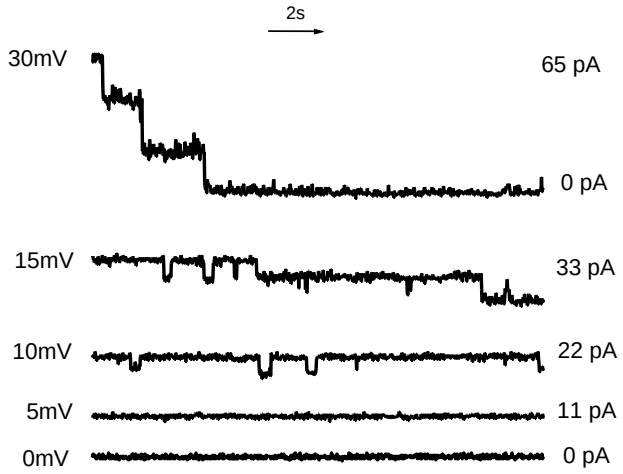

Figure 4.3: Current versus time graph shows the closing of three embedded channels into the bilayer due to voltage-induced gating. At +15 mV the pores started to gate, and holding the potential at +30 mV closed all three pores (150 mM KCl, 20 mM HEPES/KOH, pH 7).

Applying different amounts of negative voltages across the three open Lysenin channels did not produce any non-ohmic behavior as a result of the current flowing through them, as shown in Figure 4.4. This provided excellent conditions to conduct the experiments of this study in this negative voltage range, so the voltage gating did not interfere with the conductance measurements.

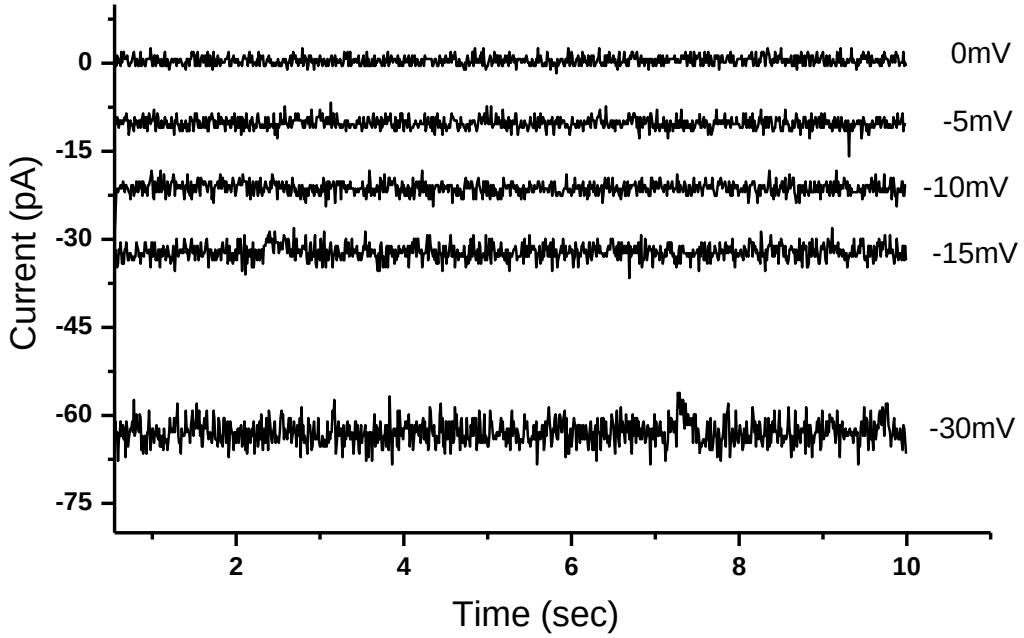

Figure 4.4: Current versus time graph shows the negative applied voltages up to -30 mV did not produce closure in any of the bilayer's three pores (150 mM KCl, 20 mM HEPES/KOH, pH 7).

Lysenin's behavior at the single-channel level, including its voltage-induced gating, was fully reflected in the I-V curve recorded for larger number of channels. Current-voltage curve (in the range of -80 mV to +60 mV) was recorded for more than 1000 channels that were inserted in the BLM (Figure 4.5). The linear and ohmic behavior observed at negative voltages demonstrated that no conformational changes (closings) occurred in that range. In contrast, voltages greater than +20 mV showed a strong non-linearity of open current. The transition from high to low conductance was gradual and underwent a negative dynamic conductance region (negative slope) followed by rectification [45].

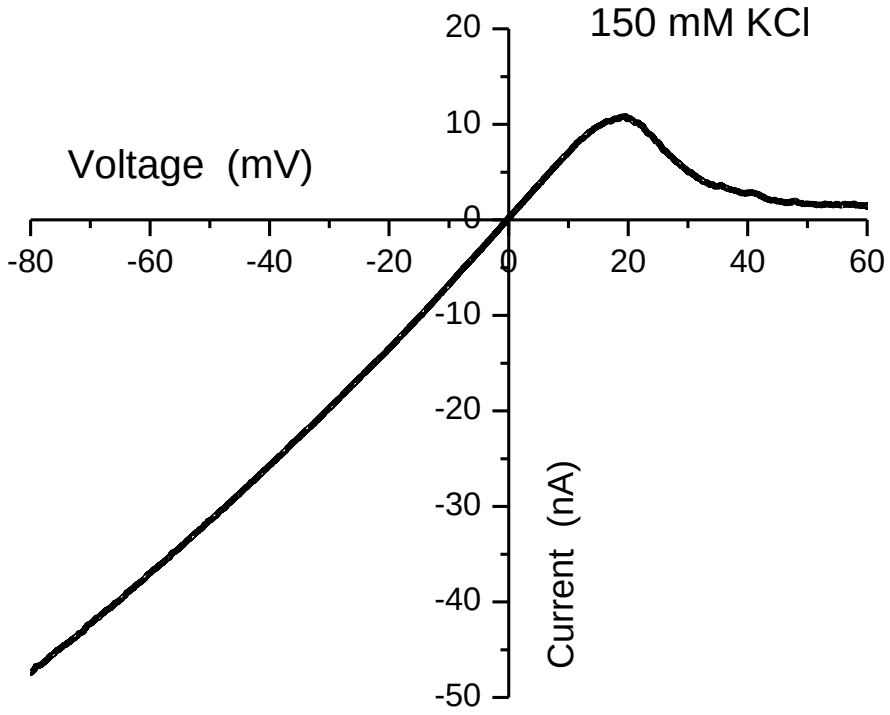

Figure 4.5: Current voltage graph shows the behavior of a population of Lysenin channels in the BLM surrounded by a supporting electrolyte solution of 150 mM KCl, 20 mM HEPES/KOH pH 7. The linearity in the negative voltage shows no rectification, while it can clearly be seen in the positive voltage region due to the voltage-induced gating of Lysenin.

This research investigated the dynamic interaction of multivalent ions with Lysenin, which was measured by calculating the conductance of Lysenin channels. The results above (Figure 4.5) recommend conducting the experiments of this research in the negative voltage region as mentioned before. The negative and positive voltage regions are related to the direction of the electric field, which was produced by the electrodes across the inserted channels and BLM. The directions of the electric fields are shown in section 4.5.1.

4.2 Effect of Monovalent Ions Concentrations on Lysenin Channels' Conductance

Changes in conductance of Lysenin channels elicited by multivalent ions were investigated by adding electrolyte metal and non-metal ions to the bulk solution in chloride form. For this study, it was essential to assess whether the addition of chloride ions to the bulk electrolyte would interfere with conductance measurements by either promoting conformational changes to Lysenin channels, or by disturbing the open current due to screening effect.

Lysenin channels' macroscopic conductance increased linearly with 50 mM NaCl/ KCl sequential increases in electrolyte concentration (Figure 4.6-a) which is consistent with the linearity in conductivity for both monovalent species (Figure 4.6-b) indicating no interference from these ions in the range of 50-900 mM KCl/NaCl.

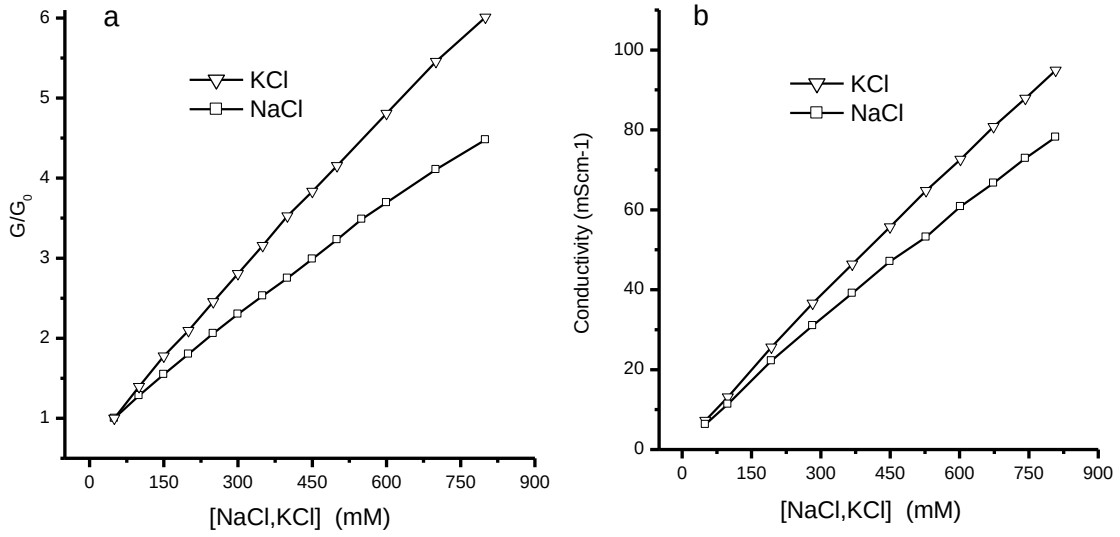

Figure 4.6: (a) The conductance of Lysenin channels linearly increased with monovalent ion concentration in the range 50mM to 900 mM, which is consistent with the conductivity curve in (b), indicating no changes in the geometry of the channels in that range. (b) K^+ and Na^+ increased the conductivity at a constant rate in the range of 50-900 mM, with the difference between the two ions due to sodium's lower mobility.

The higher conductance recorded in the presence of KCl compared to NaCl (Figure 4.6) can be explained based on the difference in relative electrophoretic mobility between Na^+ and K^+. When exposed to external electric fields in solutions, K^+ moves faster than Na^+ [33].

Previous studies of Lysenin[45] suggested that voltage gating could be affected by high monovalent ion concentration, where the pores are in their open state according to the foot-in-the-door model of gating [53]. The effect of low and high salt concentrations on gating due to monovalent ions will be discussed later in section 4.5.

Unless otherwise stated, all experiments were conducted with the same salt concentration of 150 mM NaCl or KCl, which is near physiological conditions. Thus, any changes in conductance during multivalent ion investigations are not due to monovalent ions.

4.3 Influence of Divalent Metal Ions on Lysenin Channel's Macroscopic Conductance

Unlike monovalent ions, which yielded a linear increase in Lysenin's channels conductance, divalent metal ions affected and reduced their conductance [51, 54]. The analytical response to divalent metals manifested itself as a decrease in the macroscopic conductance of Lysenin channels. This decrease was observed when the analyte was in the mM range, a value much less than monovalent concentration, although the inhibitory effect was not uniform for all tested divalent metal ions as illustrated in Figure 4.7 and Figure 4.8.

Although all the added ions carried a charge of +2, their inhibitory effect considerably varied, indicating that chemical identity might influence changes in the macroscopic conductance. The alkaline earth Ca^{2+} and Mg^{2+} were the least effective inhibitors, where the conductance of Lysenin channels has been reduced by approximately 30% at 20 mM bulk

concentration, as Figure 4.7-a depicts. On the other hand, the other divalent cations such as Mn^{2+}, Ni^{2+}, Co^{2+}, and Fe^{2+} had a higher ability to inhibit the macroscopic current: up to 90% at less than 10mM for the case of Fe^{2+}, as Figure 4.7-b depicts. The divalent ions Zn^{2+} and Cd^{2+} exhibited similar behavior to the other metal ions. Zn^{2+} reduced the macroscopic conductance by at least 80% at low bulk concentration, as illustrated in Figure 4.8. The electronic configuration of the ions is illustrated in Appendix A.

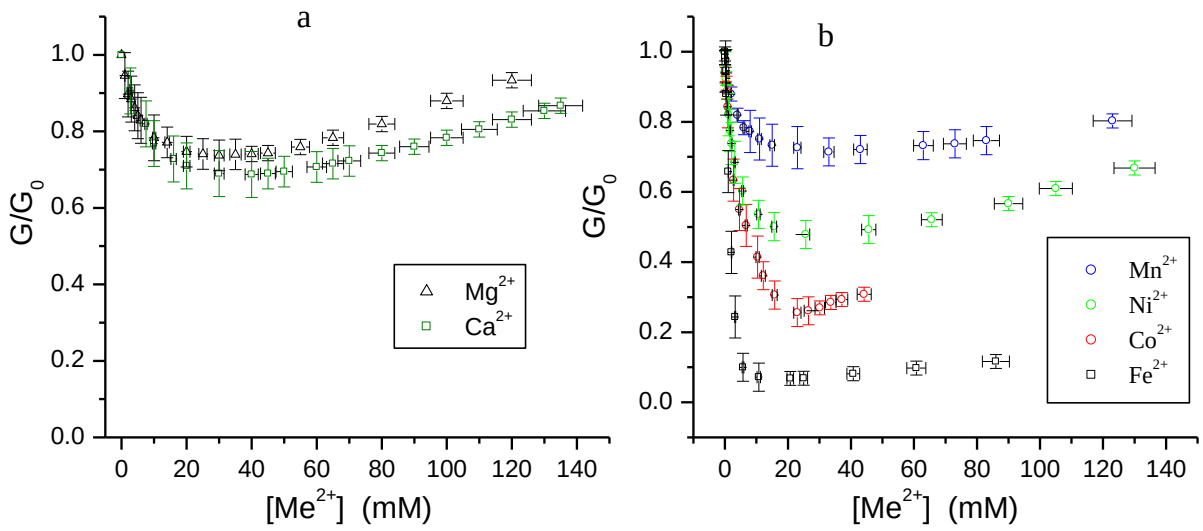

Figure 4.7: (a) $Mg^{2+}$and Ca^{2+}decreased the conductance of Lysenin channels by about 30% (b) Mn^{2+} also reduced the conductance of channels but was less efficient than Ni^{2+} and Co^{2+}. The most efficient divalent ion was Fe^{2+} and the linear increase after the minimum conductance was due to the subsequent increase in the bulk conductivity.

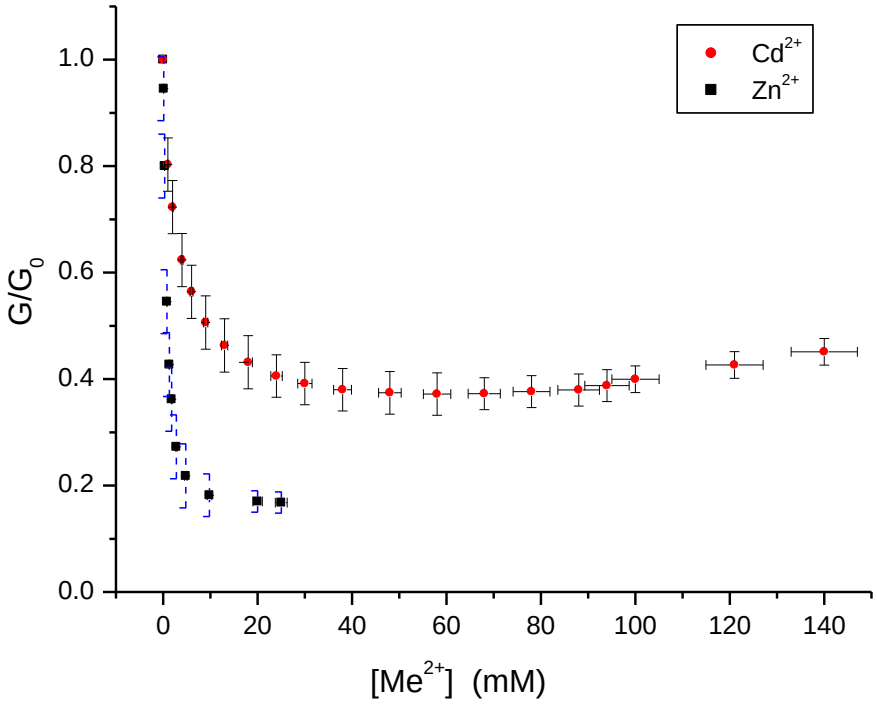

Figure 4.8: Zn^{2+} was more efficient and caused a greater reduction in Lysenin's channels conductance than Cd^{2+} and at a lower concentration range.

4.4 Effect of Trivalent Metal Ions on Lysenin Channel's Macroscopic Conductance

The addition of trivalent metal ions to the bulk solution reduced the conductance of Lysenin channels to a larger extent than most of the divalent ions [51, 54] as shown in Figure 4.9. All tested trivalent lanthanides approximately shut down the ionic transport in concentration ranges of 130 μM-650 μM.

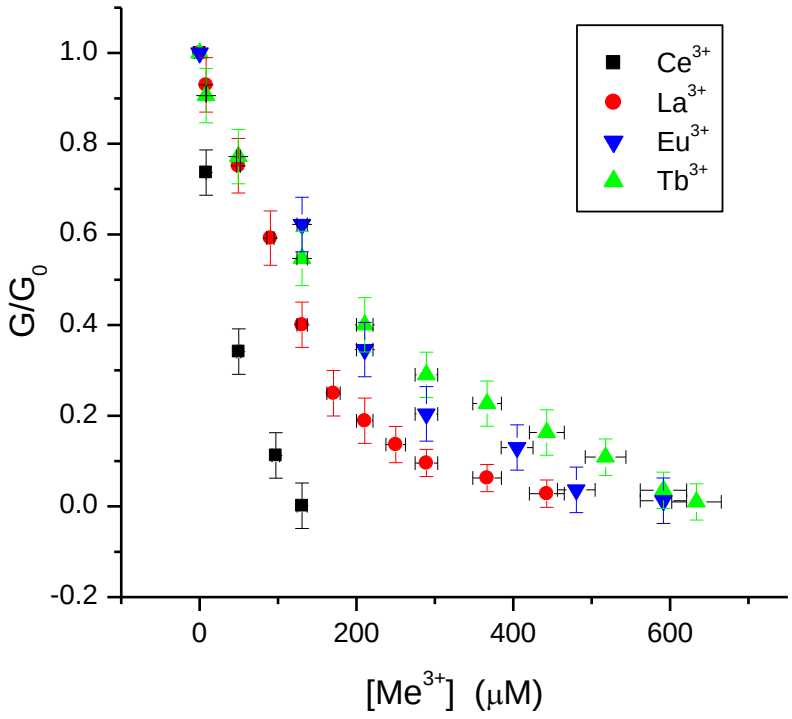

Figure 4.9: Lanthanides ions were very effective inhibitors of ionic transport through Lysenin channels, and lowering the conductance to approximately zero in ranges of 130 μM-650 μM.

The greatest efficiency was encountered for Al^{3+}, which diminished the conductance at less than 1.5 μM bulk concentration as illustrated in Figure 4.10, and in fact demonstrated the highest inhibition potential among all tested metal ions.

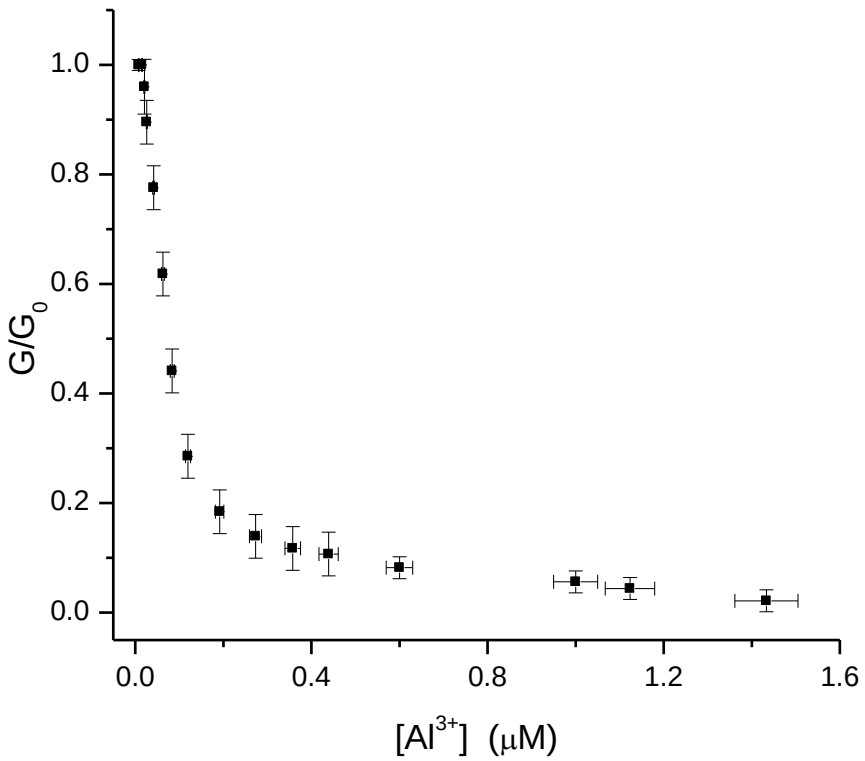

Figure 4.10: Among the tested ions, Al^{3+} was the most effective inhibitor, bringing the conductance of Lysenin channels to zero in the range of zero to 1.5 μM.

4.5 Influence of Monovalent Ions on Lysenin's Gating

4.5.1 High Monovalent Concentration Modulates Lysenin's Voltage Gating

Monovalent ions were used as a bulk solution (electrolyte) in order to measure the electrical current through Lysenin channels (i.e. determining their conductance). In fact the BLM by itself can be considered as a capacitor (see Appendix E) of dielectric constant ($\in \approx 2$) [6]. As the voltage was applied, an external electric field ($\vec{E}_{ext}$) was created across the BLM and across the inserted Lysenin channels. This external electric field (Figure 4.11) was established because of the accumulation of cations and anions of the electrolyte on both sides of the BLM, even before any channel insertion. As a result of the charge accumulation on both sides of the BLM, the dielectric material of the BLM became polarized. Accordingly, an internal electric field ($\vec{E}_{int}$), which is opposed to the external one, was produced across the BLM. Then any changes of the charge distribution on the BLM could affect their external ($\vec{E}_{ext}$) and internal ($\vec{E}_{int}$) electric fields.

Lysenin channel has two charged regions in its structure (see sections 2.7.3 and 2.7.4) creating an electric dipole moment ($\vec{p}$) along its structure (Figure 4.11). The interaction between the external electric field ($\vec{E}_{ext}$) and Lysenin's electric dipole moment ($\vec{p}$) plays the major role in its gating. The direction of the electric field affects the state of the channel, as illustrated in Figure 4.11. The channel stays in its open state because of the interaction between $\vec{E}_{ext}$ and the dipole moment ($\vec{p}$), that is $\vec{p}.\vec{E}$. If the applied voltage is reversed, as illustrated by Figure 4.12, and when the critical voltage is achieved, then the channel closes as a result of the dipole-electric field interaction ($\vec{p}.\vec{E}$).

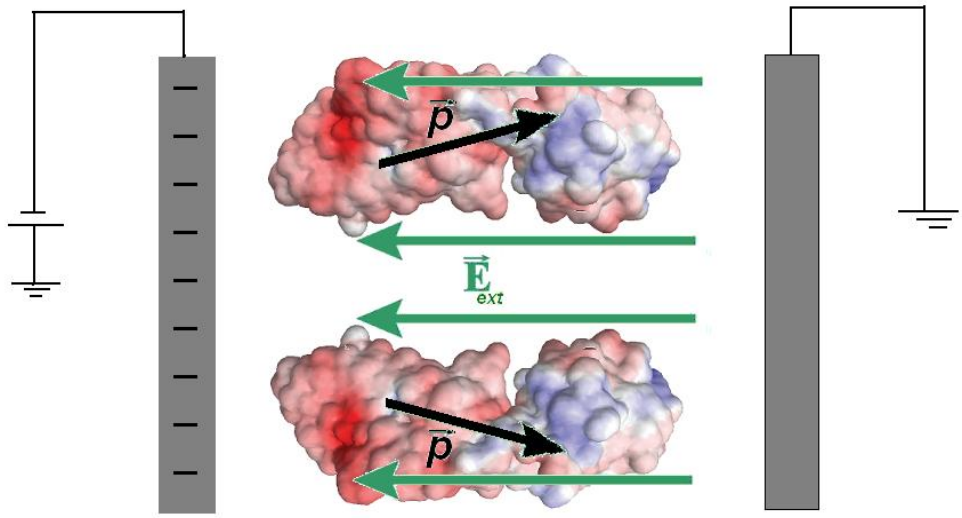

Figure 4.11: A Lysenin channel in its open state. The structure shows just two of the six Lysenin proteins with their dipole moments interacting with the external electric field across the BLM and the channel. The blue and red colors represent the positive and negative charged regions (inside the lumen) respectively [42]. The interaction between ($\vec{E}_{ext}$) and ($\vec{p}$) that is ($\vec{p}.\vec{E}$) forces the channel to stay open.

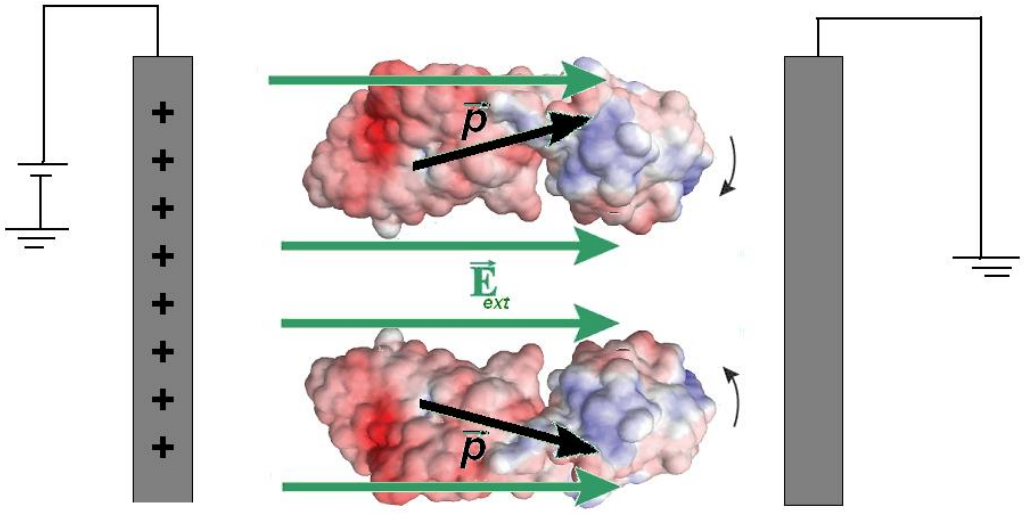

Figure 4.12: The positive voltage is applied across the BLM and the channel. The Lysenin channel starts to gate when this voltage exceeds the critical voltage, proposing that the main cause for voltage gating is the dipole-electric field interaction ($\vec{p}.\vec{E}$).

Since all multivalent ions that have been used in this research were in the chloride form, it was essential to inspect the effect of different concentrations of chloride ions (monovalent ions) on the conductance of Lysenin channels and their functionality (gating).

The influence of monovalent ion concentration on the voltage-induced gating of Lysenin was investigated for a large number of Lysenin channels as illustrated in Figure 4.13. The critical voltage of Lysenin channels has been shifted from about 30 mV at a concentration of 300 mM KCl to about 60 mV at a concentration of 600 mM KCl. A close inspection of Figure 4.13 shows a leakage current in the positive voltage region either at 300 mM (after 60 mV) or at 600 mM (after 80 mV), which could be either through the membrane or through the channels themselves, or both. The high leakage current at higher monovalent ion concentration could be due to the increase in the conductivity of the bulk, or due the lack of closing of Lysenin channels. These findings indicated that monovalent ions (K^+ and Cl^-) electrostatically interacted with Lysenin via its charged regions within its structure (see Figure 2.12), where potassium cations accumulated on the negatively charged region and chloride anions accumulated on the positively charged region of Lysenin. This accumulation of charges weakened the strength of Lysenin's dipole moment which affected its interaction with the external electric field ($\vec{E}_{ext}$) as shown in Figure 4.12. As the concentration of monovalent ions increased Lysenin's dipole moment strength decreased, then the required external electric field for gating increased, which explained the shift in the voltage-induced gating of Lysenin from 30 mV at 300 mM KCl to 60 mV at 600 mM KCl.

On the other hand, the slope of each straight line in the negative region (negative voltage and negative current) represents the conductance of the channels. The increase of the slopes, which is proportional to the increase in concentration, does not signify an increase in the

channels' conductance but rather, it was due to the increase in the conductivity of the bulk solution itself.

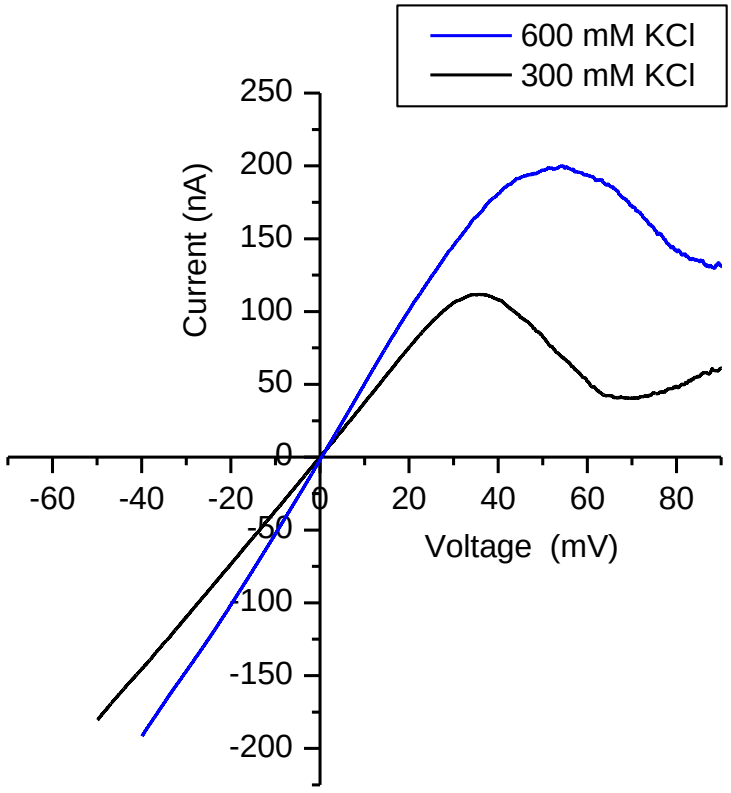

Figure 4.13: Current versus voltage graph shows the shift in the critical voltage of Lysenin as a result of the electrostatic interaction of monovalent ions and the voltage sensor of Lysenin channels. In the negative region, the slopes of the straight lines increased because of the increase in the conductivity of the solution.

4.5.2 Monovalent and Multivalent Ions Compete Lysenin's Binding Site

Usually the region in the protein structure which electrostatically interacts with an external electric field and causes the voltage gating is called the voltage-sensing domain or the voltage sensor [19, 55], while, as introduced before (sec.2.7.2), the one for ligand gating is called the binding site.

The behavior of Lysenin channel's conductance over a wide range of cerium trivalent cation concentrations and at different monovalent salt concentrations showed how high salt concentration affected the sensitivity of Lysenin channels toward cerium ions. At high concentration of monovalent ions (900 mM KCl), the conductance of Lysenin was decreased (due to the interaction with 500 μM Ce^{3+}) just by approximately 40% as illustrated in Figure 4.14. While at 300 mM KCl, Lysenin's sensitivity has affected less, and at 150 mM KCl or 75 mM KCl the effect of monovalent ions on Lysenin channels' conductance was even less.

These findings indicated that monovalent cations (K^+) competed for the binding site with trivalent cations, (supported by our model in the next chapter) where this binding site was proposed to be the negatively charged regions among Lysenin's structure (i.e. the two acidic amino acids mentioned in sec 2.7.4). Since the concentration of (K^+) was much higher than that for (Ce^{3+}) the binding site would be occupied by these monovalent ions. Being heavily occupied by (K^+), the electrostatic interaction between the binding site and trivalent cations (Ce^{3+}) was reduced, which eventually minimized their probability of binding.

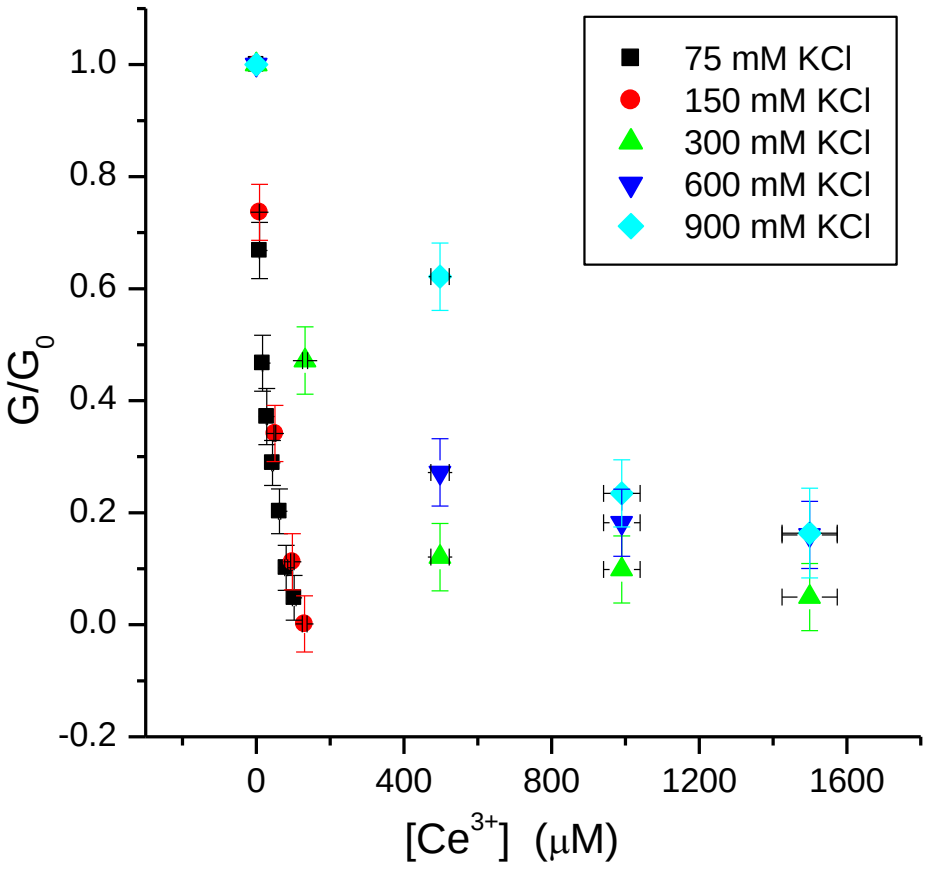

Figure 4.14: The behavior of the conductance of Lysenin channels versus concentration of monovalent concentrations shows the sensitivity of Lysenin towards trivalent cations (Ce^{3+}) at low monovalent ion concentrations. This sensitivity became weaker as the monovalent ion concentration increased.

Since high monovalent concentration modulated the voltage gating and reduced the sensitivity of Lysenin toward cerium trivalent cations, it was important in this research to investigate Lysenin's voltage gating under the influence of divalent cations. Unlike trivalent cations, divalent ones did not totally inhibit the ionic current through Lysenin channels (they partially closed Lysenin channels). For this reason, comparing voltage-induced gating before and after adding divalent cations would help in explaining Lysenin's mechanism of gating. This comparison was important because it revealed the relationship between the binding site and the

domain sensor of Lysenin. To distinguish between Lysenin's voltage sensor and its binding site, a series of experiments were conducted, where an I-V curve was recorded before and after adding magnesium divalent cations (Figure 4.15).

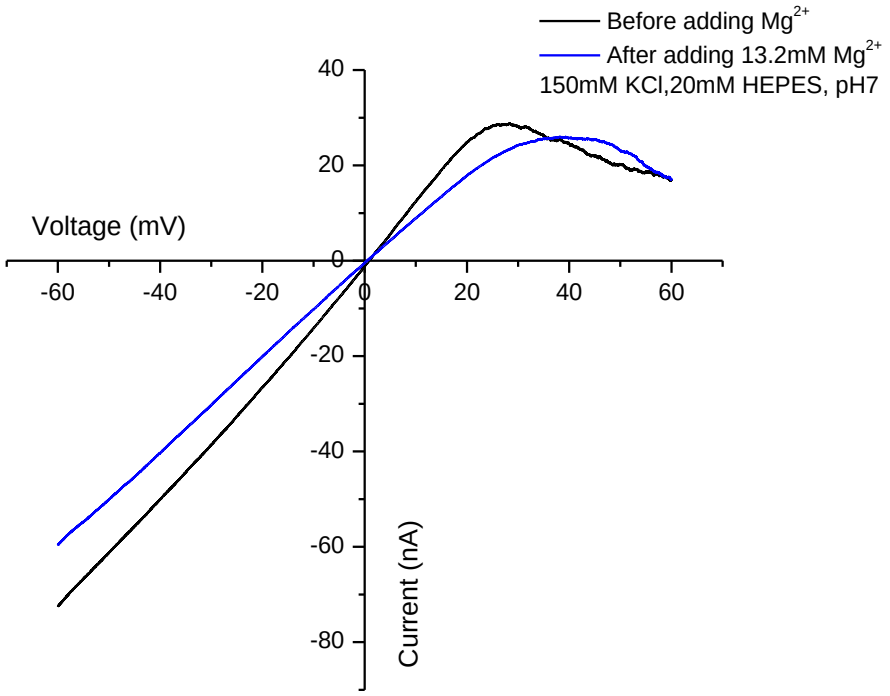

Figure 4.15: Divalent ions modify the voltage gating of Lysenin. A notable shift in the critical voltage before and after adding Mg^{2+} was recorded. The critical voltage was shifted from 20 mV to 40 mV before and after adding Mg^{2+} respectively.

As expected, before adding Mg^{2+}, the critical voltage of Lysenin at electrolyte condition (150 mM KCl) was about 20 mV. After adding Mg^{2+} the behavior of the I-V curve was different where a shift (from 20 mV to 40 mV) in the critical voltage appeared. This indicated that the Mg^{2+} electrostatically interacted with the negatively charged region of Lysenin (Red color in Figure 4.12). This negatively charged region is located within the hydrophobic region in the protein's structure [41]. Since both negatively and positively charged regions form Lysenin's

voltage sensor, this experiment proposes that binding site of Lysenin to be part of its voltage sensor.

The previous experiments in this section showed how high monovalent concentration modulated the voltage gating, reduced the sensitivity of Lysenin toward trivalent cations, and caused a shift in voltage gating. All of these findings indicate that the negatively charged region of the dipole moment has been electrostatically affected. The two acidic negatively charged amino acids (two Glutamate amino acids) are located inside the channel itself (i.e. within the hydrophobic part or the N-terminus). The significance of these findings is that they indicate the position of the presumed binding site to be inside the channel.

4.5.3 Monovalent Ions affect the Transport of Lysenin's Channels

The strength of the electric dipole moment of Lysenin was modulated by monovalent ion concentrations. Since the strength of this dipole moment plays a major role of Lysenin's gating, it was crucial to investigate the effect of different monovalent ion concentrations on the conformational changes of Lysenin's channel (i.e. the geometry of the channel). Conductance "G" is directly proportional to conductivity "*k"*, where the proportionality constant or (the geometry of the channel) is the cross sectional area per channel's length, that is $G = k\frac{A}{l}$ (see Appendix C). The importance of this experiment was that it led to better understanding of the mechanism of Lysenin's gating (Sec. 2.7.2).

A series of experiments were conducted at different KCl concentrations, to measure the conductance of one single Lysenin channel. The experiments covered the concentration range from 1 mM to 900 mM of potassium chloride buffered with HEPPES/KOH. The experimental

results (Figures 4.16) indicated that the channel's conductance was not affected by the monovalent concentrations in the range of 50 mM to 900 mM KCl as shown in sec.4.2. However, results were also consistent with monovalent ions attaching to the negative site and saturating at about 50 mM.

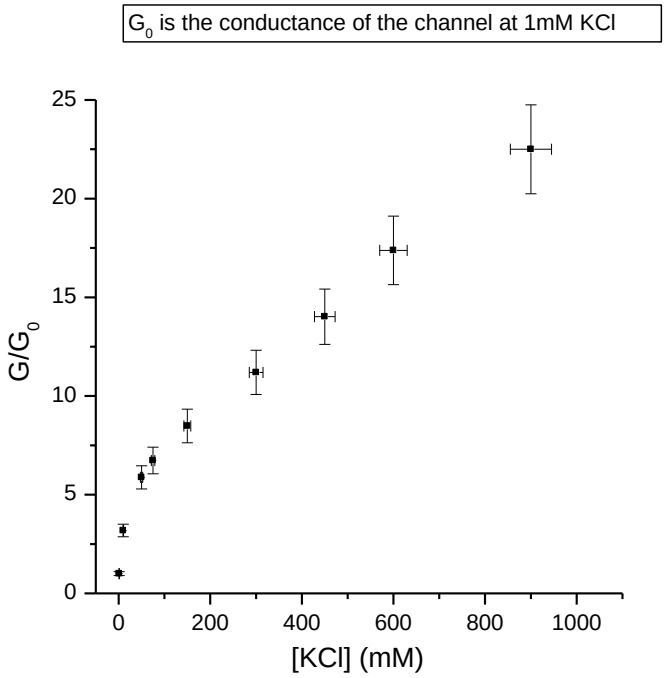

Figure 4.16: The measurement of the conductance of single Lysenin channel shows its nonlinear and linear behavior in the ranges of 1 mM to 50 mM and 50 mM to 900 mM KCl respectively.

As Figure 4.17 depicts, in the range of 1 mM to 50 mM KCl, the channels underwent conformational changes appeared as a nonlinear behavior of the channels' conductance with their corresponding conductivities. A close inspection of Figure 4.17 revealed that the steepest slope (the slope is the cross sectional area per channel's length ($\frac{A}{l}$)) was in the lowest concentration (1 mM to10 mM), then the geometry of the channels was less affected in that range. These results could not explain exactly whether the area of the channel, the length, or both has changed under

the influence of monovalent ions. This important finding shows how the strength of Lysenin's dipole moment was sensitive to monovalent ions, and indicates more sensitivity toward multivalent ions.

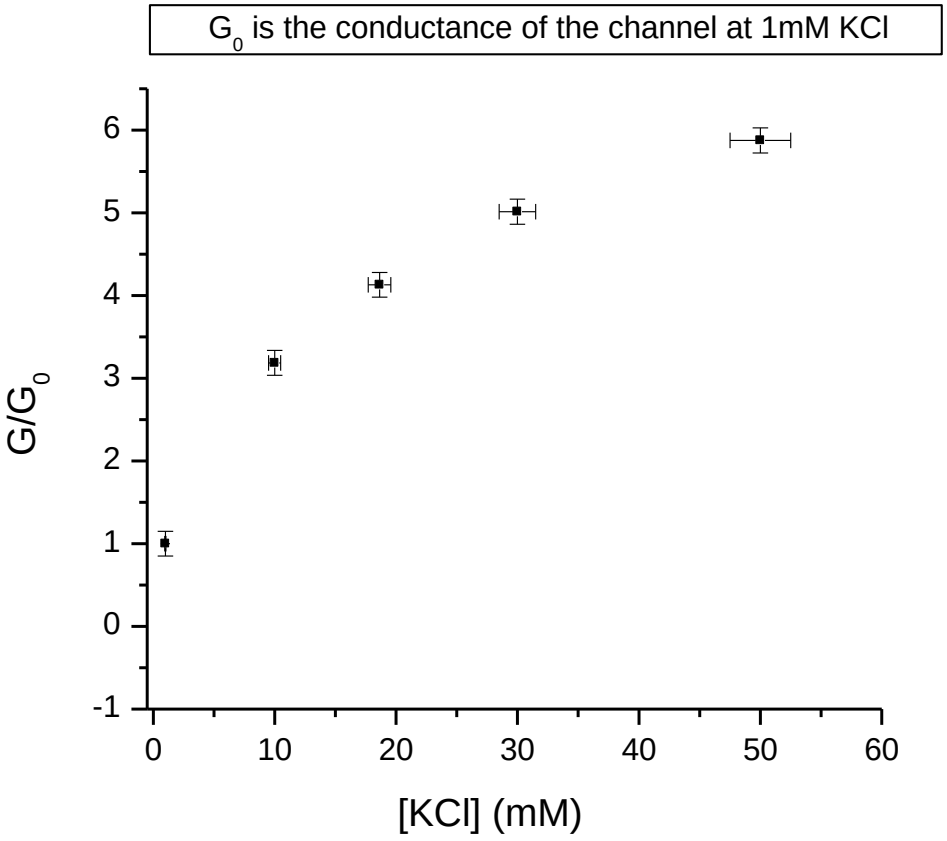

Figure 4.17: The measurement of the conductance of single Lysenin channel shows its nonlinear behavior with the conductivity of KCl bulk upon increasing its concentration from 1 mM to 50 mM. The differences in slopes of the segments indicate a change in the geometry of the channel.

4.5.4 Sensitivity of the Lysenin-BLM Biosensor

Since monovalent ions affected the electrostatic interaction between Lysenin's dipole moment and multivalent ions (in the range of 1 mM to 50 mM KCl), then it was essential for this research to look for the ideal conditions of the minimum influence of monovalent ions on the

channel's geometry. A set of experiments were conducted in the micromolar range (Figure 4.18), where the KCl bulk concentration was diluted from 1 mM to 50 μM. The results show an excellent linear relationship between the conductance of Lysenin channel and the concentration of the monovalent ions.

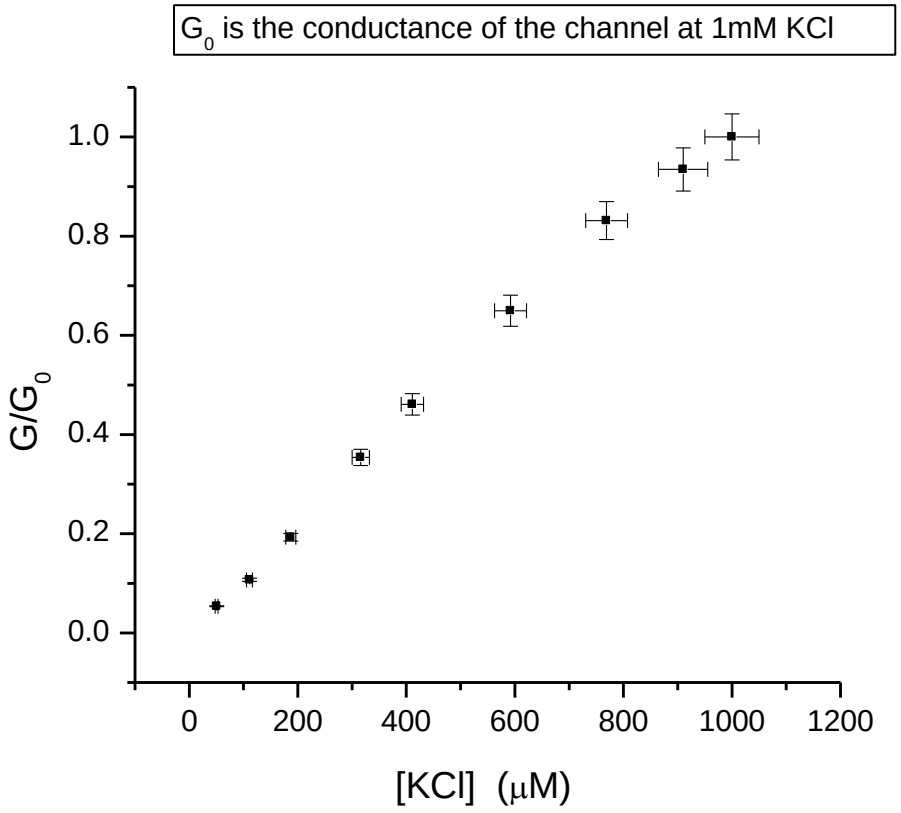

Figure 4.18: The linearity of the conductance versus bulk concentrations of one single channel indicates that the geometry of the channel is not affected at very low monovalent ion concentrations.

The linearity of the conductance and monovalent ion concentration reveal no influence of monovalent ions on the channels' geometry in this low-range concentration. This finding recommends the best experimental conditions for Lysenin use in biosensing applications that detect multivalent ions in biological samples. These conditions simply eliminate the influence of

monovalent ions on the electrostatic interaction between Lysenin's binding site and multivalent ions.

In this line of inquiry, a set of experiments were conducted in order to inspect the sensitivity of Lysenin channels under the influence of multivalent ions. Different concentrations of cobalt divalent ions were added to the Lysenin channels at very low monovalent ion concentrations (Figure 4.19). Compared with the behavior of Lysenin at 150 mM KCl, the results showed that Lysenin was more sensitive toward Co^{2+} at a very low monovalent ion concentration. This finding supports the competition concept between multivalent and monovalent ions for the binding site. Cobalt divalent ions won the competition for the binding site at this low monovalent ion concentration.

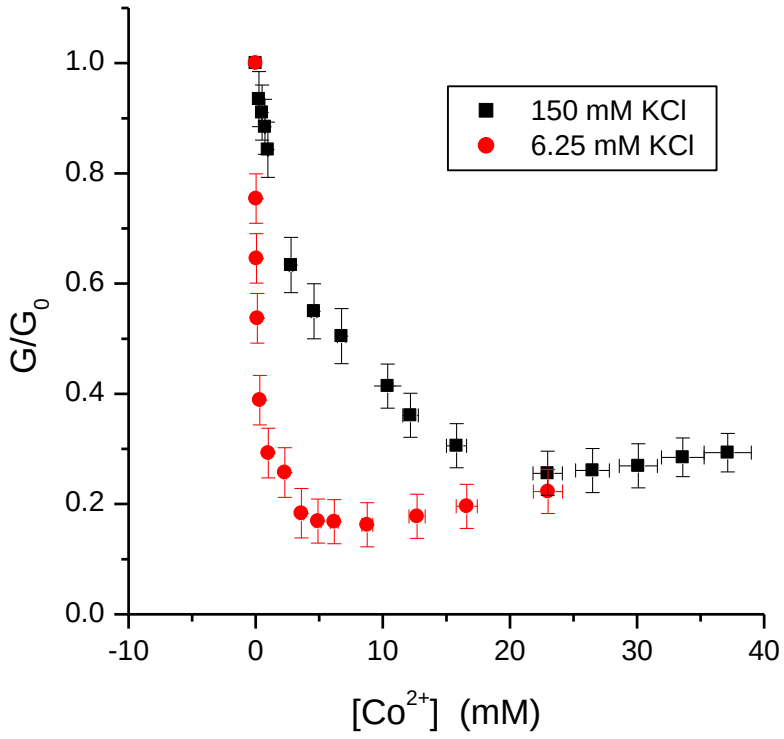

Figure 4.19: Lysenin channels show more sensitivity to Co^{2+} at the lowest monovalent ion bulk concentrations.

4.6 Charge Impact on Lysenin Channel's Conductance

The previous experiments showed how Lysenin channels' conductance was influenced by different multivalent ions. All tested multivalent metal ions inhibited partially or totally the Lysenin channels' transport capabilities according to their respective efficiencies, which were considerably varied. Although the experiments did not offer enough information to help in deciphering the intimate mechanisms behind this observed decrease in conductance, some general trends may be described.

As concluded before, the effect of monovalent ions (in the micromolar range) was almost negligible on the conductance of Lysenin channels. That is, monovalent ions did not reduce the macroscopic conductance. Divalent ions did not affect the conductance as efficiently as ions with charges greater than +2, which eliminated the conductance in the μM range. These observations proposed electrostatic interaction as the primary source of the decrease in conductance.

In order to explore the influence of charge on the inhibitory potency, experiments involving the same ion (Fe) in two different redox states, +2 and +3, were conducted. The divalent ferrous ion Fe^{2+} was a very efficient inhibitor where the macroscopic conductance was decreased by more than 90% at about 10 mM concentration as Figure 4.20 depicts. However, the trivalent form of the same ion reduced the transport capabilities by approximately 95% at much lower concentration (about 250 μM), and demonstrated that the charge, and not the chemical identity, modulated the inhibition efficiency of Lysenin channels [51].

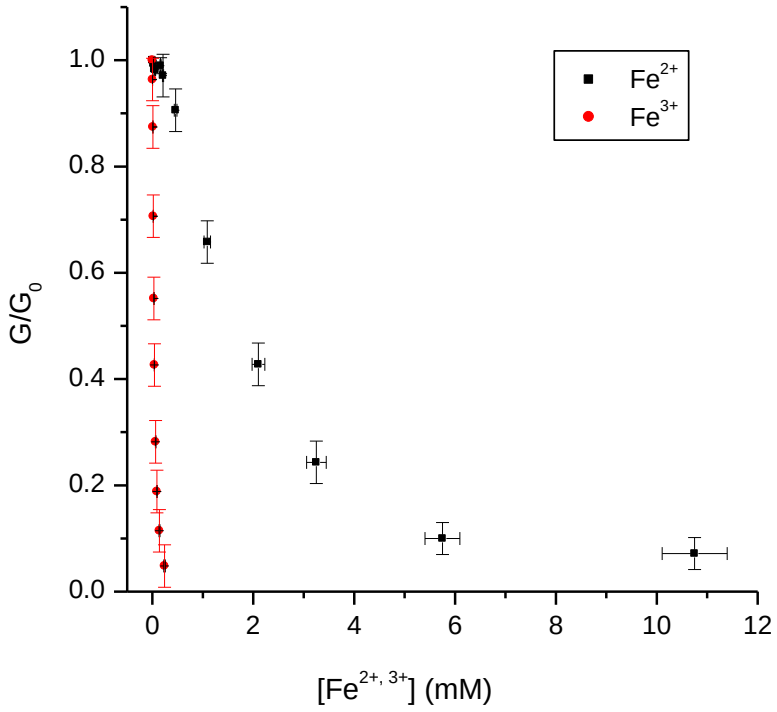

Figure 4.20: Trivalent ferric ions (Fe^{3+}) reduced the conductance of Lysenin much more effectively than divalent ferrous ions (Fe^{2+}), indicating the irrelevance of chemical identity to changes in Lysenin's conductance.

4.7 Hydrated Radius and Charge Density Effects on Lysenin Channel's Conductance

The different sensitivities encountered for ions of the same charge indicated that other physical properties might play a role in modulating the macroscopic conductance of Lysenin channels. The most uniform response was encountered for the trivalent lanthanides, which carry the same charge but have different ionic radii.

With this in mind, ion size was hypothesized to be responsible for the different sensitivities, as steric hindrance might impede accessibility to the binding site [56]. While the ion size hypothesis would explain why Al^{3+}, with an ionic radius of approximately 0.55 Å, was more efficient than any of the lanthanides, ranging from 1.05 to 1.20 Å, it did little to account for

divalent ions such as: Zn^{2+} (0.74 Å radius), Ni^{2+} (0.715 Å radius), Mn^{2+} (0.86 Å radius), and Co^{2+} (0.74 Å radius) [57].

Nevertheless, the ionic radii as reported does not take in consideration the fact that the ions were hydrated with one or more layers of water molecules (effective hydrated radii), where the effective size of the ions would be larger and should be considered in the reaction with Lysenin's binding site. All trivalent cations have the same hydrated radii (9 Å) [33]. Taking into account that Lysenin makes a pore with radius of about 15 Å then diminishing the conductance of the channel by blocking is a plausible mechanism. The ionic and hydrated radii for the ions that used in this research are listed in Appendix A.

For a better understanding of the influence of ionic size on Lysenin's gating, a set of experiments were performed using the huge polyamines (nonmetals) spermidine^{3+} "SPD^{3+}" and spermine^{4+} "SPM^{4+}", whose chemical structures are displayed in Figure 4.21 [58].

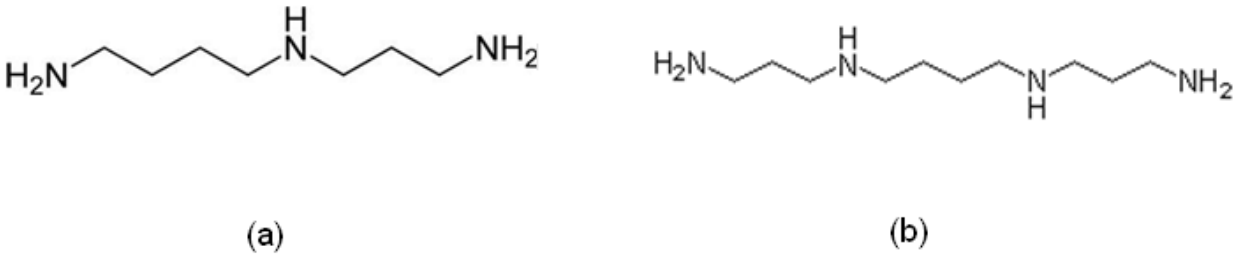

Figure 4.21: The chemical structure of (a) Spermidine^{3+} and (b) Spermine^{4+}

The addition of Spermidine and Spermine to the bulk electrolyte of concentration 150 mM NaCl, as Figure 4.22 depicts, did not reduce macroscopic conductance to the same degree as the trivalent metals did. The addition of 5 mM Spermidine reduced the conductance by approximately 40% despite the fact that Spermidine is trivalent. This low sensitivity resembled

the inhibition induced by divalent metals rather than trivalent ones. The addition of 4 mM Spermine to the electrolyte reduced the conductance of Lysenin channels by more than 50%, similarly to divalent metal ions. The slightly higher sensitivity recorded for Spermine may be linked to its higher ionic charge compared to Spermidine.

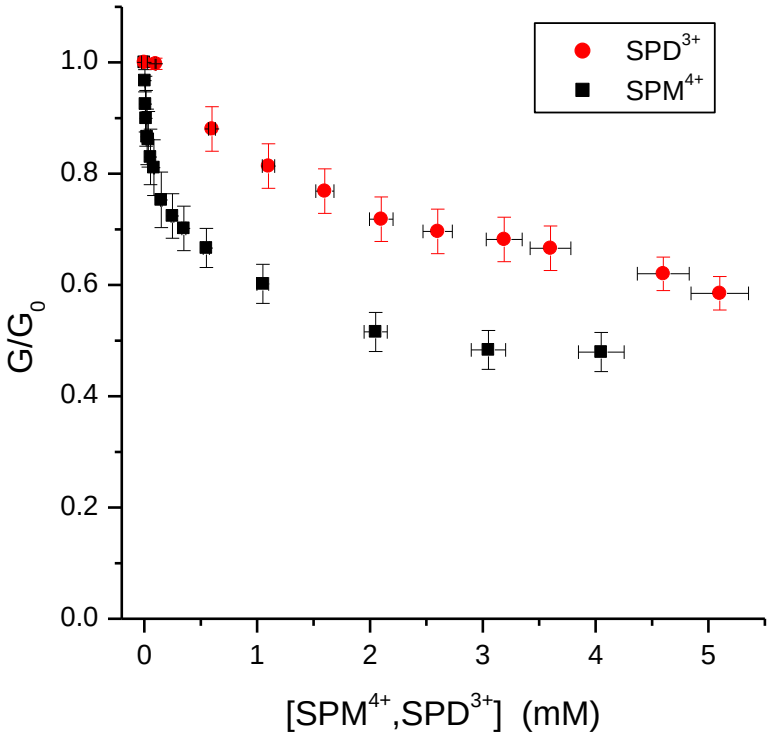

Figure 4.22: The effects of (a) trivalent Spermidine and (b) quatrovalent Spermine on conductance of Lysenin channels were similar to those of divalent ions.

Spermine has a linear structure (cylindrical shape) and is considered to be the longest among other polyamines with about (20 Å in length) and (4 Å in diameter) [30]. Taking into account the diameter of Lysenin channel which lies between 30 Å [40] and 57 Å [41], then Spermine would pass through the Lysenin's channel. The low inhibition observed for both

voluminous organic ions provided supplementary evidence to indicate that the modulation of the channel conductance could be governed by both ionic charge and size [51, 54].

4.8 Reversibility

The interaction of multivalent ions with Lysenin channels yielded a concentration-dependent decrease in macroscopic conductance upon their addition to the bulk solution of monovalent ions. The experimental results indicate that electrostatic interaction played a major role in modulating Lysenin's sensitivity to multivalent ions, without offering any further clues to the mechanistic processes resulting from such interaction.

The stability of Lysenin channels in the BLM was investigated in the presence of multivalent ions to determine whether these channels were functioning reversibly, that is opening and closing, or were simply removed from the BLM. Such studies required the consequent removal of the multivalent ions from the bulk electrolyte. The simplest approach for this task would be to flush the bilayer chamber with fresh electrolyte until all multivalent ions were completely removed. Practically, however, the well-known fragility of the unsupported BLM seriously impeded such an approach.

An experiment was conducted in order to measure the changes in macroscopic conductance of Lysenin channels upon addition of La^{3+}. Lysenin was added to the BLM and an open current of approximately 11.5 nA was reached. The measurements were performed in voltage clamp conditions of -80mV bias, and sampling rate 100 ms. The addition of 10 μM La^{3+} reduced the conductance significantly (channels closed) in about 2 minutes (Figure 4.23-a), then

the addition of 1mM EDTA, a chelator, reinstated (in much shorter time) the initial conductance properties and demonstrated reversibility [51, 54].

Accordingly, the capabilities of various chelating or precipitating agents, in the bulk electrolyte, were investigated to reduce the amount of free ions and help in analyzing reversibility.

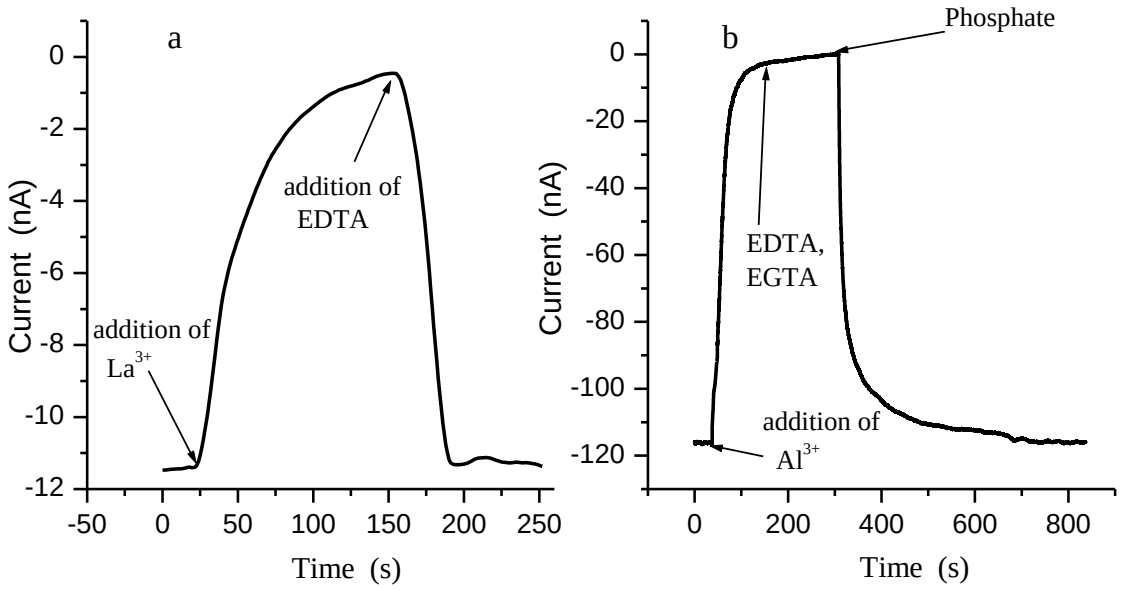

Figure 4.23: Chelators' or precipitators' effect on recovering the current through closed Lysenin channels. The fast recovery of the current indicated that these channels were functioning in the BLM. (a) Addition of EDTA chelated La^{3+}; as a result the channels reopened again. (b) Phosphate ions precipitated Al^{3+}; the channels reopened quickly.

Another experiment was conducted to investigate this property with regards to Al^{3+}. The bilayer preparation and the Lysenin insertion were performed as described in chapter three. The measurements were performed in voltage clamp conditions of -40 mV bias, and the changes in the macroscopic currents upon multivalent ion addition were recorded as a function of time (sampling rate 1 s).

Before the addition of any multivalent ions, the free Lysenin in solution was carefully removed by flushing the ground side of the chamber with 30 ml of fresh buffered electrolyte. As a result, the total amount of Lysenin was drastically reduced to only the few thousand proteins inserted into the BLM.

Addition of 100 μM of Al^{3+} rapidly shut down the open current in a matter of minutes as Figure 4.23-b depicts, and neither the addition of EDTA or EGTA as chelating agents provided any reversal. Since these particular agents however are not reported as effective removers of Al^{3+}, the lack of conductance recovery did not necessarily disprove the reversibility. In fact, subsequent addition of 5 mM of phosphate ions quickly reinstated the open current through Lysenin channels. Phosphate ions have the ability to interact with free Al^{3+} and the resulting phosphate has a very low solubility in water at neutral pH [54]. As a result, it was concluded that the interaction between Al^{3+} and Lysenin was indeed reversible, and that the changes in conductance were cancelled by precipitating the inhibitors.

The insertion process of Lysenin channels in the BLM was a slow and stable process that took about one hour (see Figure 4.1) and reversibility indicated that these channels were not pulled out of the BLM as a result of their interactions with multivalent ions. If this removal had indeed occurred, and the channels had been released to the solution, they would have reinserted at an extremely slow rate after chelation or precipitation, as their bulk concentration would be very low. Instead, the rapid reversibility of these channels indicated their firm establishment in the BLM.

The reversibility of macroscopic conductance induced by multivalent ions ruled out the hypothesis that these ions caused irreparable damage to Lysenin channels. In fact, it was evidence showing that the pores did not come out of the membrane.

The noted reversibility has profound implications for the possibility of Lysenin's use in biosensing purposes. The distinctive conductance changes of this protein's channels could make it a novel biosensor for multivalent ions, and its reversibility would allow the analysis of multiple samples with one sensing system [51, 54]. Reversibility as a fundamental feature separates multiple-use sensors from single-use probes. Additionally, the Lysenin-BLM setup could be used to detect and distinguish between chelators and precipitators such as detecting phosphate in water samples.

4.9 Single Channel Investigation and Mechanism of Conductance Decreasing

The macroscopic conductance of Lysenin channels decreased with the increase of the concentration of multivalent ions. The physical determinants of the observed changes in conductance and the intimate mechanisms leading to such functionalities are yet to be determined.

Lysenin inserts stable channels into bilayer membranes [1, 39, 43, 59], and the channels are regulated by voltage and ligands [1, 43, 45, 51, 54, 60]. These conducting paths are not really ion channels, but are simply pores in a bilayer with some similar behaviors to ion channels (see chapter 2). Both structures are capable of high transport rate, but Lysenin lacks the selectivity function [1, 43]. Selectivity is an extremely important characteristic of ion channels that enables the cell to discriminate and control biomolecules exchange with its surroundings [4], in other words it is the transport of only a certain type of ions for maintaining the electrochemical gradient, whereas such a function would not be a stringent requirement when it comes to, for example, a pore-forming toxin (Lysenin) that kills its host cell by dissipating its electrochemical

gradient. The interaction between wild type pore-forming proteins and multivalent ions is not well documented [51, 61-64] and no feasible mechanisms have been advanced so far to explain it.

In contrast, ion channel regulation has been reviewed for decades [22, 65-68]. Based on the functional similarities between Lysenin and ion channels, one might assume similar mechanisms behind their interactions with multivalent ions. Ion-channel regulation by multivalent ions is a very complex process. Ligand-gated ion channels experience a conformational change upon the binding of a specific ligand [69], or the pathway of the ion channels is blocked by these ions [22].

The analysis of the macroscopic current through Lysenin channels during their dynamic interaction with multivalent ions offered some important clues to the mechanism of interaction. Reversibility of Lysenin channels, which showed fast recovery of conductivity upon the removal of the inhibitory ions, ruled out the possibility of permanent damage to the Lysenin channels or their expulsion from the supporting bilayers. This was key evidence on the gating process of Lysenin.

Furthermore, the graph of conductance inhibition displayed a fall-off shape with much higher sensitivity in the low concentration range, while the higher concentrations indicated saturation. As multivalent ion concentration increases, the probability of their time-interaction with the binding site increases until it reaches its maximum capacity of ions (saturation). At high concentration, saturation was observed as a flattening in response. This behavior indicates the presence of a binding site interacting with those multivalent ions, which is consistent with the previous findings in sec.4.5.

Another significant clue is the interaction between ions and Lysenin which can be considered electrostatic interaction. The different sensitivities of Lysenin to multivalent cations support such kind of interaction. The modulation of the voltage gating upon addition of multivalent ions and the competition between monovalent and multivalent ions for the binding site (sec.4.5) are strong evidence to propose electrostatic interaction.

The final shape and size of Lysenin channel after assembled in the BLM is unknown. The diameter of the entrance (mouth) of Lysenin pore was reported [40, 41] to be either (30 Å) or (47 Å), while the internal size of the pore (whether it is narrower or fatter) is for sure ambiguous. But based on the similarities between pore-forming proteins and ion channels, we may assume the same internal-structural size. The sizes of potassium ion channel gets narrower below the entrance of the pore [19, 31, 70, 71]. Accordingly, it is hypothesized that Lysenin channel follows the same sense and have a narrower pathway below its entrance. Taking in consideration the hydrated sizes of ions (lanthanides 18 Å in diameter), then blocking the pathway of Lysenin pore is a plausible mechanism. In fact, the experimental data is consistent with this mechanism either for divalent or trivalent ions without excluding other possible mechanisms.

However, it may still possible that Lysenin possesses multiple binding sites, and a cluster of ions could completely occlude the conducting pathway. Open current measurements performed on a large population of Lysenin channels could not offer further information to help in discriminating between various current-blockage mechanisms, so at this time of inquiry, analysis of the single-channel level was conducted.

Insertion of a small number of Lysenin channels into a planar BLM was performed by adding extremely small amounts of Lysenin, approximately 10 pM of final concentration, to the trans chamber while applying a negative voltage of -80mV across the membrane. After inserting

a small number of channels as illustrated in Figure 4.24-a, the trans chamber was flushed with about 30ml of fresh electrolyte in order to prevent any further insertion. The insertion of each channel changed the current by approximately -48 pA, as Figure 4.24-a depicts. Adding 300 μM of La^{3+} to both sides of the chamber decreased the open current in a stepwise manner, as shown in Figure 4.24-b.

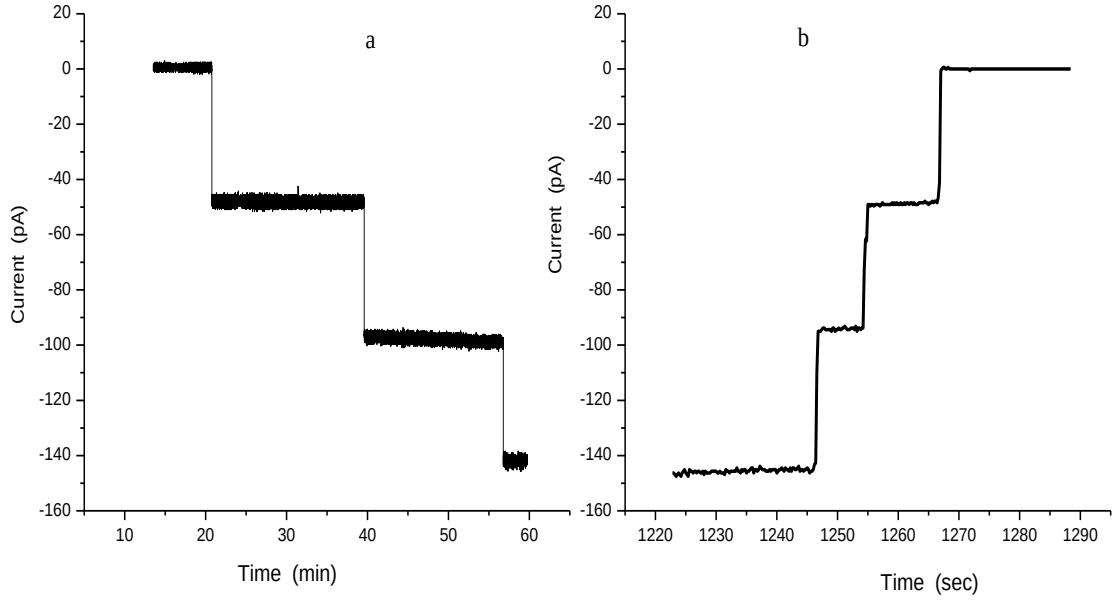

Figure 4.24: (a) The kinetic process of inserting three Lysenin channels in the BLM increased current in three discrete steps. (b) The inhibition of the current through these channels in a similar manner as they closed upon addition of La^{3+}. The noise was higher in (a), so the recorded line is thicker than (b).

This observation was crucial in establishing the mechanism of the dynamic interaction of Lysenin channels with multivalent ions. An eventual occlusion of the Lysenin channels by clusters of ions attached to multiple binding sites should produce a monotonical and gradual variation in the open current. From a thermodynamics standpoint the binding process is described in statistical terms and it is impossible for all the binding sites to be simultaneously

occupied and to produce a sudden and uniform change in the open current. The most probable mechanism compatible with the observed current variation, then, is the pore-blocking mechanism.

Since single channel analysis proved to be an excellent tool in deciphering the effect of La^{3+} on Lysenin channels, the experiment was repeated to analyze the influence of Ca^{2+} on the macroscopic currents through single channels. After inserting a few Lysenin channels into the BLM and adding 40 mM Ca^{2+} to the bulk solution, a high resolution current recording (-80 mV bias voltage) was performed. Although the initial salt concentration and voltage conditions were identical to the La^{3+} experiment, Ca^{2+} followed the same pattern but in smaller current steps, as Figure 4.25-b depicts. The changes in the open current were characterized as steps of approximately 22 pA, indicating partial closing of these channels.

The sub-closed state of conductance under the influence of divalent ions could be explained with two scenarios. The first would be that all individual channels went through single conformational transitions to sub-conducting states, that is

Four open channels ⟶ Four sub-conducting channels

The other scenario is that some channels remained in their open state while others closed partially before closing completely, or

Four open channels ⟶ {Two sub-conducting state ⟶ {Two non-conducting state

+ Two open channels} + Two open channels}

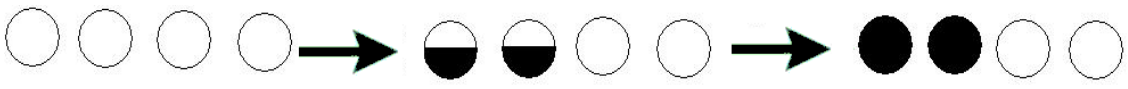

The first scenario of partial change for all channels is most probable. If the second scenario were true then eventually all channels would be switched to the fully closed state because divalent ions were still in the bulk and would continue to interact with Lysenin.

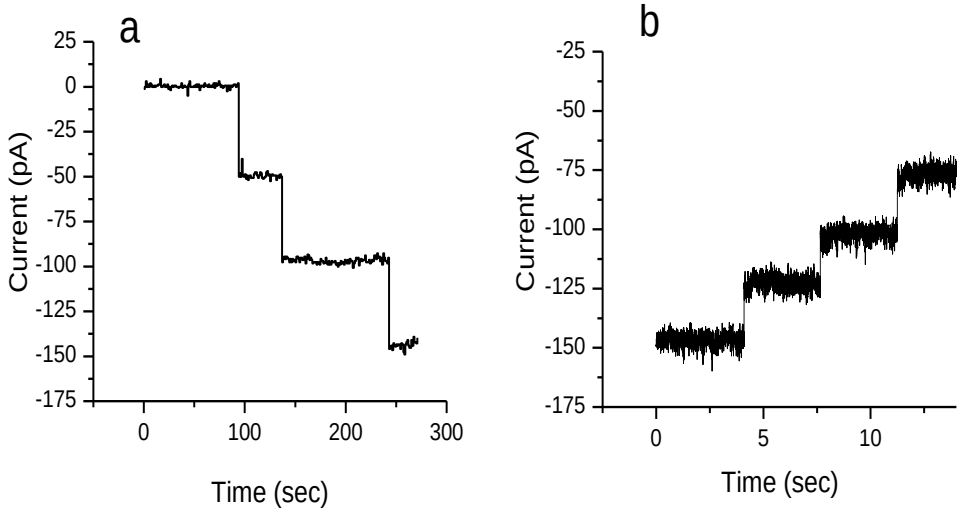

Figure 4.25: (a) The kinetic process of inserting three Lysenin channels in the BLM increased current in three discrete steps. (b) The addition of Ca^{2+} decreased open current in a similar manner to La^{3+} with approximately half amplitude steps indicating a sub-conducting state. The noise was higher in (b), so the recorded line is thicker than (a).

The binding of divalent ions (3-8 Å in diameter) produced small transients in the open current but their amplitudes were extremely low as illustrated in Figure 4.25-b. It was proposed that the binding partially blocked the conducting pathway and reduced the current but the conductance was never completely nullified. The result of this experiment indicated that Ca^{2+} (6 Å in diameter) attached to the binding site, and accordingly the pore was partially blocked as shown by the small decreased steps in the current.

The differences in sensing various divalent or various trivalent ions by Lysenin (see Figures 4.7, 4.8 and 4.9) could be due to the ion-binding affinity between these ions and the binding site of Lysenin. The electric field across a Lysenin channel is on the order of 10^7 V/m which is a massive field, and may force the ions inside the channel to leave the binding site, unless there was an interaction process between the binding site and the ions. The behavior of Lysenin channels under the influence of ions indicated a dynamic interaction between the channels and the binding site, which was governed by the ion-protein binding affinity.

The investigation of the dynamic interaction between ions and Lysenin indicate the pore-blocking mechanism because it is consistent with the experimental data. However, this does not rule out the possibility that other mechanisms, such as, conformational change, were playing a role in limiting transport. However, we could say that the hydrated ions were playing a role.

Chapter 5 Modeling the Dynamic Interaction between Ions and Lysenin

5.1 Kinetics of the Dynamic Interaction between Lysenin and Ions

The history of biological-ion channel modeling goes back more than 100 years [35]. In the beginning of the premolecular era, the analysis of those simple models was considered the main source of information on channel structure. Early suggested models depended mainly on the simplified approximations that lead to mimic the function of the channel.

As science advanced, more molecular biological structures became known; and through the use of computer software the modeling of these structures has achieved great progress [72]. Modeling enhances our understanding of the structure-function relation of different proteins, especially ion channel or pore-forming proteins.

In this work, a mathematical model is proposed for Lysenin channel's kinetic process, which assumes based on the reaction-rate approach [72] that the binding site of Lysenin dynamically interacts with metal ions. The ions jump between the binding site and the bulk solution according to a rate constant that governs the kinetic process. The closing of Lysenin channels (or the sub-closing) is considered to be a forward reaction process between Lysenin and multivalent ions, while the reopening of these channels is considered to be a backward reaction of the kinetic process.

Single channel experiments were performed in order to investigate the dynamic process of the interaction between ions and a Lysenin channel. A minute amount of Lysenin was added to a BLM formed in 150 mM KCl buffered with 20 mM HEPES/KOH. A single channel was observed to be inserted in the BLM (48 pA) as illustrated by Figure 5.1. A small concentration of La^{3+} was added (60 μM) to interact with this channel so it would not induce sustained full

closing. The purpose of adding La^{3+} was to examine the dynamic interaction between metal ions and Lysenin. According to Figure 5.1, the fluctuation of the recorded current indicated that the Lysenin channel switched from its open state (-48 pA) to partially closed one (-15 pA) for some time as a result of the dynamic interaction between La^{3+} and the binding site; then the La^{3+} left the binding site, resulting in reopening the channel again, and so on. The behavior of the channel, in terms of the current fluctuations, provided extra evidence of the dynamic interaction between the binding site of the Lysenin channel and the metal ions.

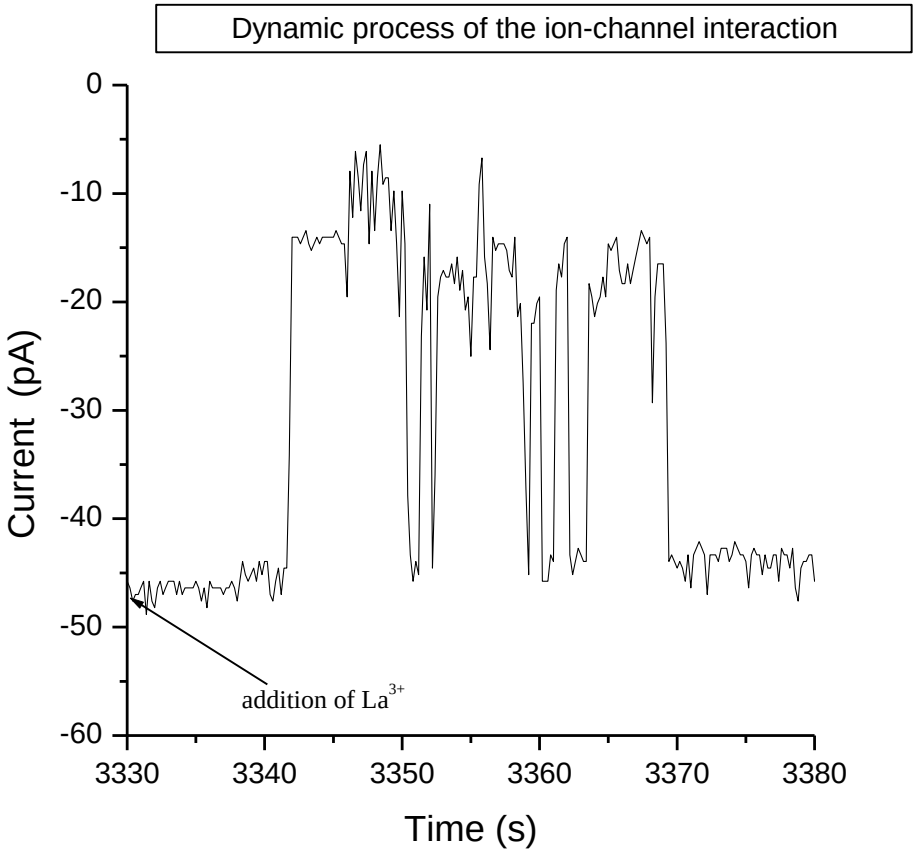

Figure 5.1: La^{3+} ions interacted with Lysenin channel and caused a fluctuation in current revealing the dynamic interaction between them. The status of the channel was switched between partially closing and reopening according to the dynamic interaction with ions.

The purpose of modeling Lysenin's interaction with multivalent ions was to understand and predict their influence on the Lysenin's macroscopic conductance and measure the equilibrium rate constants of these dynamic interactions.

The model was established by estimating the macroscopic current response to different concentrations of multivalent ions in single-channel analysis. In addition, the bulk conductivity, applied voltage and the channels' geometry were considered in this model.

Some essential assumptions and approximations were proposed in order to build this model: Lysenin-ion interaction was assumed to be a single step, the concentration of ions was approximately constant, and all ions were able to pass through the Lysenin channel.

5.2 Mathematical Model for Ligand Gating of Lysenin Channels

According to the experimental results, regarding dynamic interaction (Figure 5.1) and reversibility shown in Figure 4.23 and), the interaction between multivalent ions and Lysenin was reversible. Reversibility as a process can be defined in terms of forward and reverse reactions of a dynamic equilibrium process between ions and Lysenin. The significance of this approach is that it will enable us to estimate the equilibrium rate constants for these reactions.

5.2.1 Equilibrium Rate Constant

The equilibrium rate constant is defined as: $K = \frac{k_f}{k_b}$, where

k_f is the forward rate constant

k_b is the back (reverse) rate constant

For the general elementary reaction $\mathrm{A} + \mathrm{B} \rightleftharpoons_{k_b}^{k_f} \mathrm{AB}$

The rate laws for the forward and reverse reactions are [34]

$\mathrm{r}_f = \mathrm{k_f}[\mathrm{A}]^{\varepsilon}[\mathrm{B}]^{m}$, $\mathrm{r}_b = \mathrm{k_b}[\mathrm{AB}]^{\gamma}$, and at equilibrium $\mathrm{r_f} = \mathrm{r_b}$, so

$$K = \frac{\mathrm{k_f}}{\mathrm{k_b}} = \frac{[\mathrm{AB}]^{\gamma}}{[\mathrm{A}]^{\varepsilon}[\mathrm{B}]^{m}} \qquad 5.1$$

ε *and* m are integers or half integers and the reaction is said to have order "ε" with respect to A, or order "m" with respect to B [34].

The experimental results revealed that the interaction between Lysenin and multivalent ions switched Lysenin to either a sub-closed state with divalent ions, or a fully closed state with trivalent ions. Even for higher degree ions than trivalent (n>3) the interaction must remain within these two possibilities.

That is

Open channels + divalent ions $\rightleftharpoons$ sub-closed channels, or

Open channels + trivalent ions $\rightleftharpoons$ fully closed channels

Let us introduce the following parameters:

$\mathrm{N_0(t = 0)}$ is the number of open channels before adding multivalent ions $=$ constant

$\mathrm{N_1(t)}$ is the number of open channels afteradding multivalent ions

$N_2(\mathrm{t})$ is the number of sub $-$ closed channels after adding divalent ions,

or the number of the fully $-$ closed channels after adding trivalent ions

It is clear that at any time

$$\mathrm{N_0(t = 0) = N_1(t) + N_2(t)} \qquad 5.2$$

Let x be the ratio of the number of the sub-closed (or fully closed) channels to the number of open channels as shown in Equation (5.3).

$$x = \frac{N_2(t)}{N_0(t=0)} \quad 5.3$$

The interaction of Lysenin with "*m*" multivalent ions ($m\mathrm{Me}^{n+}$) can be expressed as:

$$N_1(t) + m\mathrm{Me}^{n+} \underset{k_b}{\overset{k_f}{\rightleftharpoons}} N_2(t) \quad 5.4$$

According to Equation (5.1), the equilibrium rate constant in Equation (5.4) can be written as:

$K = \frac{[N_2]}{[N_1][Me^{n+}]^m}$, or

$$K = \frac{N_2}{N_1[Me^{n+}]^m} \quad 5.5$$

Plug Equation (5.2) in Equation (5.5), then

$$K = \frac{N_2}{(N_0 - N_2)[\mathrm{Me}^{n+}]^m} \quad 5.6$$

Now plug Equation (5.3) into Equation (5.6)

$K = \frac{N_0 x}{(N_0 - N_0 x)[\mathrm{Me}^{n+}]^m}$, or

$K = \frac{x}{(1-x)[Me^{n+}]^m}$, then

$$x = \frac{K[Me^{n+}]^m}{1 + K[Me^{n+}]^m} \quad 5.7$$

5.2.2 Electric Current Before and After Adding Multivalent Ions

Before adding Me^{n+}:

Let us define

I_0 is the total current through all channels before adding Me^{n+}

I_s is the current through a single open channel before adding Me^{n+}, then

$$I_0 = N_0 I_s = N_0 w \kappa_0 V \quad (5.8)$$

Where "w" is the area per unit length of the channel (channel's geometry)

κ_0 is the specific conductivity of the bulk before adding Me^{n+}

V is the bias voltage across the channel

After adding Me^{n+}:

Let us define

I is the total current through all channels after adding Me^{n+}

I_1 is the current through an open channel during the ineraction with Me^{n+}

I_2 is the current through a sub − conducting channel during the ineraction with Me^{n+}, then

$$I = N_1 I_1 + N_2 I_2 \quad (5.9)$$

But $I_2 \propto I_1$, then

$$I_2 = f\, I_1 \quad (5.10)$$

$f = 0 \Rightarrow$ all channels are closed, which is the case for trivalent ions. In general for any partially conducting (sub-closed) state, this value should be $0 < f < 1$, which is the case for the interaction of Lysenin with divalent ions.

By plugging Equation (5.10) in Equation (5.9) we get

$\mathrm{I} = \mathrm{N}_1\mathrm{I}_1 + \mathrm{N}_2 f \mathrm{I}_1$ and with the use of Equation (5.2) and Equation (5.3)

$$\mathrm{I} = \mathrm{I}_1\mathrm{N}_0\{1 - (1 - f)\mathrm{x}\} \qquad 5.11$$

If we assume that the channels' geometry is not going to be affected by the interaction with multivalent ions, that is "w" is going to be the same before and after adding $\mathrm{Me}^{\mathrm{n}+}$, then the current "$\mathrm{I}_1$" can be expressed as

$$\mathrm{I}_1 = \mathrm{wV}\kappa_1 \text{ , where} \qquad 5.12$$

κ_1 is the specific conductivity after addition of $\mathrm{Me}^{\mathrm{n}+}$, and by plugging Equation (5.12) in Equation (5.11) and divide Equation (5.11) by Equation (5.8) we get

$\frac{I}{I_0} = \frac{N_0 w V \kappa_1\{1 - (1 - f)x\}}{N_0 w V \kappa_0}$, which can be reduced to

$$\frac{\mathrm{I}}{\mathrm{I}_0} = \frac{\kappa_1\{1 - (1 - f)\mathrm{x}\}}{\kappa_0} \qquad 5.13$$

The electrical conductivity of the bulk solution after adding divalent ions, such as Ca^{2+}, stays linear (see Figure 5.2) according to the following relationship:

$$\kappa_1 = \kappa_0 + \mathrm{b}[\mathrm{Me}^{\mathrm{n}+}] \qquad 5.14$$

where "b" is a constant that can be determined from the slope of the line.

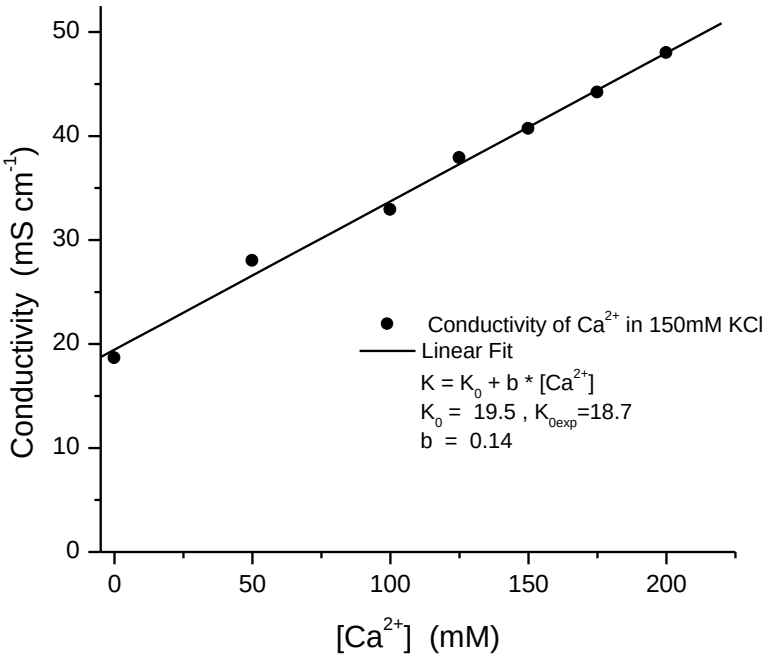

Figure 5.2: Addition of Ca^{2+} to a bulk of 150 mM KCl linearly increases the conductivity of the bulk. The linear fit gives the value of the parameter "b" which is the slope of line.

By plugging Equation (5.14) in Equation (5.13) we get

$\frac{I}{I_0} = \frac{\kappa_0 + b[Me^{n+}]}{\kappa_0}\ (1-(1-f)x)$, by using Equation (5.7) we get

$$\frac{I}{I_0} = \frac{\kappa_0 + b[Me^{n+}]}{\kappa_0}\left\{\frac{1+fK[Me^{n+}]^m}{1+K[Me^{n+}]^m}\right\} \qquad 5.15$$

For low concentration of multivalent ions i.e. $[Me^{n+}]\ in\ \mu M$ then

$b \approx 0$ and Equation(5.15) becomes

$$\frac{I}{I_0} = \frac{1+fK[Me^{n+}]^m}{1+K[Me^{n+}]^m} \qquad 5.16$$

If we have full closure then $f = 0$ and this equation reduced to

$$\frac{I}{I_0} = \frac{1}{1 + K[Me^{n+}]^m} \qquad 5.17$$

The parameters in Equation 5.15 can be defined as:

I is the total current through all channels after adding Me^{n+}

I_0 is the total current through all channels before adding Me^{n+}

κ_0 is the specific conductivity of the bulk before adding Me^{2+}

b is the slope of the conductivity linear relation after adding Me^{2+}

K is the equilibrium rate constant

f is a fraction that describes the status of the channel $0 < f < 1$

n is an integer denotes the charge of multivalent ions

$[Me^{n+}]$ is the concentration of multivalent ions

m is the cooperativity number which is the required number of ions interacting with Lysenin to cause either full or partial closure.

Chapter 6 Comparison between Theory and Experiment

The purpose of fitting the experimental data to the model was to provide evidence for an explanation of the type of interaction between the binding site and the ions. In addition, the intent was to reveal the mechanism of gating of the Lysenin channel. The strength of the dynamic interaction of ions with Lysenin was related to the estimated values of the equilibrium rate constant "*K"*.

6.1 Fitting Data of Divalent Metal Ions

Lysenin channels sensed divalent ions differently as shown in Figures (4.7-4.8). The fraction number "*f"*, which described the status of the channel according to its definition in Equation (5.10), was estimated by considering the best fit of the experimental data using the mathematical model (Equation 5.15). The model estimated the values of the equilibrium rate constants "*K"* for each dynamic interaction, while the cooperativity number "*m"* was chosen to be one for all divalent ions except for copper, where it was proposed to be two according to the case study described in section 8.1.

The variables that appeared in the model were taken as follows: $\kappa_0 = 18.7$ mS/cm, and b=0.14 for all other divalent ions as illustrated in Figure 5.2, where the slope "b" was calculated from the linear relationship of conductivity versus concentrations of divalent ions.

The experimental results of the dynamic interaction between Lysenin and divalent ions were fit to the model (Equation 5.15) and showed an excellent prediction as illustrated in Figures 6.1-6.8.

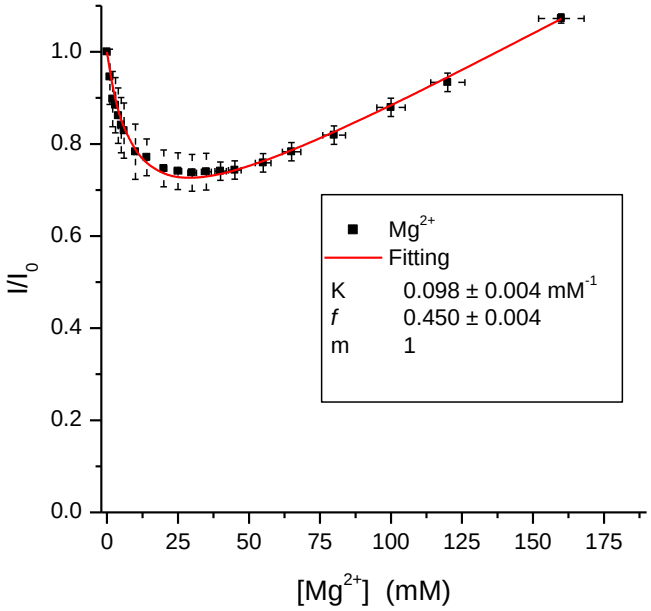

Figure 6.1: The model successfully predicted a stable sub-conducting state of Mg^{2+}. As indicated by the graph, the macroscopic current decreased at low divalent ion concentrations was followed by a linear increase due to the subsequent increase in conductivity of the bulk.

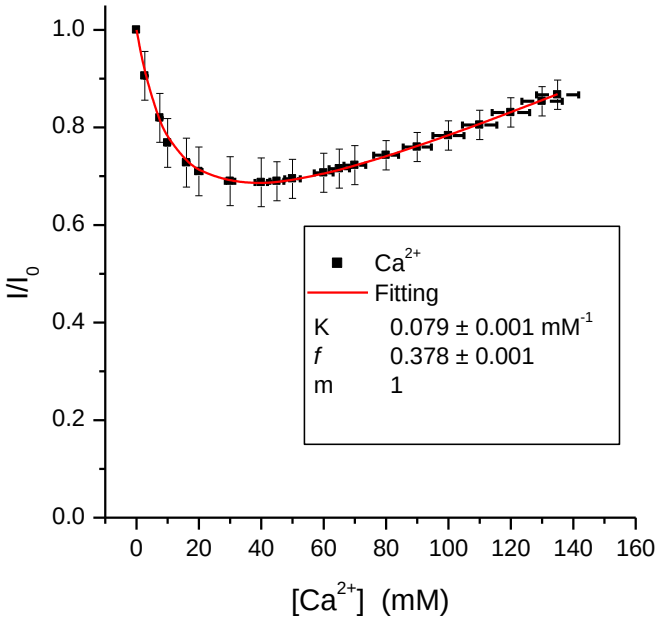

Figure 6.2: Fitting the experimental data of Ca^{2+}.

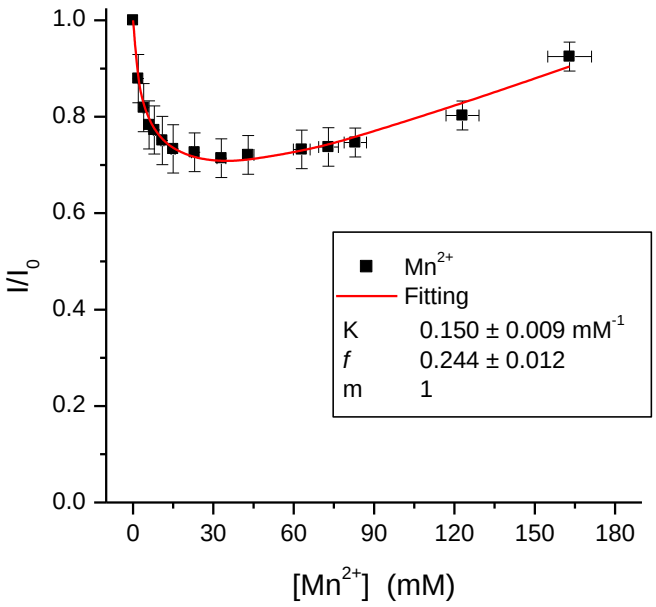

Figure 6.3: Fitting the experimental data of Mn^{2+}.

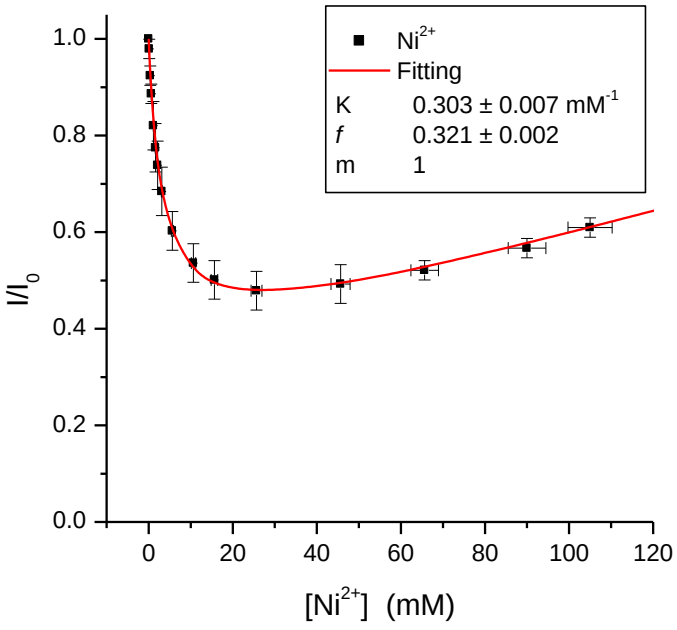

Figure 6.4: Fitting the experimental data of Ni^{2+}.

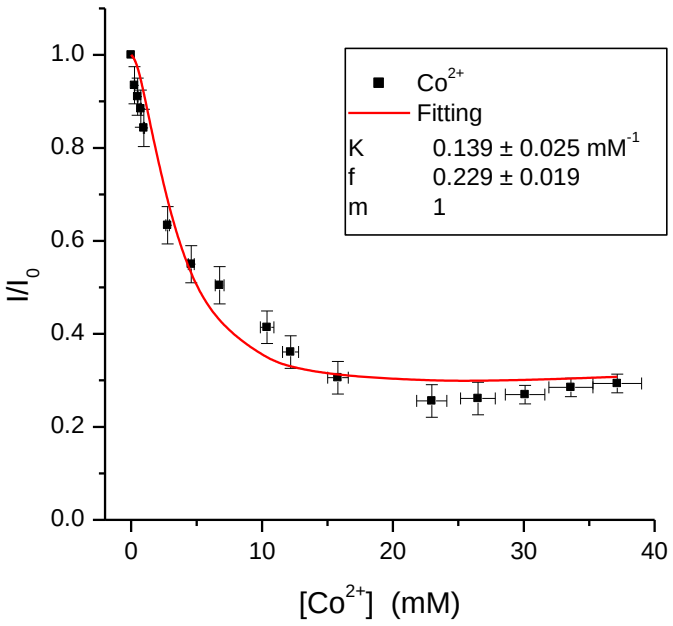

Figure 6.5: Fitting the experimental data of Co^{2+}.

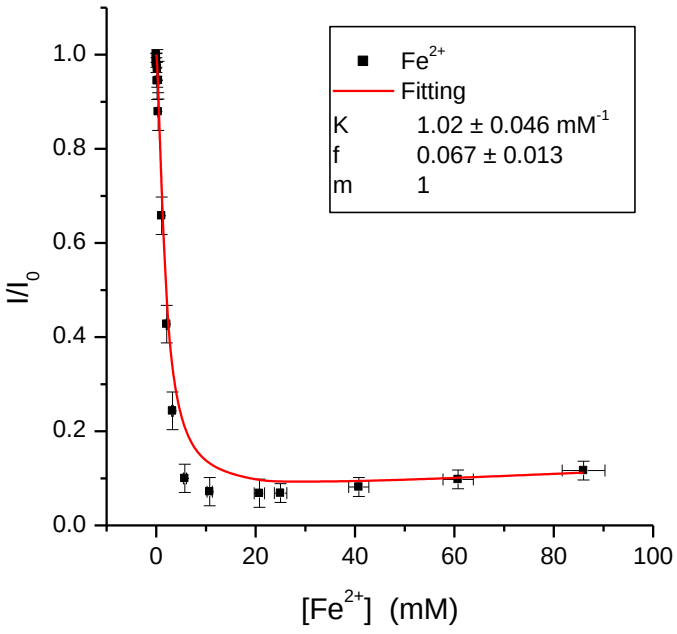

Figure 6.6: Fitting the experimental data of Fe^{2+}.

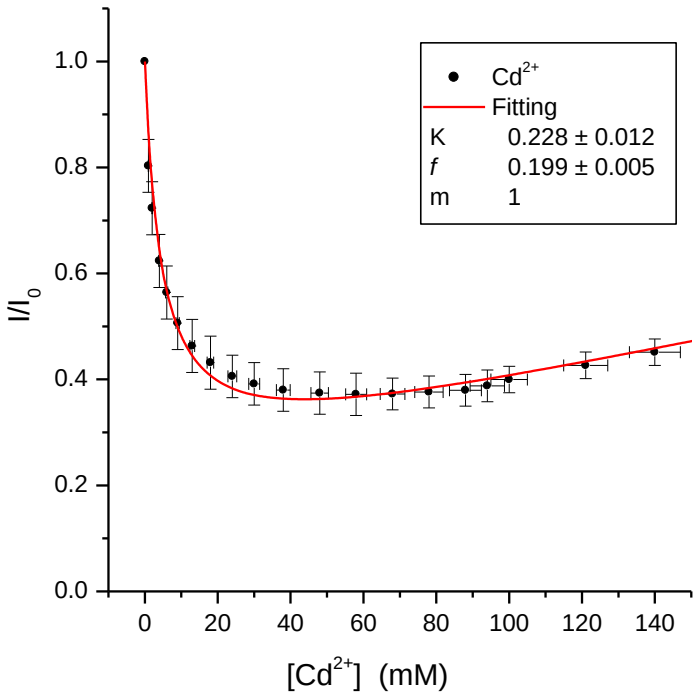

Figure 6.7: Fitting the experimental data of Cd^{2+}.

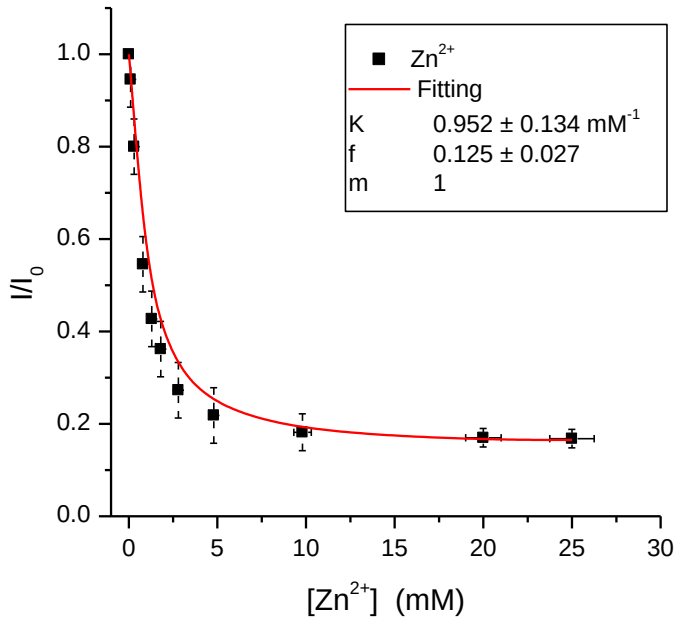

Figure 6.8: Fitting the experimental data of Zn^{2+}.

The estimated values of the equilibrium rate constants along with the fraction numbers "*f*" of divalent ions are enumerated in Table 4. The different values of the equilibrium rate constants are related to the ion-binding affinity between the ions and Lysenin.

Table 4: predicted values of equilibrium rate constants and the fraction numbers "*f*" for divalent ions.

Divalent ion	***f***	**Equilibrium rate constant** ***K* in mM^{-1}**
Mg^{2+}	0.450	0.098
Ca^{2+}	0.378	0.079
Mn^{2+}	0.244	0.150
Ni^{2+}	0.321	0.303
Cd^{2+}	0.199	0.228
Co^{2+}	0.229	0.139
Zn^{2+}	0.125	0.952
Fe^{2+}	0.067	1.02

6.2 Fitting Data of Trivalent Metal Ions

The effect of the trivalent ions was uniform in that they caused a full closure of Lysenin channels. Accordingly the fraction number "*f=0",* and the very low concentration "μM" indicates no significant increase in the bulk concentration (that is b≈0) of all tested trivalent ions.

This allows simplification of the model and we can use Equation (5.17) below to fit the data for trivalent ions $\frac{I}{I_0} = \frac{1}{1+K[Me^{n+}]^m}$

The dynamic interaction of Lysenin and aluminum trivalent experimental results were fit to the model and showed an excellent prediction as illustrated in Figure 6.9

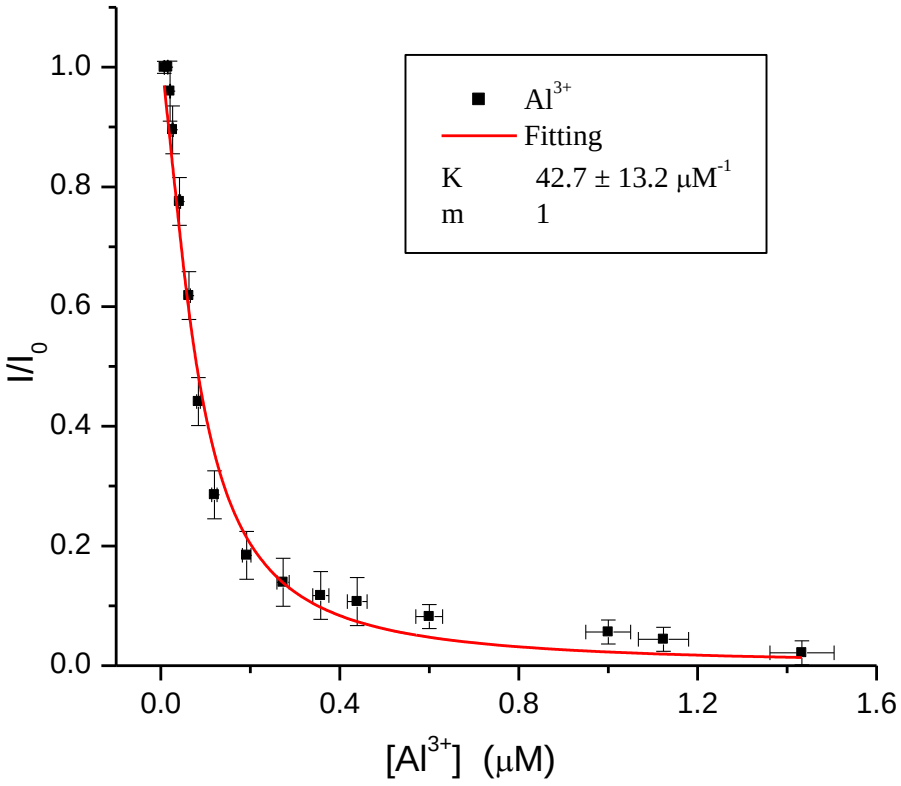

Figure 6.9: The model successfully predicted a non-conducting state. As indicated by the graph, the macroscopic current decreased at very low aluminum trivalent ion concentrations.

The fitting graphs of other trivalent ions to the model are shown in Figures 6.10-6.14, and the estimated values of the equilibrium rate constant for each trivalent ion are listed in Table 5, where it can be noticed their decrease with Lysenin's sensitivity to them.

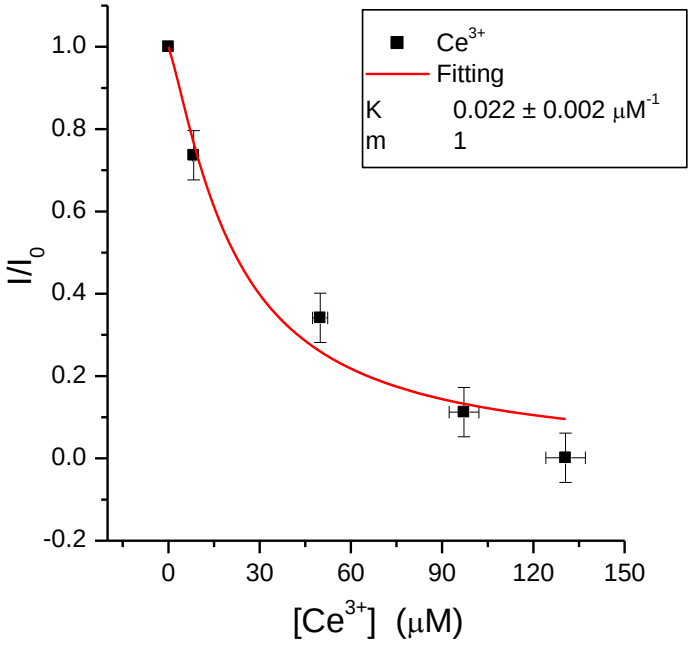

Figure 6.10: Fitting the experimental data of Ce^{3+}.

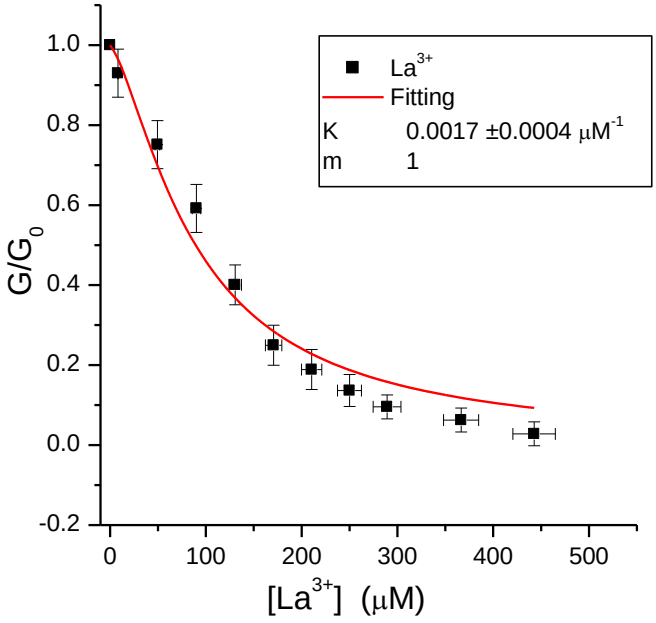

Figure 6.11: Fitting the experimental data of La^{3+}.

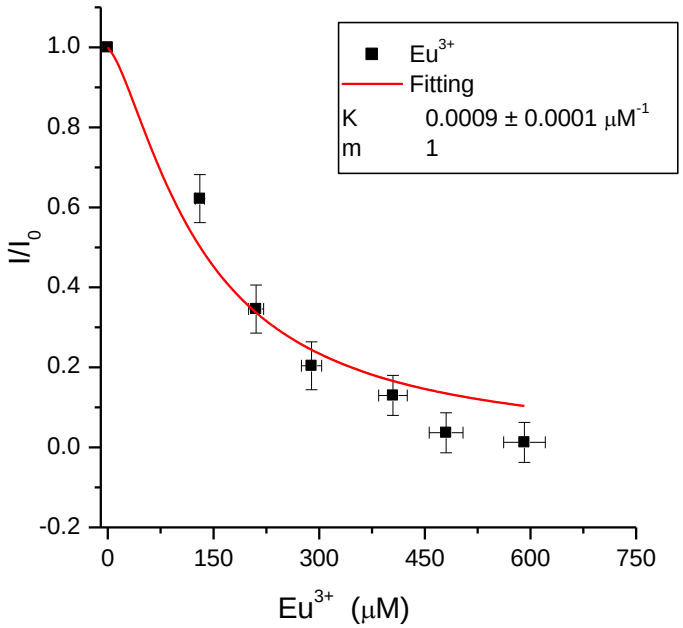

Figure 6.12: Fitting the experimental data of Eu^{3+}.

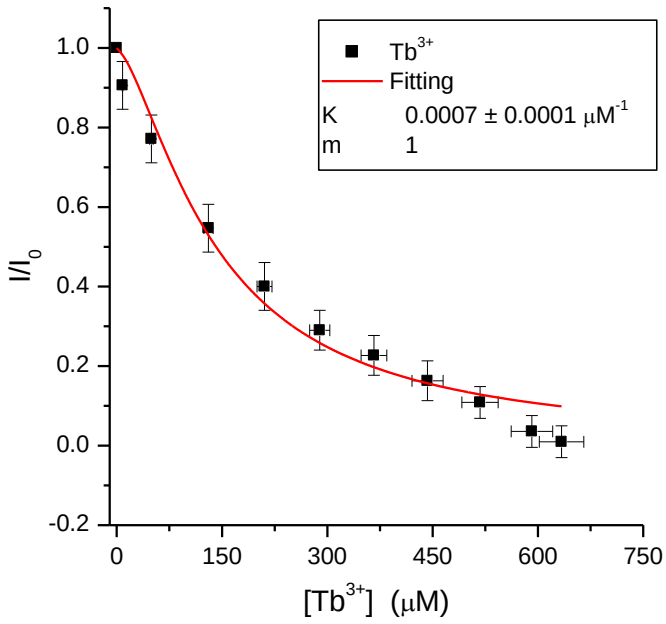

Figure 6.13: Fitting the experimental data of Tb^{3+}.

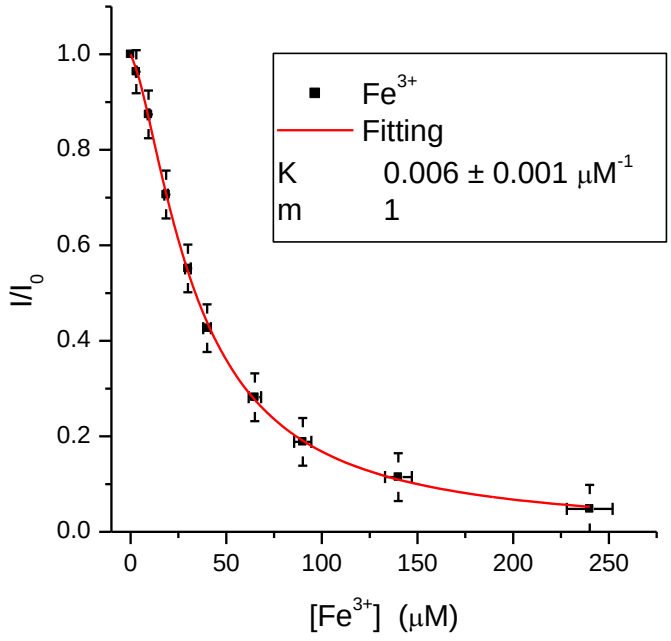

Figure 6.14: Fitting the experimental data of Fe^{3+}.

Table 5: predicted values of equilibrium rate constants for trivalent ions

Trivalent ion	**Equilibrium rate constant** ***K*** **in** μM^{-1}
Al^{3+}	42.70
Ce^{3+}	0.0220
Fe^{3+}	0.0060
La^{3+}	0.0017
Eu^{3+}	0.0009
Tb^{3+}	0.0007

6.3 Fitting the Data for High Monovalent Ion Concentration

The experimental data sec.4.5.2 that considered the competition between monovalent and trivalent ions was also fitted by using the proposed model (Equation 5.17). The model predicted the values of "K" where it decreased with increasing monovalent ion concentration (Figures 6.15-6.19). The ratio of trivalent to monovalent ions was kept the same as monovalent ion concentration increased which was considered as evidence on the competition for the binding site between monovalent and trivalent ions. The general trend, of Lysenin's conductance with trivalent ions in the presence of different concentrations of monovalent ions, was that Lysenin turned to be less sensitive to trivalent at high monovalent ion concentrations. Being heavily occupied by monovalent ions, the electrostatic interaction between the binding site and trivalent ions (Ce^{3+}) was reduced, which eventually minimized their probability of binding.

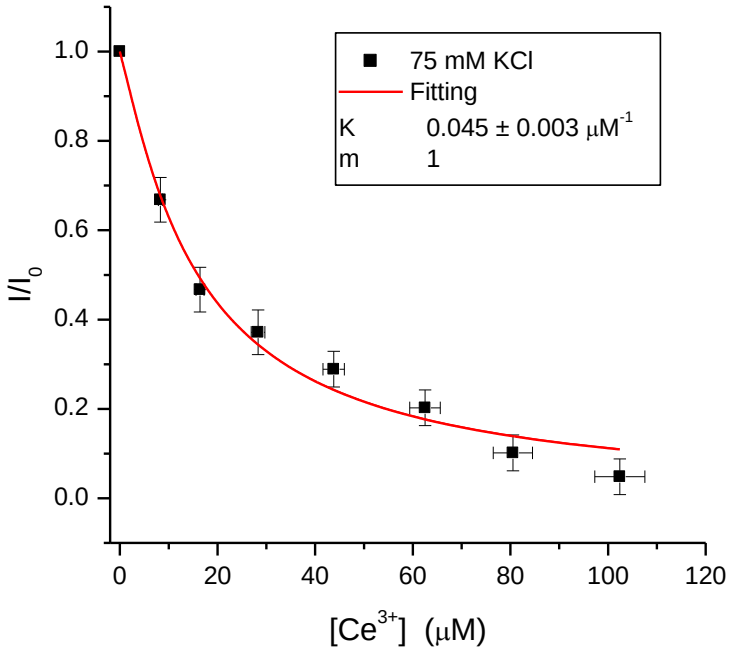

Figure 6.15: Fitting the experimental data of Ce^{3+} at 75 mM KCl.

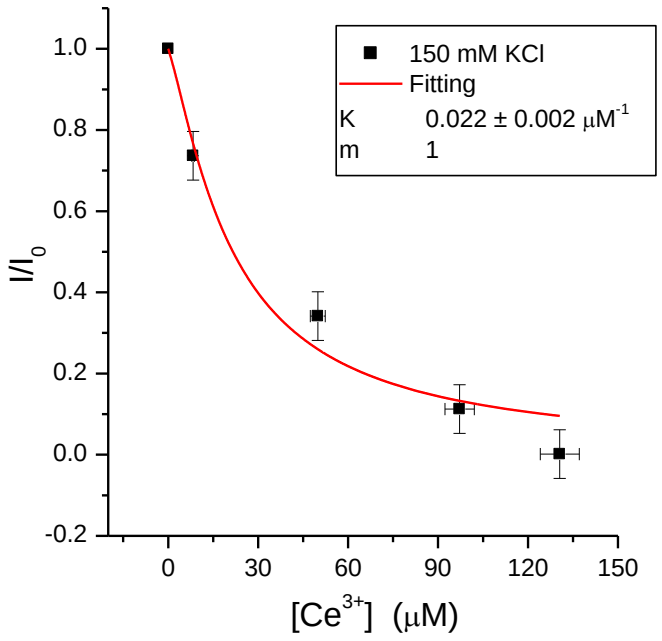

Figure 6.16: Fitting the experimental data of Ce^{3+} at 150 mM KCl.

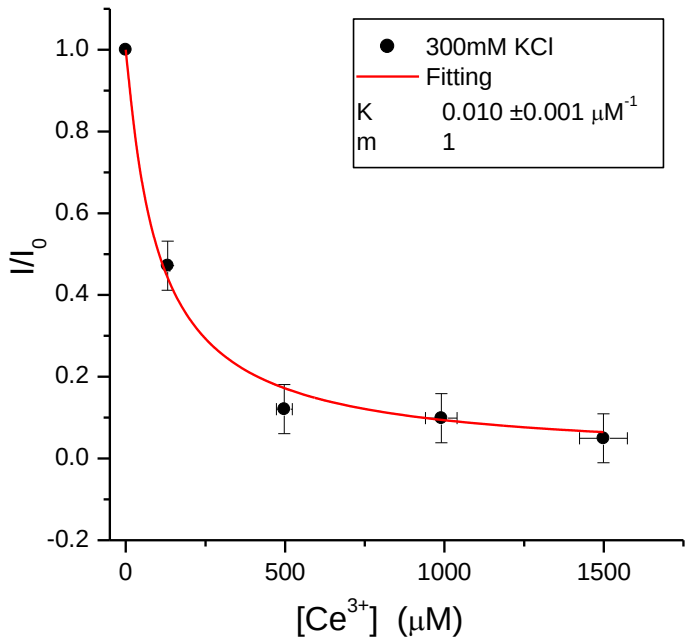

Figure 6.17: Fitting the experimental data of Ce^{3+} at 300 mM KCl.

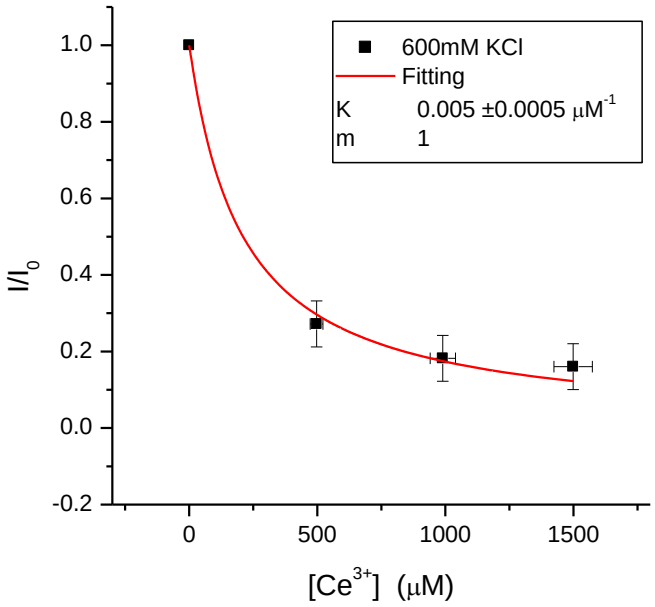

Figure 6.18: Fitting the experimental data of Ce^{3+} at 600 mM KCl.

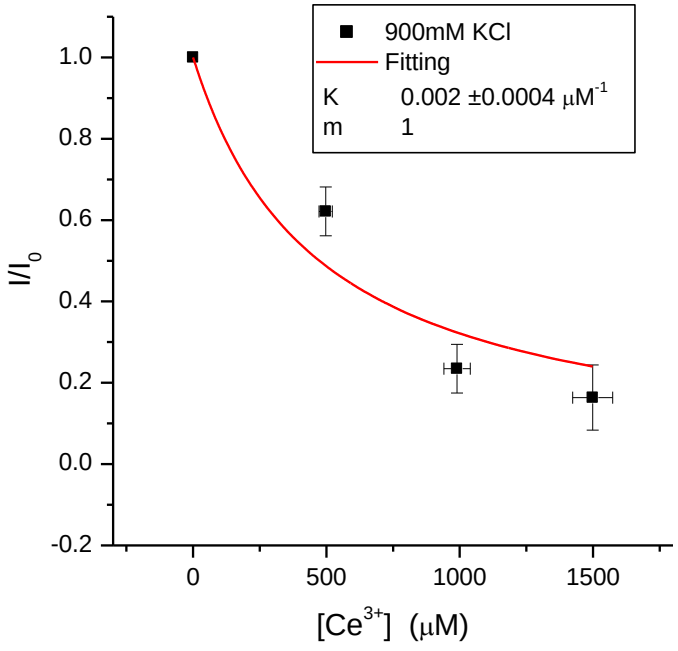

Figure 6.19: Fitting the experimental data of Ce^{3+} at 900 mM KCl.

Chapter 7 Conclusions

The main objective of this study was to investigate the mechanism of gating of Lysenin as a pore-forming toxin under the influence of multivalent ions, and to further explore the potential of this setup for use in biosensing applications. This work added useful scientific information to previous studies in the field of ligand gating and its uses in biosensing applications.

In the conducted experiments, Lysenin gated noticeably under the influence of most divalent ions, and fully closed when interacting with trivalent metal ions. Lysenin's voltage-gating process, which was observed in the positive voltage range, indicated that each Lysenin channel could have what is called a voltage sensor. Accordingly, the dynamic interaction between Lysenin and the external electric field appeared to be electrostatic. On the other hand, Lysenin channels did not show any voltage-gating when negative voltages were applied, remaining in their open state over the entire negative voltage range. The open state of Lysenin channels at negative voltages provided the ideal conditions for the investigation of the electrostatic interaction between Lysenin's binding site and multivalent ions. The experimental data was consistent with a model that assumed that binding site was a negatively charged region inside the lumen of the channel.

The analytical response of the conductance of Lysenin channels was not the same for divalent and trivalent ions. Trivalent metal ions approximately inhibited the transport through the Lysenin channels by blocking their open pathway, which appeared as discrete steps. The experimental data was also consistent with a pore-blocking mechanism, but did not exclude the role of additional mechanisms such as conformational changes. The hydrated sizes of the ions relative to

the size of the pore supported this hypothesis. The size of the charge was not the only reason for ligand gating; in addition, ionic size and the ion-binding affinity which led to the ligand gating mechanism (pore-blocking).

The suggested mathematical model was built according to a pseudo-first order kinetic process based on the dynamic interaction process between the ions and Lysenin's binding site. The model predicted successfully the behavior of Lysenin under the influence of different multivalent ions. Upon their interaction, the equilibrium rate constant was estimated by fitting the experimental data to the model. The experimental data were fitted successfully according to the proposed model, where it follows the behavior of Lysenin under the influence of different multivalent ions and concentrations. The data and model together provided values of the equilibrium rate constants of each multivalent ion, reflecting the channel's sensitivity to these ions.

Reversibility as a fundamental feature separates multiple-use sensors from single-use probes. Additionally, the Lysenin-BLM setup could be used to detect and distinguish between chelators and precipitators such as detecting phosphate in water samples. The noted reversibility has profound implications for the possibility of Lysenin's use in biosensing purposes. The distinctive conductance changes of this protein's channels could make it a novel biosensor for multivalent ions, and its reversibility would allow the analysis of multiple samples with one sensing system.

Lysenin was the most sensitive toward aluminum trivalent ions. The sensitivity of Lysenin to multivalent ions indicated its potential for use as a sensor for the detection of metal ions in biological samples. As a sensor we found that the Lysenin's sensitivity to multivalent ions increased for low monovalent ion concentration.

Chapter 8 Future Work

8.1 Full Closing versus Partial Closing: a Cu^{2+} Study

The conducted experiments, under the same conditions (voltage and resolution), showed a one-step full closing state for La^{3+} and a one-step partially closing state for Ca^{2+} divalent ions [51]. All tested trivalent ions followed the same pattern, in which they caused direct closure of the open channel in one step; but some divalent ions such as Cu^{2+} did partially close the channel not in one step but rather in an additional transient step.

It was hypothesized that a single trivalent ion was interacting with each Lysenin channel's binding site and causing the channel to close. On the other hand, Lysenin demonstrated a lower and varied sensitivity to divalent ions, with its highest sensitivity to Cu^{2+} (Figure 8.1).

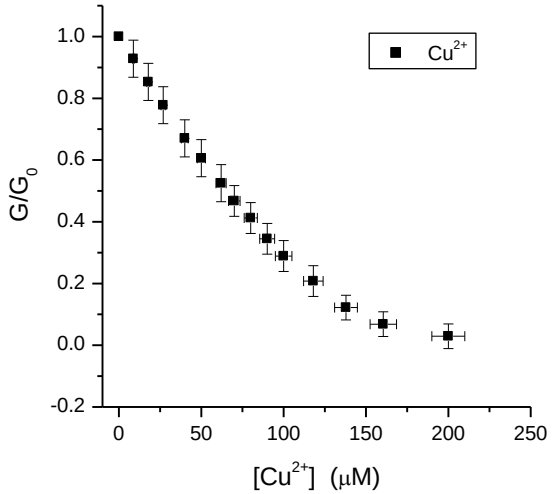

Figure 8.1: Among all tested divalent ions, Cu^{2+} demonstrated the greatest conductance reduction effect on Lysenin channels, requiring only 200 μM to almost completely shut them.

In order to understand the mechanism that ruled the dynamic interaction of Lysenin with copper divalent ions (Cu^{2+}), another experiment was conducted under the same conditions of voltage (-80mV bias voltage across the BLM) but with higher sampling rate (50 ms^{-1}). The addition of minute concentrations of Lysenin resulted in the insertion of only two channels (-48 pA each) in the BLM (Figure 8.2-a). The addition of 500 μM Cu^{2+} almost completely nullified the conductance at much lower concentrations than other divalent ions. The open channels switched to the closed state, but with an intermediate transient step as Figure 8.2-b depicts. Addition of EGTA with a final concentration of 10 mM recovered the initial (open) current, showing the same intermediate step for the reopening of channel as shown in Figure 8.2-c.

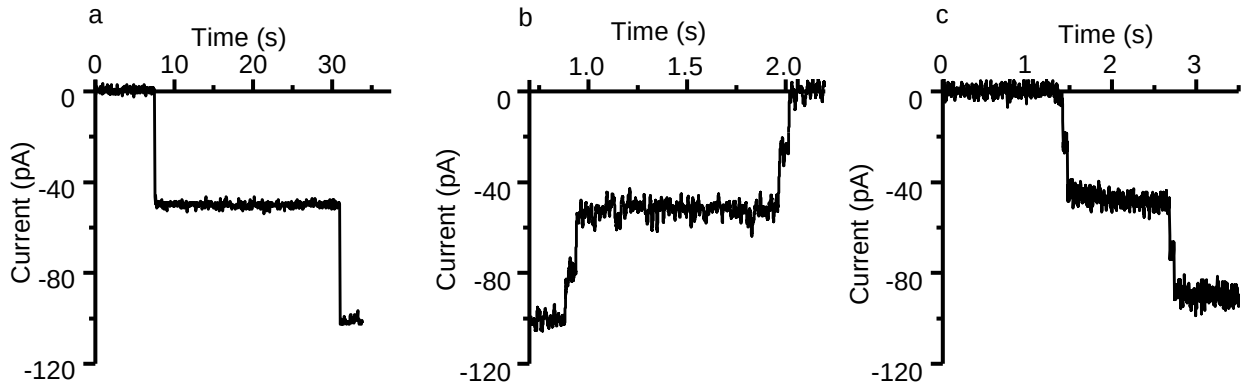

Figure 8.2: (a) Two Lysenin channels opening. (b) Full closure of Lysenin channels in two steps as induced by Cu^{2+} with brief transitional periods between them. (c) The channels reopen with similar transitional states upon Cu^{2+} chelation.

The full closure of Lysenin in the presence of Cu^{2+} through transient steps indicated that more than one Cu^{2+} was needed. If we assumed one single divalent ion per each intermediate step, then two ions would be required to switch each channel to its fully closed state. To determine the equilibrium rate constant of copper, the data (Figure 8.1) was fitted according to the proposed model as Figure 8.3 depicts, where "m" was chosen to be "2".

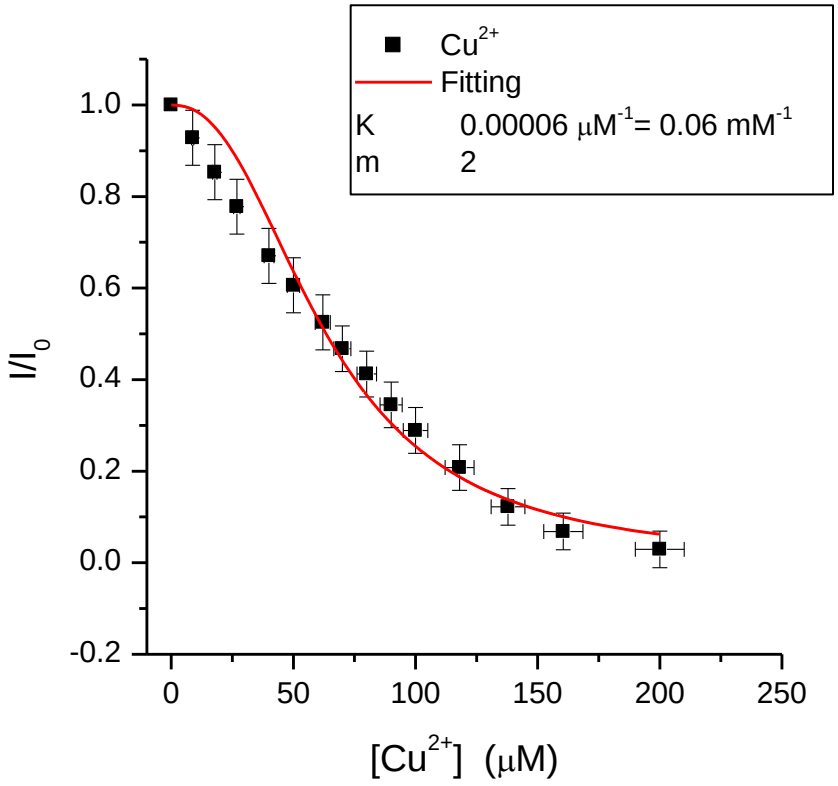

Figure 8.3: The model provided the value of the equilibrium rate constant of the interaction between copper divalent ions and the binding site of Lysenin.

8.2 The Influence of Lipid Composition on Lysenin Channel Insertion and Activity

The objective of such a plan is to expand our understanding of Lysenin channel activity. This investigation will have a direct impact on this research because it expands our knowledge of the protein-lipid interaction in the case of Lysenin and its influence on the mechanism of Lysenin channel gating.

The influence of lipid composition on the Lysenin functionality will be investigated from the electrophysiological measurements. Planar lipid bilayers composed of various lipid types including neutral, zwitterionic, saturated and non-saturated with different tail lengths will be formed by well-established painting or folding techniques. Channel insertion and functionalities such as voltage/ligand gating and selectivity will be analyzed by measuring the ionic currents under various environmental conditions.

8.3 Ion-Lipid Interaction Effect on Lysenin Channel Functionality

The objective of this investigation is to understand how ion-lipid interaction influences the activity of Lysenin channels.

Their ability to be used as tools to analyze biological structures and functioning was the main drive to use them in order to examine the activities of Lysenin. Their potential toxicological effect at higher concentrations in biological media, and their strong relevant and association with different biological functions is another reason to study ion-lipid interaction.

The investigation of ion-lipid interaction will answer some significant questions in this research such as, how ion-lipid interaction affects the oligomerization (channel insertion), the voltage and ligand gating of Lysenin channels.

Determining the nature of interaction between ions and lipids has a direct impact on explaining the interaction between ions and Lysenin that leads to better understanding of Lysenin's channel performance (mechanism).

8.4 Controlled Molecular Transport

The objective of this project is to produce a novel method for drug delivery by using liposomes. Lysenin is an excellent model for transmembrane complexes, transporters with multimeric organization, pore-forming toxins, and ion channels. A better understanding of their interactions and functionalities, and the novel approaches developed would be of large interest for a research team focused on physiological regulation, signaling, communication, and membrane trafficking. The implications of potential applicability in developing more efficient drug delivery systems and in designing host-specific antimicrobial peptides can have a lasting impact on human health.

Unlike many other pore-forming toxins, the Lysenin channel is regulated by voltage and ligand binding, and these abilities open new perspectives for controlled drug delivery. The proposed approach uses Lysenin channels to be reconstituted into spherical bilayer lipid membranes (liposomes) as shown in Figure 8.4 loaded with the drug of interest.

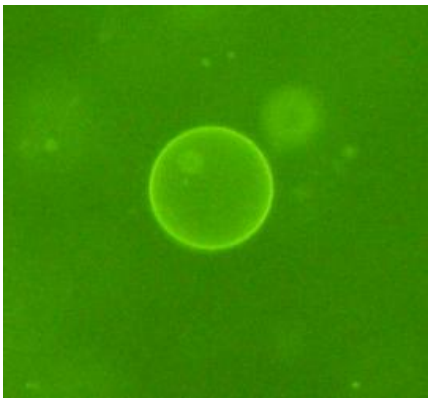

Figure 8.4: Fluorescent giant unilamellar vesicle (GUV).

Since Lysenin inserts constitutively open channels in artificial membranes at rest, the pores will be forced to close by creating a diffusion potential of positive value (> +20 mV) or by ligand binding such as Al^{3+}. The transmembrane voltage and the ligand concentration can be further controlled by external stimuli such as electric fields, temperature, or ionizing and non-ionizing radiation. A convenient externally-triggered change in transmembrane voltages or inhibitory-ligand concentrations reopens the channels and releases the load at the desired location in a controlled manner. This work puts together the significant results of this research on Lysenin in the service of a rapidly growing medical application field such as drug delivery.

8.5 Modulate the Charge on Lysenin Structure

The objective of this plan is to identify the amino acids that function in binding multivalent ions and also to reveal the role of the Lysenin's charge in its gating process (voltage/ligand).

The structure of Lysenin is still under investigation and locating the charged amino acids among its structure is of great interest to the people who are in this field of research. The investigation of the influence of protein's charge on its activity in the membrane leads to better understanding of both protein-lipid interaction and protein-protein interaction.

Modulating the charge of Lysenin will have a great impact on this research. It will enhance in determining the position and the structure of the binding site of Lysenin channels, which is responsible for the electrostatic interactions between Lysenin and ions.

A newly published structure of Lysenin [41] shows the presence of two acidic amino acids in a region of Lysenin that extends into the hydrophobic core of a lipid bilayer. Since charged amino acids are unlikely to be found at the lipid interface, it is hypothesized these two amino acids are facing the interior of the pore, which is consistent with the sensitivity of Lysenin to trivalent cations; conductance through Lysenin is blocked by addition of trivalent cations (Figure 4.9). In order to examine the role of these amino acids, site directed mutagenesis of Lysenin complementary DNA (cDNA) could be used to change the two acidic residues to neutral amino acids such as Alanine.

References

1. Ide, T., et al., *Lysenin forms a voltage-dependent channel in artificial lipid bilayer membranes.* Biochemical and Biophysical Research Communications, 2006. 346: p. 288-292.

2. Hubner, C.A. and T.J. Jentsch, *Ion channel diseases.* Human Molecular Genetics, 2002. 11(20): p. 2435-2445.

3. Garcia, M.L., *Ion channels: Gate expectations.* Nature, 2004. 430: p. 153-155.

4. Campbell, N.A., et al., *Biology*. 8th ed. 2008: Pearson.

5. Johnson, G.B., *The Living World*. 7th ed. 2012: McGraw-Hill.

6. Tien, H.T. and A. Ottova-Leitmannova, *Membrane Biophysics As Viewed From Experimental Bilayer Lipid Membranes*. 1st ed. 2000: Elsevier.

7. Becker, W.M., et al., *The World of the Cell*. 7th ed. 2009: Pearson Education Inc.

8. Lodish, H., et al., *Molecular Cell Biology*. 6th ed. 2007: W.H Freeman and Company.

9. Ishitsuka, R. and T. Kobayashi, *Lysenin: A new tool for investigating membrane lipid organization.* Anatomical Science International, 2004. 79: p. 184-190.

10. Atlas, R.M., *Principles of Microbiology*. 2nd ed. 1997: Wm. C. Brown.

11. Berg, J.M., J.L. Tymoczko, and L. Stryer, *Biochemistry*. 6th ed. 2007: W.H. Freeman and Company.

12. Gilbert, T.R., et al., *Chemistry*. 2nd ed. 2009: W.W. Norton&Company, Inc.

13. Akutsu, H. and j. Seelig, *Interaction of Metal ions with Phosphatidylcholine Bilayer Membrane.* Biochemistry, 1981. 20: p. 7366-7373.

14. Yamaji, A., et al., *Lysenin, A novel sphingomyelin-specific binding protein.* Journal of Biological Chemistry, 1998. 273(February 27): p. 5300-5306.

15. *Sigma-Aldrich.* http://www.sigmaaldrich.com.2012.

16. *Avanti Polar Lipids.* http://www.avantilipids.com.2012.

17. Chang, S.H., O.S. Andersen, and V. Krishnamurthy, *Biological Membrane Ion Channels Dynamics, Structure, and Applications*. 2007: Springer.

18. Schaefer, T.J. and R.W. Wolford, *Disorders of Potassium.* Emergency Medicine Clinics of North America, 2005. 23: p. 723-747.

19. Ashcroft, F.M., *Ion Channels and Disease*. 2000: Academic Press.

20. Kibble, J.D. and C.R. Halsey, *The Big Picture Medical Physiology*. 2009: McGraw-Hill.

21. Woolley, G.A. and T. Lougheed, *Modeling ion channel regulation.* Current Opinion in Chemical Biology, 2003. 7: p. 710-714.

22. Elinder, F. and P. Arhem, *Metal ion effects on ion channel gating.* Quarterly Reviews of Biophysics, 2004. 36(4): p. 373-427.

23. Silberberg, M.S., *Principles of General Chemistry*. 2007: Thomas D. Timp.

24. *Westfield State University.* http://www.westfield.ma.edu/cmasi/gen_chem1/nomenclature/periodic_table.html.2012.

25. Lippard, S.J. and J.M. berg, *Principles of Bioinorganic Chemistry*. 1994.

26. Manahan, S.E., *Environmental Chemistry*. 7th ed. 2000: Lewis Publishers.

27. Glusker, J.p., A.K. Katz, and C.w. Bock, *Metal Ions in Biological Systems.* The Rigaku Journal, 1999. 15: p. 8-16.

28. Chang, R., *Chemistry*. 10th ed. 2010: McGraw-Hill.

29. Kirberger, M., et al., *Statistical analysis of structural characteristics of protein Ca^{2+}-binding sites.* Bilo Inorg Chem, 2008. 13: p. 1169-1181.

30. Lopatin, A.N., E.N. Makhina, and C.G. Nichols, *The Mechanism of Inward Rectification of Potassium Channels: "Long-pore Plugging" by Cytoplasmic Polyamines.* J. Gen. Physiol, 1995: p. 923-955.

31. Jiang, Y., et al., *The open pore conformation of potassium channels.* Nature, 2002. 417: p. 523-526.

32. Tortora, G.J. and S.r. Grabowski, *Principles of Anatomy and Physiology*. 7th ed. 1993.

33. Harris, D.C., *Quantitative Chemical Analysis*. 8th ed. 2010: W.H. Freeman and Company.

34. Levine, I.N., *Physical Chemistry*. 6th ed. 2009: McGraw Hill.

35. Hille, B., *Ionic Channels of Excitable Membranes*. 2nd ed. 1992: Sinauer Associates.

36. Sherman-Gold, R., *The Axon Guide for Electrophysiology & Biophysics Laboratory Techniques*. 1993, Axon Instruments.

37. Parker, M.W. and S.C. Feil, *Pore-forming protein toxins: from structure to function.* Progress in Biophysics & Molecular Biology, 2005. 88: p. 91-142.

38. Fologea, D., et al., *Potential analytical applications of lysenin channels for detection of multivalent ions* Analytical and Bioanalytical Chemistry, 2011. 401: p. 1871–1879.

39. Aoki, T., et al., *Single channel properties of lysenin measured in artificial lipid bilayers and their application to biomolecule detection.* Proceedings of the Japan Academy, Ser. B, Physical and Biological Sciences, 2010. 86: p. 920-925.

40. Yamaji-Hasegawa, A., et al., *Oligomerization and pore formation of a sphingomyelin-specific toxin, lysenin.* Journal of Biological Chemistry, 2003. 278(June 20): p. 22762-22770.

41. Colibus, L.D., et al., *Structures of Lysenin Reveal a Shared Evolutionary Origin for Pore-Forming Proteins And Its Mode of Sphingomyelin Recognition.* Structure, 2012. 20: p. 1498-1507.

42. TJ, D., et al., *PDB2PQR: an automated pipeline for the setup, execution, and analysis of Poisson-Boltzmann electrostatics calculations.* Nucleic Acids Research 2004: p. W665-7.

43. Kwiatkowska, K., et al., *Lysenin-His, a sphingomyelin-recognizing toxin, requires tryptophan 20 for cation-selective channel assembly but not for membrane binding.* Molecular Membrane Biology, 2007. 24(2): p. 121-134.

44. Kiyokawa, E., et al., *Spatial and Functional Heterogeneity of Sphingolipid-rich Membrane Domains.* The Journal of Biological Chemistry, 2005. 280: p. 24072-24084.

45. Fologea, D., et al., *Controlled Gating of Lysenin Pores.* Biophysical Chemistry, 2010. 146: p. 25-29.

46. Delmouly, K., et al., *HEPES inhibits the conversion of prion protein in cell culture.* Journal of General Virology, 2011. 92: p. 1244-1250.

47. Matsuno, Y., et al., *single- Channel Recordings of Gramicidin at Agarose-Supported Bilayer Lipid Membranes Formed by the Tip-Dip and Painting Method.* Analytical Sciences, 2004. 20: p. 1217-1221.

48. Suzuki, H., et al., *Highly Reproducible Method of Planar Lipid Bilayer Reconstitution in Polymethyl Methacrylate Microfluidic Chip.* Langmuir, 2006. 22: p. 1937-1942.

49. Mueller, P., Rudin, D.O., Tien H.T. & Wescott, W.C, *Reconstitution of cell membrane structure in vitro and its transformation into an excitable system.* Nature, 1962. 194: p. 979-980.

50. Fologea, D., et al., *Multivalent ions control the transport through lysenin channels.* Biophysical Chemistry, 2010. 152: p. 40-45.

51. Fologea, D., et al., *Multivalent ions control the transport through lysenin channels.* Biophysical Chemistry, 2010. 152(1-3): p. 40-45.

52. Fologea, D., et al., *Bi-stability, hysteresis, and memory of voltage-gated lysenin channels.* Biochimica et Biophysica Acta, Biomembranes, 2011. 1808: p. 2933-2939.

53. Demo, S.D. and G. Yellen, *Ion effects on gating of the Ca^{2+} -activated K^{+} channel correlate with occupancy of the pore.* Biophysical Journal, 1992. 61(3): p. 639-648.

54. Fologea, D., et al., *Potential analytical applications of lysenin channels for detection of multivalent ions.* Analytical and Bioanalytical Chemistry, 2011. 401: p. 1871-1879.

55. Schow, E.V., et al., *Down-State Model of the Voltage-Sensing Domain of a Potassium Channel.* Biophysical Journal, 2010. 98: p. 2857-2866.

56. Smith, M.B. and J. March, *March's Advanced Organic Chemistry*. 6th ed. 2007: Willey-Interscience.

57. Persson, I., *Hydrated metal ions in aqueous solution: How regular are their structures?* Pure Appl.Chem., 2010. 82: p. 1901-1917.

58. Bancroft, D., et al., *The Low-Temperature Crystal Structure of the Pure-Spermine Form of Z-DNA Reveals Binding of a Spermine Molecule in the Minor Groove.* Biochemistry, 1994. 33: p. 1073-1086.

59. Shakor, A.-B.A., E.A. Czurylo, and A. Sobota, *Lysenin, a unique sphingomyelin-binding protein.* FEBS Letters, 2003. 542: p. 1-6.

60. Fernandez, J.A., et al., *Voltage- and cold-dependent gating of single TRPM8 ion channels.* Journal of General Physiology, 2011. 137(2): p. 173-195.

61. Bayley, H., O. Braha, and L.-Q. Gu, *Stochastic Sensing with Protein Pores.* Advanced Materials, 2000. 12(2): p. 139-142.

62. Braha, O., et al., *Simultaneous stochastic sensing of divalent metal ions.* Nature Biotechnology, 2000. 18: p. 1005-1007.

63. Braha, O., et al., *Designed protein pores as components for biosensors.* Chemistry & Biochemistry, 1997. 4: p. 497-505.

64. Menestrina, G., *Ionic Channels Formed by Staphylococcus aureus Alpha-Toxin: Voltage-Dependent Inhibition by Divalent and Trivalent Cations.* Journal of Membrane Biology, 1986. 90: p. 177-190.

65. Armstrong, C.M. and G. Cota, *Calcium block of Na^{+} channels and its effect on closing rate.* Proceedings of the National Academy of Sciences of the United States of America, 1999. 96: p. 4154-4157.

66. Armstrong, C.M. and S.R. Taylor, *Interaction of Barium Ions with Potassium Channels in Squid Giant Axons.* Biophysical Journal, 1980. 30: p. 473-488.

67. Lansman, J.B., *Blockade of Current through Single Calcium Channels by Trivalent Lanthanide Cations.* Journal of General Physiology, 1990. 95: p. 679-696.

68. Lansman, J.B., P. Hess, and R.W. Tsien, *Blockade of Current through Single Calcium Channels by Cd^{2+}, Mg^{2+}, and Ca^{2+}*. Journal of General Physiology, 1986. 88: p. 321-347.

69. Sheng, M. and D.T.S. Pak, *Ligand-Gated Ion Channel Interactions with Cytoskeletal and Signaling Proteins.* Annu. Rev. Physiol., 2000. 62: p. 755-778.

70. Roux, B., et al., *Ion selectivity in channels and transporters.* The Journal of General Physiology, 2011. 137: p. 415-426.

71. Chena, X., et al., *Structure of the full-length Shaker potassium channel Kv1.2 by normal-mode-based X-ray crystallographic refinement.* PNAS, 2010. 107: p. 11352-11357.

72. Levitt, D.G., *Perspective Modeling of Ion Channels.* J.Gen.Physics, 1999. 113: p. 789-794.

73. Dean, J.A., *Lange's Handbook of Chemistry*. 15th ed. 1999: McGraw-Hill.

74. Holm, R.H., P. Kennepohl, and E.I. Solomon, *Structural and functional Aspects of metal Sites in biology.* Chemical Reviews, 1996. 96: p. 2239-2314.

75. Khandpur, R.S., *Handbook of Biomedical Instrumentation*. 2nd ed. 2003.

76. Taylor, J.R., *An Introduction To Error Analysis*. 1997: University Science Books.

77. Gross, L.C.M., et al., *Determining Membrane Capacitance by Dynamic Control of Droplet Interface Bilayer Area.* Langmuir, 2011. 27: p. 14335-14342.

78. M.C.Hegg and A.V.Mamishev, *Influence of Variable Plate Separation on Fringing Electric Fields in Parallel-Plate Capacitors*, in *IEEE International Symposium on Electrical Insulation*. 2004: Indianapolis.

79. Niles, W.D., R.A. Levis, and F.S. Cohen, *Planar Bilayer Membranes Made from Phospholipid Monolayers Form by a Thinning Process.* Biophysics., 1988. 53: p. 327-335.

Appendix A: Characteristics of Metal Ions

Table 6: Biological classification, ionic and hydrated radii [22, 33, 57, 73].

Atomic number	**Element**	**Oxidation state**	**Biological classification**	**Effective ionic radii,** Å	**Effective hydrated radii,** Å
11	Na	+1	Bulk	1.09	4.50
12	Mg	+2	Bulk	0.76	8.00
13	Al	+3		0.55	9.00
19	K	1+	Bulk	1.50	3.00
20	Ca	+2	Bulk	1.12	6.00
25	Mn	+2	Essential	0.86	6.00
26	Fe	+2	Essential	0.78	6.00
		+3	Essential	0.66	9.00
27	Co	+2	Essential	0.74	6.00
28	Ni	+2	Beneficial	0.715	6.00
30	Zn	+2	Essential	0.74	6.00
48	Cd	+2	Toxic	0.96	5.00
57	La	+3		1.18	9.00
58	Ce	+3		1.20	9.00
63	Eu	+3		1.085	9.00
65	Tb	+3		1.05	9.00

Table 7: Electronic configurations of elements and ions [12, 74].

Atomic number	Element	Electron configuration of Atom	Ion	Oxidation state	Electron configuration of ions
11	Na	[Ne]$3s^1$	Na^+	+1	[Ne]
12	Mg	[Ne]$3s^2$	Mg^{2+}	+2	[Ne]
13	Al	[Ne]$3s^2$ $3p^1$	Al^{3+}	+3	[Ne]
19	K	[Ar]$4s^1$	K^+	1+	[Ar]
20	Ca	[Ar]$4s^2$	Ca^{2+}	+2	[Ar]
25	Mn	[Ar]$4s^2 3d^5$	Mn^{2+}	+2	[Ar]$4s^0$ $3d^5$
26	Fe	[Ar]$4s^2$ $3d^6$	Fe^{2+}	+2	[Ar]$4s^0$ $3d^6$
			Fe^{3+}	+3	Ar]$4s^0$ $3d^5$
27	Co	[Ar]$4s^2$ $3d^7$	Co^{2+}	+2	[Ar]$4s^0$ $3d^7$
28	Ni	[Ar]$4s^2$ $3d^8$	Ni^{2+}	+2	[Ar]$4s^0$ $3d^8$
30	Zn	[Ar]$4s^2$ $3d^{10}$	Zn^{2+}	+2	[Ar]$4s^0$ $3d^{10}$
48	Cd	[Kr]$5s^2 4d^{10}$	Cd^{2+}	+2	[Kr]$5s^0 4d^{10}$
57	La	[Xe]$6s^2 5d^1$	La^{3+}	+3	[Xe]$6s^0 5d^0$
58	Ce	[Xe]$6s^2$ $4f^1 5d^1$	Ce^{3+}	+3	[Xe]$6s^0$ $4f^1 5d^0$
63	Eu	[Xe]$6s^2$ $4f^7$	Eu^{3+}	+3	[Xe]$6s^0$ $4f^6$
65	Tb	[Xe]$6s^2$ $4f^9$	Tb^{3+}	+3	[Xe]$6s^0$ $4f^8$

Appendix B: Chelating Agents and Buffers

B.1 Chelating Agents and Precipitators

EDTA, EGTA and phosphate were used in this research as chelating agents and precipitators respectively. EDTA, a hexadentate ligand, contains two amine groups and four carboxylic acid groups. By ionizing the acid groups, EDTA introduces six coordinate binding sites, which can be bound to a metal ion. EGTA, a polyamino carboxylic acid that is related to EDTA, has a higher affinity for calcium than magnesium ions. The chemical structure of EDTA and EGTA is illustrated in Figure B.1.

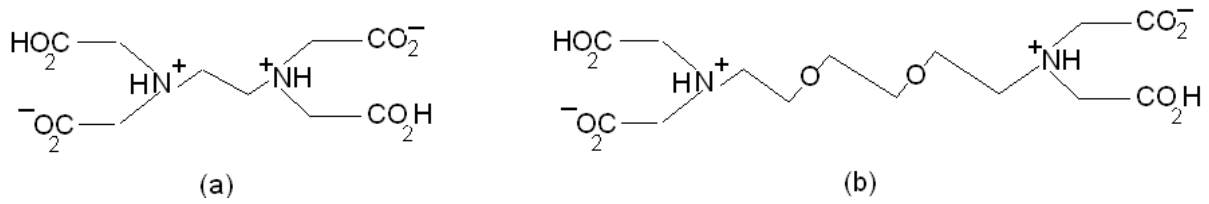

Figure B.1: The chemical structure of (a) EDTA, and (b) EGTA

Phosphate also was used in this research to precipitate couple of metal ions such as aluminum trivalent and copper divalent ions. The chemical structures of phosphate precipitator and some common functional groups of chelating agents are illustrated in Figure B.2.

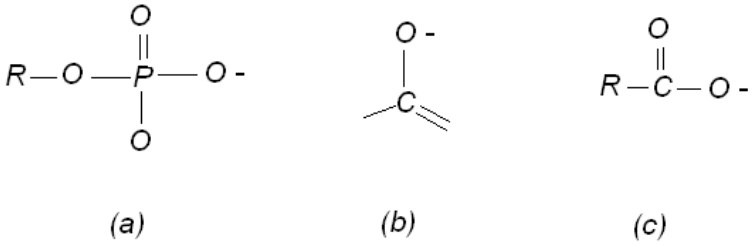

Figure B.2: The chemical structure of (a) Phosphate (b) Phenoxide (c) Carboxylate

B.2 HEPES

Buffered solutions are essential in biological investigations. Cell biology, for instance, uses cell-cultural media mixed with HEPES buffer in many applications. Compared to other agents, HEPES exhibits solubility, stability and experiences minimum interaction with metal ions [46].

In this study, the pH of the electrolyte was kept constant by adding HEPES/KOH buffer. The chemical structure of HEPES is shown in Figure B.3 [33]. When NaCl electrolyte solution was used, the produced NaOH, a base, increased the pH (see equation C.4 in Appendix C). In order to maintain a constant pH, HEPES bound the OH- molecule and kept the bulk at a constant pH.

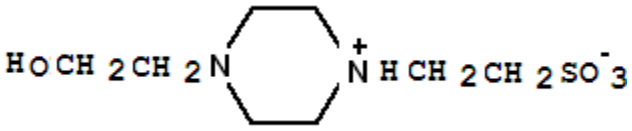

Figure B.3: The chemical structure of HEPES.

Appendix C: Conductivity and Electrochemical Reactions

C.1 Electrical Conductivity

Electrical conduction is a transport effect in which electrical charge (carried by electrons or ions) moves through the system [34].

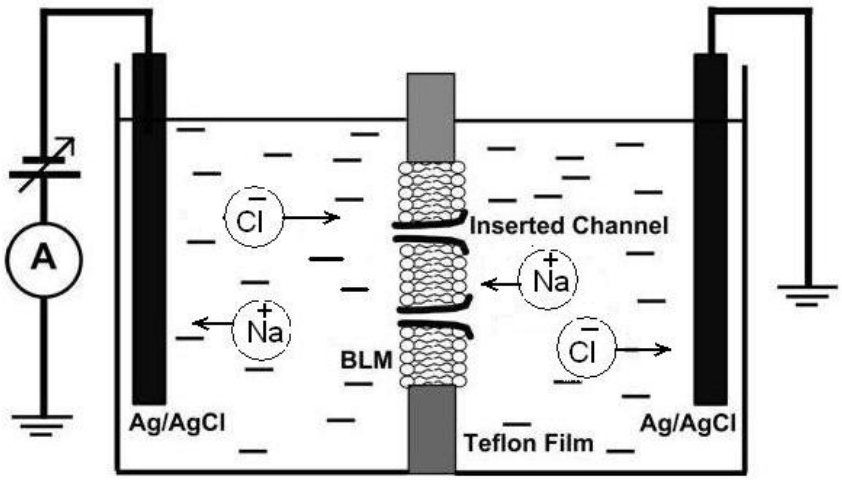

Figure C.1: An electrolysis cell

Two Silver/silver chloride electrodes at each end of a cell— filled with electrolyte solution as illustrated in Figure C.1— were used to apply a potential difference by connecting them to a power supply. The conductivity 'k" of a the electrolyte; that is the reciprocal of resistivity " $1/\rho$" is defined as $k = j/E$, where "E" is the electric field, and *"j"* is the electric current density or the electric current per unit cross sectional area that is $j = I/A$.

Since Ohm's law applies to aqueous ionic solutions, then if we assume that the electric field is constant and along the x-direction, then

$E = \left|\frac{dV}{dx}\right| \Rightarrow \Delta V = El$, then $\Delta V = \frac{l}{kA} I$, or $\Delta V = \rho \frac{l}{A} I$

The term $\rho\frac{l}{A}$ is called the resistance, that is $R = \rho\frac{l}{A}$ and its reciprocal is called the conductance G, so $G = k\frac{A}{l}$

Conductance is the reciprocal of resistance, and it is convenient to deal with conductance rather than resistance when discussing channels in membrane. Simply, the total conductance of the channels is just the sum of each individual channel's conductance [36]. The SI units of conductivity and conductance are S/cm and S respectively, where S denotes siemens.

C.2 Ions in Solution and Electrochemical Reactions

The electrochemical reactions occurring at, the silver/silver chloride electrodes (Ag/AgCl), the anode and cathode (see Figure C.2) along with chemical reactions in the electrolyte can be described in simple chemical equations. The electrolyte of sodium chloride, for instance, and water undergoes ionic dissociation as shown in equation C.1.

$$NaCl_{(s)} \xrightarrow{H_2O} Na^{+}_{(aq)} + Cl^{-}_{(aq)} \qquad C.1$$

As the potential difference is applied between the electrodes, positive ions (Na^+) move towards the negative electrode (cathode) and negative ions (Cl^-) move towards the positive one (anode). Reactions of sodium ions at the cathode and of chlorine at the anode are described by the following equations [75].

$$2Na^{+} + 2H_2O + 2e^{-} \rightarrow 2NaOH + +H_{2(g)} \qquad C.2$$

$$Cl^{-} \rightarrow 1e^{-} + Cl \qquad C.3$$

The neutralized chloride ion (Equation C.3) interacts with the chloride layer that covers the anode (see Figure C.2). The base NaOH dissociates according to equation C.4.

$$NaOH \rightleftharpoons +Na^{+} + OH^{-} \qquad C.4$$

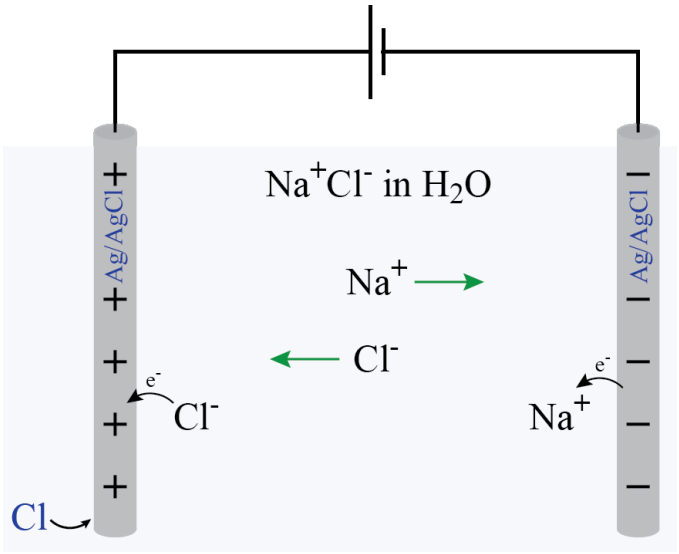

Figure C.2: Sodium ions become sodium atoms after they gain electrons at the cathode, while chloride ions turn to chlorine atoms at the anode.

Since the electric current can flow in both directions, then the electrochemical reactions at the electrodes are reversible. The silver/silver chloride electrodes (Ag/AgCl) provide the best conditions to enhance both a flow of electrons in the wires, and a flow of ions in solution. The AgCl, which covers the Ag electrodes, dissociates to Ag atoms and Cl^{-1} ions after the electrons pass through these electrodes. As a result, the hydrated Cl^{-1} ions enter the solution, as illustrated by equation C.5 and Figure C.3.

$$AgCl_{(s)} + e^{-} \rightleftharpoons Ag_{(s)} + Cl^{-} \qquad C.5$$

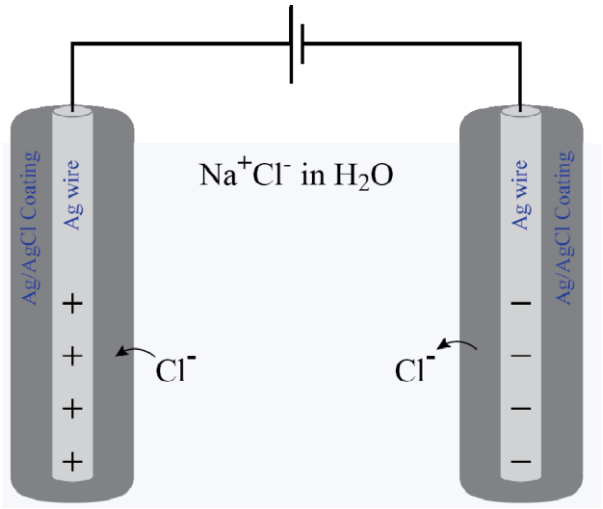

Figure C.3: The chemical reactions of the chloride ions at the Ag/AgCl electrodes

Appendix D: Conductance Calculations, Uncertainties and Errors

In order to estimate the conductance of Lysenin channels, a linear voltage ramp was applied across the BLM. That linear ramp was defined by using the episodic stimulation protocol (0 mV: -60 mV:0 mV, 0.5 mV/5 scan rate), each run consisted of three identical voltage sweeps, that is a total of six I-V curves in the range (0 mV: -60 mV :0 mV) as shown in Figure 3.5.

D.1 Measuring the Initial Conductance and the Uncertainty

The conductance was calculated from the slope of I-V curve, which was obtained by using a Clamp fit analysis as follows:

1. Open the required file and let's assume that file has the number of (10127006.abf) as illustrated in Figure D.1 below. This graph is still the recorded current-time graph, so we need to get the current-voltage graph in order to calculate the conductance.

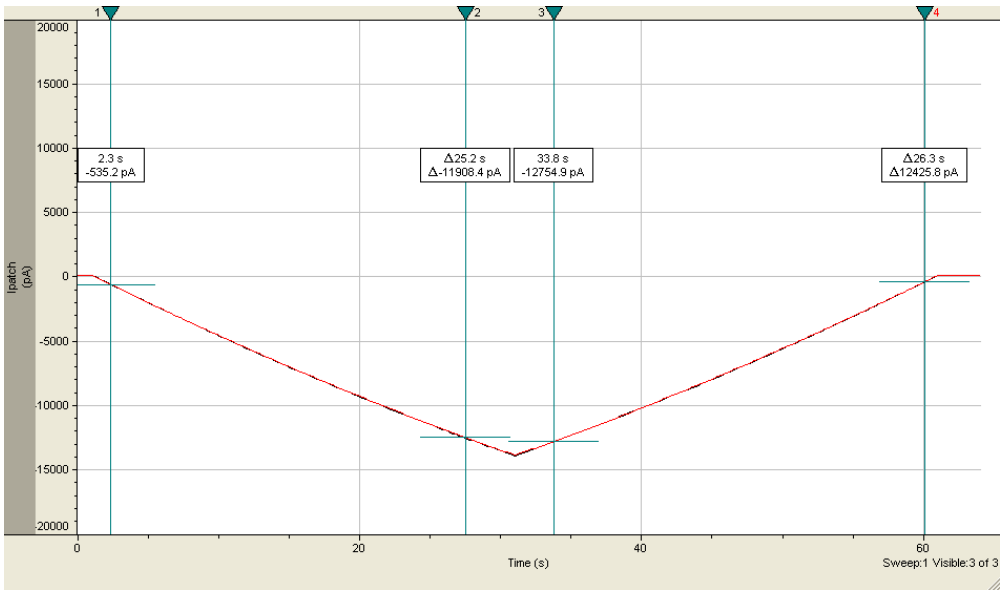

Figure D.1: Recording of current versus time of an electric ramp of (0 mV: -60 mV: 0 mV). This electric ramp was applied across the BLM containing Lysenin channels.

2. Execute "Analyze" then "quick graph" then choose "trace vs. trace" this will open a trace vs. trace dialog box. On the X-Axis trace, choose "sweep#1" and highlight the waveform Cmd0

(mV). On the Y-Axis trace, choose “sweep#1” and highlight the signal “Ipatch (pA)”, then on region choose “EpochA which is the straight line between the cursers 1 and 2” (see Figure D.1) and then choose “Replace” under the “destination”. By executing “OK” we get an I-V graph as illustrated in Figure D.2.

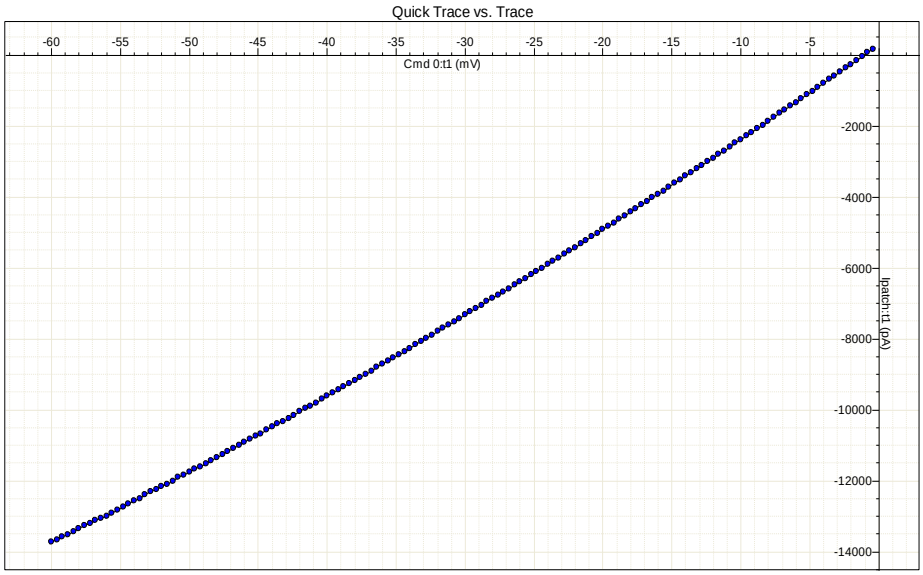

Figure D.2: Current versus voltage of Epoch A.

3. The conductance is just the slope of the line in Figure (D.2) above.

4. To consider the second straight line (Epoch B), which lied between cursers 3 and 4 we repeat the same steps in (2) above but we change to Epoch B and choose “Apend” under the “destination” and by clicking “OK” we get the second I-V curve as illustrated in Figure D.3.

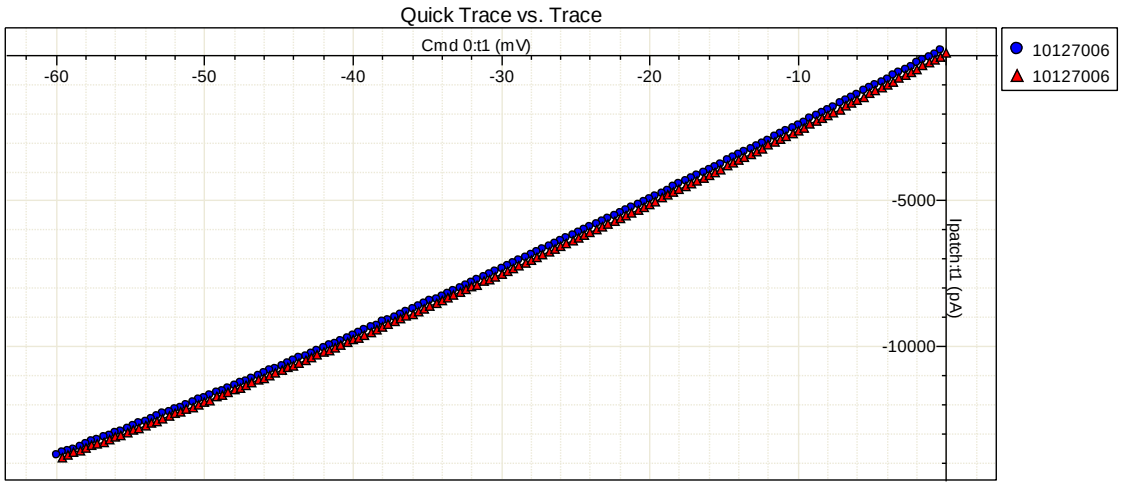

Figure D.3: Current versus voltage for one ramp (0 mV: -60 mV: 0 mV) of the first sweep.

5. The analysis above covered the first sweep, and for the other two sweeps we need to repeat the above procedures to get the six straight lines as shown in Figure D.4.

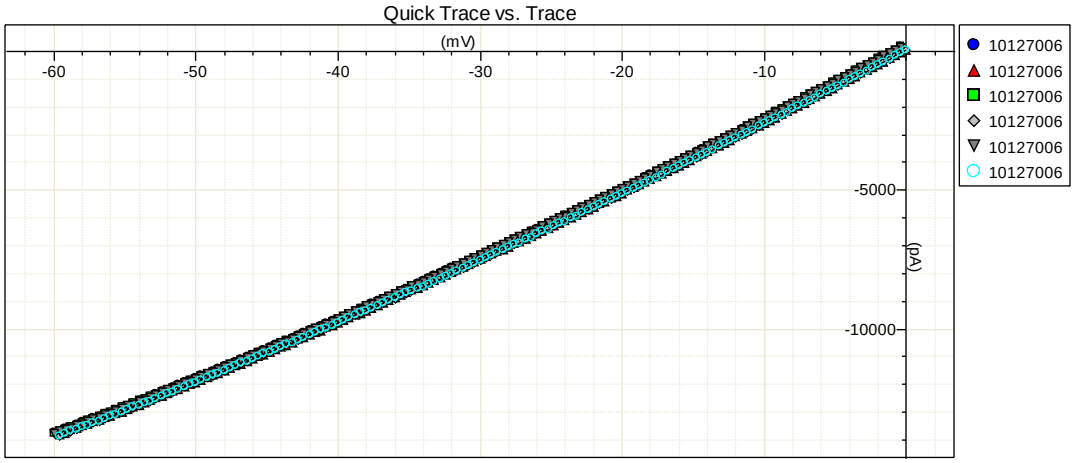

Figure D.4: Current versus voltage for the six ramps (three sweeps). The slope is almost the same for all of these lines indicating small errors in the calculations of conductance.

6. The conductance of the BLM was just the mean of the slopes of these lines. The root mean square (RMS) of these measurements was taken as the standard deviation of the slopes i.e. the estimated values of the conductance, which are listed in Table 8.

Table 8: The estimated values of the electrical conductance of Lysenin channels before adding ions

m1	m2	m3	m4	m5	m6
233.8 x10^{-9}	233.5 x10^{-9}	234.5 x10^{-9}	233.5 x10^{-9}	234.5 x10^{-9}	233.3 x10^{-9}

7. In order to calculate the uncertainty, the standard deviation for these measurements was considered. $\sigma = \sqrt{\frac{\sum_{i=1}^{N}(m_i - \tilde{m})^2}{N-1}}$ [76], where N is the number of measurements which is 6 in this case and (m_i) is the *ith* measurement and ($\tilde{m}$) is the mean measurement. According to this equation the mean conductance was calculated to be $\tilde{m} = 233.9x10^{-9}$, and the standard deviation was $\sigma_1 = 0.5x10^{-9}$, And since the measurements should be expressed as: $\boxed{Best\ value\ \pm Uncertainty}$ [76]. Then the measurement of the conductance before adding ($Me^{n+}) = (233.9 \pm 0.5)\ nS.$

D.2 Measuring the Conductance after adding Me^{n+} and Estimating the Uncertainty

Follow the previous procedures (1-7) for a file that contains the recorded data of the current ramp. Say this file was (10127009.abf). The slopes are shown in the Table 9.

Table 9: The estimated values of the electrical conductance of Lysenin channels after adding ions

m1	m2	m3	m4	m5	m6
224.0 x10^{-9}	223.0 x10^{-9}	223.6 x10^{-9}	224.2 x10^{-9}	224.1 x10^{-9}	223.9 x10^{-9}

According to the data in Table 9, the mean of the conductance (slopes) after adding multivalent ions would be $\tilde{m} = 223.8x10^{-9}$ and the standard deviation would be $\sigma_2 = 0.4x10^{-9}$, then the measurement of conductance after adding $(Me^{n+}) = (223.8 \pm 0.4)\, nS$.

Some of the figures that have been introduced in this dissertation considered the conductance versus concentrations, that is $\frac{G}{G_0}$, where G is the slope of the current-voltage curve after adding Me^{n+} and G_0 is the slope of the current-voltage curve before addingMe^{n+}. That is $G_0 = (233.8 \pm 0.5)x10^{-9}\, S, and\ \ G = (223.8 \pm 0.4)x10^{-9}\, S.$

The following formula has been used [76] to calculate the uncertainty of the conductance:

$The\ vale\ of\ \frac{G}{G_0} = \frac{\tilde{G}}{\tilde{G}_0}\left(1 \pm \left[\frac{\sigma_1}{\tilde{G}_0} + \frac{\sigma_2}{\tilde{G}}\right]\right)$, Then $\frac{G}{G_0} = \frac{223.8}{233.9}\left(1 \pm \left[\frac{0.5}{233.9} + \frac{0.4}{223.8}\right]\right)$

$$\frac{G}{G_0} = 0.96(1 \pm 0.004) = 0.9600 \pm 0.0038$$

This means during the same experiment the standard deviation (error) of conductance $\frac{G}{G_0}$ is almost negligible.

D.3 Sources of Errors and Error Bars

The main source of errors in the conducted experiments appeared to be due to the evaporation of the electrolyte solution. This was because the average time of conducting one experiment was about 4-6 hours, and in some cases it took about more than that. The evaporation affected the concentration of the bulk (either KCl or NaCl) and accordingly the calculations of concentrations of metal ions were affected. the evaporated amount of solution was measured to be $50\,\mu M$ out of $1000\,\mu M$. This produced about 5% error in calculating concentrations, and would be considered as the x-error bars in all the graphs. On the other hand, the y-error bars were estimated from calculating the standard deviation of the same experimental value but from different experiments.

Appendix E: Capacitance and Electric Field Across BLM

E.1 The Capacitance of BLM

A planar lipid bilayer membrane (BLM) can be considered as a biological parallel plate capacitor (Figure E.1) [77]. When a potential difference ΔV is applied across the leaflet of the membrane, then the capacitance (C in Farads) of that membrane can be expressed as [36]:

$$CV = Q \qquad E.1$$

Where (Q) is the stored charge in these leaflets.

Figure E.1: Bilayer lipid membrane is considered as a Parallel plate capacitor

It is known that Fringing effect is found between any two parallel-plate capacitor [78], and to reduce this effect we usually make the separation between the plates too small. Since the thickness of the lipid bilayer is too small (less than 10 nm), so we expect the electric field to be uniform and no Fringing effect. Accordingly the Capacitance (SI base units) of the BLM can be expressed as:

$$C = \frac{\epsilon}{t_m} A \qquad E.2$$

Where ϵ denotes the membrane dielectric constant,

A denotes the area of the planar bilayer lipid membrane, and

t_m denotes the thickness of the bilayer lipid membrane.

It is most common to use the capacitance per unit area for membranes [6].

In order to measure the capacitance of the bilayer lipid membrane, a train of triangular voltage waves was applied across the BLM. As a result, a train of square current waves was recorded as illustrated in Figure E.2. The amplitude of the recorded square waves (the capacitive current) was proportional to the area of the BLM and hence to its capacitance.

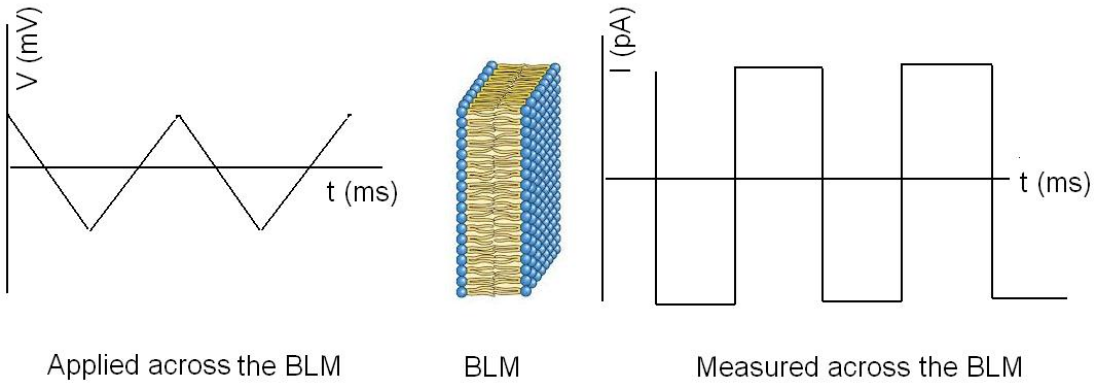

Figure E.2: The formation of a bilayer lipid membrane (BLM) was inspected by applying a train of triangular voltage waves across the BLM and recording a train of square current waves.

The capacitive current can be theoretically estimated by using Equation E.1, so if we differentiate both sides with respect to time we get:

$$C\frac{dV}{dt} = \frac{dQ}{dt}\ , or\ \ C\frac{dV}{dt} = I \qquad E.3$$

If we apply a triangular voltage which varies with time with a slope of ± 1 ($\frac{dV}{dt} = \pm 1$) then we expect the current to be equivalent to the capacitance (Equation E.3), and this is why we do call it by the capacitive current.

Theoretically, we can estimate the values of the capacitive current that tells us about the formation of the bilayer lipid membrane from multilayer ones. According to Equation E.2, the

capacitance and the thickness of the bilayer membrane are inversely proportional, and since the radius of the aperture is (70-100 μm) and the measured values of the capacitance per unit area of a BLM (0.7-0.86 μF/cm^2) [79] then the square capacitive current "I" can be calculated as follows:

If the radius of the aperture is 100μm and the radius of the formed BLM is approximately 50μm, then the area of the BLM is $A = \pi r^2$, that is $A \approx 78.5 * 10^{-6}\ cm^2$. If we accept the measured experimental capacitance per unit area to be 0.7 μF/cm^2, then the capacitance (or the capacitive current) would be $C \approx 0.7 \frac{\mu F}{cm^2} * 78.5 * 10^{-6}\ cm^2 \approx 55\ pF$. According to this value, if the capacitive current is greater than 50pA, then we expect BLM formation.

E.2 Electric Fields across the BLM

The electric fields that are considered and influenced the BLM are just the ones who are across it and not inside the electrolyte solution. In fact we can neglect the electric field within the solution. These electric fields are illustrated in Figure E.3, and the equivalent electric circuit of the BLM and the electrolyte solution is shown in Figure E.4.

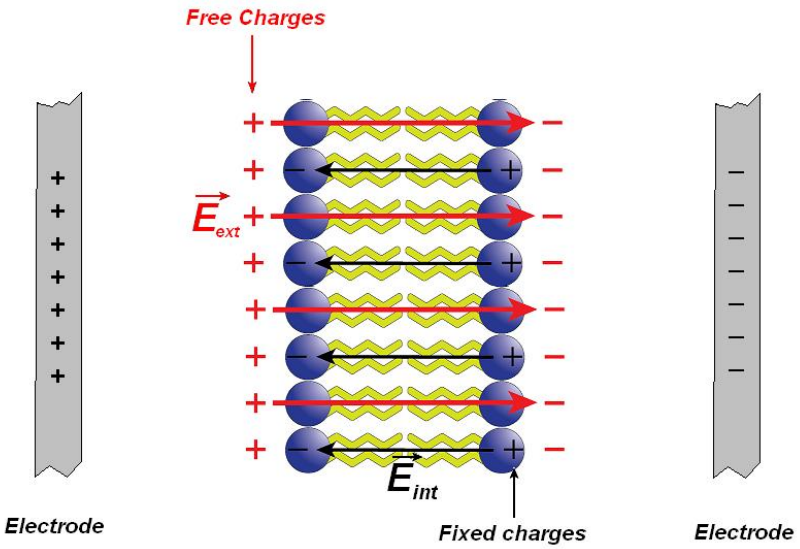

Figure E.3: The external electric field ($\vec{E}_{ext}$) across the BLM was created due to the charge accumulation of monovalent ions (K^+ and Cl^-). These charges were driven by the positive and negative electrodes. The accumulation of these charges polarized the dielectric material of the BLM creating an opposing electric field ($\vec{E}_{int}$).

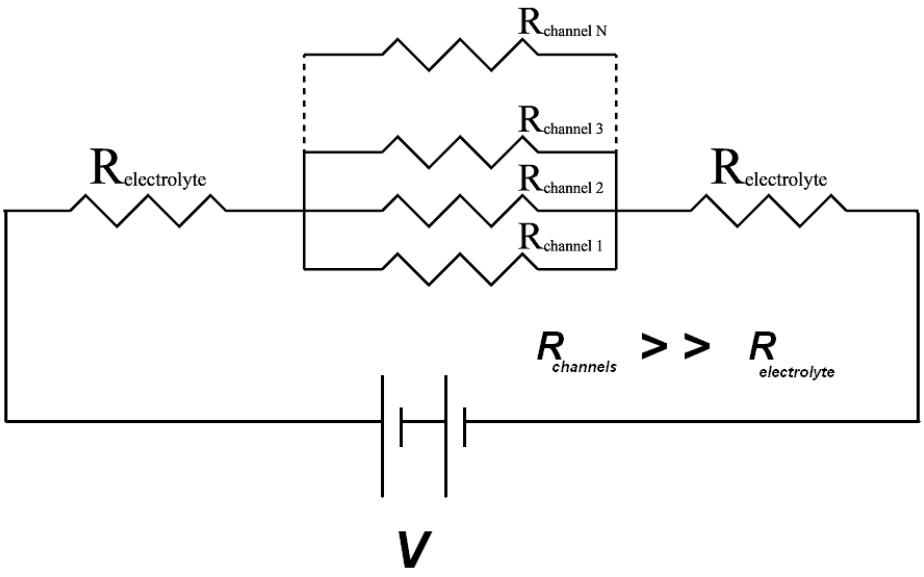

Figure E.4: The equivalent electric circuit of the lysenin channels inserted in the BLM and surrounded by the electrolyte solution.